UNIVERSITA' VITA-SALUTE SAN RAFFAELE

CORSO DI DOTTORATO DI RICERCA INTERNAZIONALE IN MEDICINA MOLECOLARE

Curriculum in

Immunologia e Oncologia di Base e Applicate

CXCR4-mediated antitumor immunization

Supervisore: Prof. Marco E. Bianchi

Co-supervisore: Prof. Jürgen Bernhagen

Tesi di DOTTORATO di RICERCA di Francesca Caprioglio

matr. 022051

Ciclo di dottorato XXXVIII

SSD BIO/11

Anno Accademico 2024/2025

CONSULTAZIONE TESI DI DOTTORATO DI RICERCA

Il/la sottoscritto	Francesca Caprioglio
Matricola	022051
nata a	Casale Monferrato (AL)
il	12/03/1997

autore della Tesi di Dottorato di Ricerca dal titolo

CXCR4-mediated antitumor immunization

X AUTORIZZA la Consultazione della Tesi

☐ NON AUTORIZZA la Consultazione della Tesi per …… mesi a partire dalla data di sottomissione della domanda di conseguimento titolo

Poiché:

□ l'intera ricerca o parti di essa sono potenzialmente soggette a brevettabilità*;*

□ ci sono parti di Tesi che sono già state sottoposte a un editore o sono in attesa di pubblicazione*;*

□ la Tesi è finanziata da enti esterni che vantano dei diritti su di esse e sulla loro pubblicazione*.*

E' fatto divieto di riprodurre, in tutto o in parte, quanto in essa contenuto

Data .....30/11/2025..... *Firma* ……Francesca Caprioglio……

DECLARATION

This thesis has been:

- composed by myself and has not been used in any previous application for a degree
- written according to the editing guidelines approved by the University.

All figures derived from open access articles except for:

- Figure 20 Created in BioRender.com (Caprioglio, F. (2025) jslqu6j)

For the following images, it was not possible to obtain permission and are therefore included in the thesis under the "fair use" exception (Italina legislative Decree no. 68/2003): Figure 5.

Throughout the text I use both 'I' and 'We' interchangeably.

All the results presented here were obtained by me, except for:

1. scRNA-seq data analysis (Figure 11D, 12, 13, 14) was performed by Dr. Sara Morelli, Chromatin Dynamics Unit, Vita-Salute San Raffaele University, Milan Italy
2. Immunohistochemistry (Figure 10, 18) was performed by Amleto Fiocchi, Animal Histopathology Facility, IRCCS San Raffaele Hospital, Milan Italy; the codes for image automatic analysis in QuPath were created by Dr. Liam S. Colley, Chromatin Dynamics Unit, IRCCS San Raffaele Hospital, Milan Italy
3. GO2 cell line was generated by Marion MacFarlane, MRC Toxicology Unit of University of Cambridge, Cambridge, UK
4. Generation of macrophages (derived from PBMC) and human co-culture setting (Figure 19) was performed by Dr. Annamaria Molinario, Chromatin Dynamics Unit, IRCCS San Raffaele Hospital, Milan Italy

All sources of information are acknowledged by means of references.

I am co-author in the following publications:

- Garcia-Manteiga JM*, Rrapaj E*, Caprioglio F*, et al (2025) Fibroblast-like Cells in Mesothelioma Can Derive from Tumor Cells *CELL DEATH DIFFER* *equal contribution
- Mantonico MV et al (2024) The acidic intrinsically disordered region of the inflammatory mediator HMGB1 mediates fuzzy interactions with CXCL12. *NAT COMMUN*
- Mezzapelle R et al (2022) CXCR4/CXCL12 Activities in the Tumor Microenvironment and Implications for Tumor Immunotherapy. *CANCERS*
- Mezzapelle R et al (2021) CXCR4 engagement triggers CD47 internalization and antitumor immunization in a mouse model of mesothelioma. *EMBO MOL MED*

Riassunto

Il Mesotelioma Maligno (MM) si sviluppa dopo un lungo periodo di infiammazione cronica causata dall'esposizione a fibre di amianto; l'esordio è sostenuto dalla proteina High Mobility Group Box 1 (HMGB1), che può legarsi a diversi recettori (CXCR4, RAGE e TLRs) per innescare risposte infiammatorie. La chemochina CXCL12 è il ligando naturale di CXCR4, al quale può legarsi da sola o in complesso con HMGB1, esercitando attività chemio-attrattiva e reclutando cellule infiammatorie. Nel contesto tumorale, l'asse CXCL12–CXCR4 favorisce la proliferazione delle cellule tumorali e la formazione di metastasi. Abbiamo identificato un meccanismo di sorveglianza immunitaria mediato da CXCR4, definito "Capitolazione Immunogenica". In breve, CXCR4 interagisce fisicamente con CD47, che funge da segnale "non-mangiarmi" legandosi a SIRPα sui macrofagi (MΦs) e inibisce la fagocitosi. Quando attivato da BoxA —una forma troncata di HMGB1— e CXCL12, CXCR4 co-internalizza con CD47, consentendo la fagocitosi di alcune cellule tumorali da parte dei MΦs. Pertanto, comprendere l'effetto di CXCL12 nel microambiente tumorale è necessario e potrebbe aprire nuove prospettive terapeutiche.

Per studiare l'effetto di CXCL12 *in vivo*, abbiamo iniettato cellule AB1 (MM murino) in topi BALB/c, generando un modello che riproduce la patologia umana, e li abbiamo trattati con CXCL12. Per testare l'effetto di CXCL12, ho eseguito saggi di proliferazione, analisi di citofluorimetria e trascrittomica a singola cellula (scRNAseq) utilizzando un sistema di co-colture 3D che mima l'interazione MΦs-cellule di MM.

La maggior parte dei topi trattati con CXCL12 ha mostrato una sopravvivenza significativamente più lunga rispetto al gruppo non trattato e, in alcuni casi, abbiamo osservato il rigetto del tumore. Le masse tumorali provenienti da topi trattati con CXCL12 presentavano un aumento di MΦs CD169+, linfociti T infiltranti (TILs) CD3+ e maggiore attivazione delle cellule T CD8+. L'effetto del trattamento veniva abolito dalla deplezione sia di cellule T CD4+ che CD8+, indicando che CXCL12 rimodella il panorama linfocitario. Esperimenti *in vitro* hanno mostrato che la proliferazione delle cellule di MM non era influenzata da CXCL12. L'analisi di scRNAseq ha rivelato che MΦs e cellule MM vengono riprogrammati trascrizionalmente downregolando le risposte cellulari e acquisendo un fenotipo più plastico e dinamico.

Questi dati suggeriscono che CXCL12 attiva la sorveglianza immunitaria promuovendo un fenotipo di MΦs favorevole al reclutamento e all'attivazione delle cellule T, e che la sua somministrazione è complessivamente benefica nei topi affetti da mesotelioma.

Abstract

Malignant Mesothelioma (MM) develops after a long period of chronic inflammation caused by exposure to asbestos fibers; its onset is supported by High Mobility Group Box 1 (HMGB1) protein which can bind to different receptors (CXCR4, RAGE and TLRs) to trigger inflammatory responses. The chemokine CXCL12 is the canonical ligand of CXCR4, to which it can bind alone or in complex with HMGB1, and it exerts chemoattractant activity and promotes the recruitment of inflammatory cells. In cancer, the CXCL12-CXCR4 axis leads to enhanced tumor cell proliferation and metastases formation. We found a mechanism of immune surveillance, named "Immunogenic Surrender", which is mediated by CXCR4. Briefly, CXCR4 physically interacts with CD47 that acts as "don't-eat-me" signal by binding to SIRPα on macrophages (MΦs), thus inhibiting phagocytosis. When engaged by some ligands, among which BoxA -a truncated form of HMGB1 antagonizing the full-length protein- and CXCL12, CXCR4 co-internalizes with CD47, and some tumor cells are phagocytosed by MΦs. Thus, understanding which is the effect of CXCL12 in the tumor microenvironment is needed and could lead to new therapeutic strategies.

To study the effect of CXCL12 *in vivo*, we injected i.p. BALB/c mice with AB1 (murine MM) cells, to generate a model that recapitulates the human disease, and we treated them with CXCL12. To elucidate the effect of CXCL12 on various cell types, both *in vitro* and *in vivo*, I performed proliferation assays, FACS analyses, and single cell transcriptomics on a 3D co-culture system –recently set up in our lab– which mimics the interaction between MΦ and MM cells.

Most of the CXCL12-treated mice showed significantly longer survival compared to the untreated group, and in some cases, there was tumor rejection at the end of the treatment. Tumor masses coming from CXCL12-treated mice displayed a larger fraction of CD169+ MΦs, a higher number of CD3+ tumor infiltrating lymphocytes (TILs) and a major CD8+ T cell activation. Concomitantly, the survival advantage induced by the treatment was abrogated upon depletion of either CD4+ or CD8+ T cells, meaning CXCL12 reshapes the T-cell landscape. *In vitro* experiments showed that MM cell proliferation was not affected by CXCL12. In parallel, scRNAseq revealed that, MΦs and MM cells undergo transcriptional reprogramming with downregulation of cellular responses and the acquisition of a more plastic and dynamic phenotype.

These data suggest that CXCL12 activates immune surveillance by promoting a MΦs phenotype conducive to T-cell recruitment and activation, and its administration is overall beneficial for mesothelioma-bearing mice.

Table of contents

LIST OF FIGURES

List of abbreviations

BAPE: Benign asbestos pleural effusion

BLI: BioLuminescence Imaging

BM: Bone marrow

BMDMs: Bone marrow-derived macrophages

CD: Cluster of differentiation

CSCs: Cancer stem cells

CTLA-4: cytotoxic T-lymphocyte 4

CTLs: Cytotoxic T lymphocytes

CXCL12: C-X-C Motif Chemokine Ligand 12

CXCR4: C-X-C chemokine Receptor type 4

DAMP: Damage-associated molecular pattern

ECM: Extracellular matrix

ER: Endoplasmic reticulum

FACS: Fluorescence-activated cell sorting

FFPE: Formalin-fixed paraffin-embedded

fr-HMGB1: Fully reduced HMGB1

GFP: Green fluorescence protein

GO: Gene Ontology

GPCR: G protein-coupled receptor

GrzB: Granzyme B

GSEA: Gene Set Enrichment Analysis

HMGB: High-mobility group box

ICD: Immunogenic cell death

ICI: Immune checkpoint inhibitor

IF: Immunofluorescence

IFN-γ: Interferon-gamma

IGS: ImmunoGenic Surrender

IHC: Immunohistochemistry

IL: Interleukin

LPS: Lipopolysaccharide

MHC-I: Major Histocompatibility Complex Class I

MM: Malignant Mesothelioma

MΦs: Macrophages

NLS: Nuclear localization sequence

PAMP: Pathogen-associated molecular pattern

PD-1: Programmed cell death-1

PDGF: Platelet-derived growth factor

RAGE: Receptor for advanced glycation end products

scRNAseq: Single-cell RNA sequencing

SDF-1: Stromal cell-derived factor-1

SIRP-α: Signal regulatory protein-α

SNP: Single nucleotide polymorphism

TAM: Tumor-associated macrophages

TCR: T cell receptor

TGF-β: Transforming growth factor-β

TILs: Tumor-infiltrating lymphocytes

TLR: Toll-like receptor

TME: Tumor microenvironment

TNF-α: Tumor necrosis factor-α

UMAP: Uniform Manifold Approximantion and Projection

1. Introduction

1.1 Malignant Mesothelioma

Malignant Mesothelioma (MM) is a tumor of the lining of the lung and chest cavity (pleura) or of the abdomen (peritoneum) which is typically related to asbestos -or other mineral fibers- exposure (Carbone M et al, 2012).

Asbestos has been determined to be a causative agent for a broad spectrum of pulmonary diseases affecting lung parenchyma and pleura and can have either benign (pulmonary and pleural fibrosis defined as asbestosis, pleural plaques, benign asbestos pleural effusion – BAPE) or malignant outcome, such as bronchogenic carcinoma and malignant mesothelioma (Solbes E & Harper RW, 2018). In fact, asbestos exposure is estimated to be responsible for 50-80% of pleural MM in men and 20-30% in women (Carbone M et al, 2012), in addition to lung cancer, ovarian cancer, laryngeal cancer and gastric cancer (Fang YJ et al, 2021). Various studies have demonstrated that asbestos fibers infiltrate the pleural tissue and cause chronic inflammation, thus promoting chronic asbestosis, pleural fibrosis/plaques and the onset of MM (Carbone M et al, 2012).

The time spanning from the first exposure to asbestos and the diagnosis of MM is defined as "latency period", and it ranges from 25 to 71 years (Bianchi C et al, 2007). Duration, quality and intensity of exposure are important factors to be considered in mineral fibers-related diseases (Carbone M et al, 2012). Unfortunately, the early diagnosis of MM is very hard, since there are no recognizable specific symptoms until the advanced stage of the disease (https://www.nhsinform.scot).

There are three main histological subtypes of MM associated to different prognosis:

- epithelioid, characterized by diffusive and invasive growth of epithelioid cells from pleural surface forming sheets of round to oval malignant mesothelial cells with abundant cytoplasm; it is the most common histotype in patients (about 80%), and it has the better prognosis, also since these patients might profit from surgical procedures;
- sarcomatoid, characterized by diffusive and infiltrative growth of spindle cells or mesenchymal cells; it has a very poor prognosis;
- biphasic, also known as mixed mesothelioma, is characterized by having at least 10% of each epithelioid and sarcomatoid component; the prognosis lies between pure epithelioid and sarcomatoid MM and the amount of the epithelioid part has a prognostic role (Brcic L & Kern I, 2020).

The median survival for MM patients is approximately 1 year, and few treatment options are available; moreover, clinical trials with cytotoxic drugs, targeted agents

and immune checkpoint inhibitors have been disappointing or with mixed results. The clinical management of MM relies on a multidisciplinary strategy integrating disease stage, histological subtype, and patient performance status. In early-stage disease, treatment consists of multimodal approaches combining platinum-based chemotherapy (commonly cisplatin plus pemetrexed) with surgery, with or without radiotherapy, to achieve macroscopic tumor control (Vogelzang NJ et al, 2003). In patients with advanced or unresectable disease, immunotherapy combining anti-programmed cell death 1 (PD-1) and anti-cytotoxic T-lymphocyte 4 (CTLA-4) antibodies, have shown survival benefit in non-epithelioid subtypes compared to chemotherapy (Baas P et al, 2021).

Nevertheless, despite incremental therapeutic advances, MM is characterized by limited treatment efficacy and poor overall survival, highlighting a substantial unmet clinical need and the importance of the development of novel therapeutic strategies.

1.2 Asbestos and related pathogenesis

Asbestos comprises a group of fibrous minerals that occur at low levels in the air, water, and soil. Serpentine and amphibole are the two groups in which asbestos is divided based on the structure of its fibers. All of them are chemically inert, durable, resistant to heat and fire and not conductive for electricity; for these properties, they started to be used for commercial application in the late 1800s, especially in construction, automotive and shipbuilding industries (Solbes E & Harper RW, 2018). Since people involved in these activities were continuously exposed to asbestos and started to develop malignancies from 1940s through the 1970s, the competent authorities found out the direct association and in 1989 the use of asbestos was banned by the Environmental Protection Agency (https://www.cancer.org).

In Italy, asbestos was widely used in the last century and the largest factory producing asbestos cement – known as Eternit – was active from 1907 to 1985 in Casale Monferrato. In the period 1946-1986, 117 workers who had been employed in Eternit died because of lung cancer, 89 due to asbestosis and 43 due to pleural malignancies (Magnani C et al, 1995). An excess of incidence of mesothelioma cases was confirmed in sites having a history of direct use of asbestos, such as Balanghero and Broni, or shipyards and harbors, such as Trieste, La Spezia, Venezia and Livorno (Binazzi A et al, 2019). Italy has banned the use of asbestos since 1992 and the European Union since 1999 (Magnani C et al, 2008).

Asbestos can break down into microscopic particles that are airborne and easily inhaled (https://www.cdc.gov); they enter the lungs and penetrate the pleural space,

where the interaction with mesothelial cells and inflammatory cells is thought to initiate prolonged cycles of local inflammation of the mesothelium, which over time will lead to carcinogenesis of MM (Sekido Y et al, 2013). The fibers are recognized by the immune system that activates an innate immune response, in particular operated by macrophages, against the foreign bodies. Macrophages are not able to digest asbestos fibers and will release high levels of reactive oxygen species (ROS). In addition, asbestos can be engulfed by mesothelial cells thus interfering with mitotic spindle formation. Finally, both asbestos-exposed mesothelial cells and macrophages release a variety of cytokines and growth factors (Toyokuni S et al, 2009) inducing inflammation and tumor promotion. These signals include tumor necrosis factor-α (TNFα), interleukin-1β (IL-1β), transforming growth factor-β (TGF-β) and platelet-derived growth factor (PDGF) (Sekido Y et al, 2013). TNFα has been shown to activate nuclear factor-κB (NF-κB) which leads to mesothelial cell survival (Yang H et al, 2006). Moreover, asbestos induces the ferroptotic cell death of mesothelial cells and the release of High-mobility group box 1 (HMGB1) in the extracellular space, which in turn recruits inflammatory cells (Yang H et al, 2010; Koruda A, 2021). In fact, HMGB1 is elevated in the blood of patients diagnosed with MM (Napolitano A et al, 2016). A likely possible mechanism is that macrophages with tissue healing phenotype favor the survival of MM cells, which contain high levels of HMGB1 and continuously secrete it, thus activating a positive loop to recruit other macrophages (Bianchi ME et al, 2017).

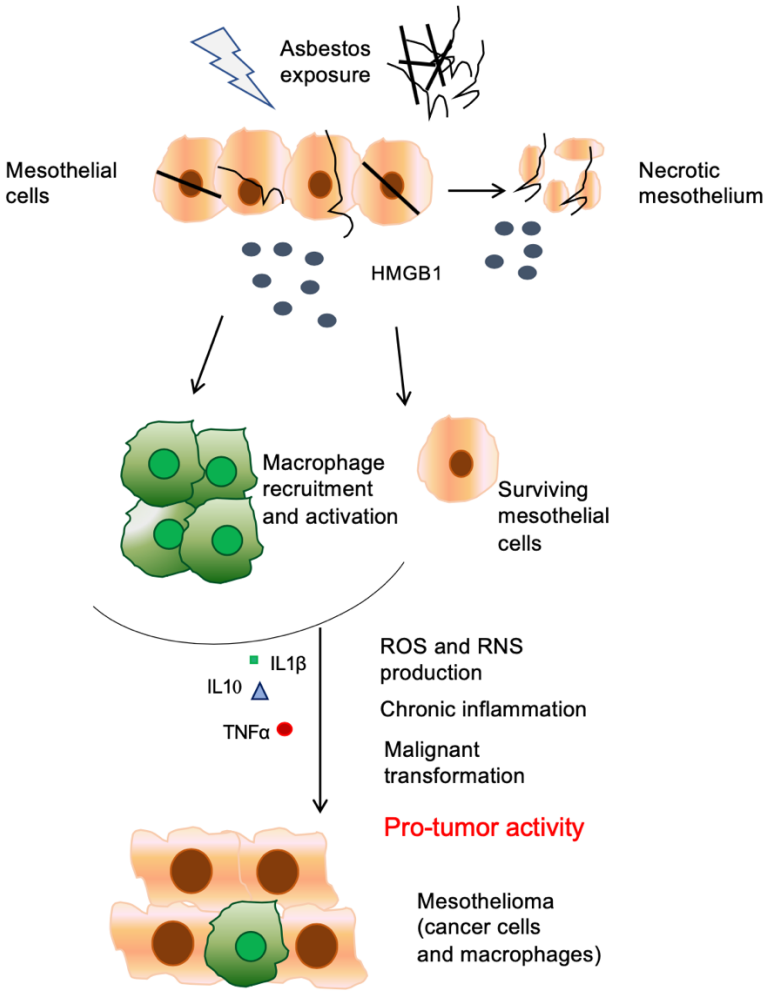

Figure 1. Schematic representation of HMGB1 pro-tumor activity (adapted from Bianchi ME et al, 2017). Mesothelial cells injured by asbestos undergo a programmed necrotic death, with HMGB1 release. Extracellular HMGB1 recruits and activates macrophages which sustains chronic inflammation thus leading to malignant transformation.

1.3 Inflammation

Inflammation is the body response to tissue damage caused by injuries, infection, external factors, or other types of traumas (Singh N et al, 2019). The inflammatory response starts with an acute phase, in which there is the recruitment of leukocytes, in particular neutrophils and monocytes; their activation leads to the release of pro-inflammatory cytokines (Vénéreau E et al, 2012). The response to pathogens is mediated via a set of receptors recognizing pathogen-associated molecular patterns (PAMPs), while traumas are recognized at cell level via receptor-mediated detection of endogenous proteins released by dead cells and defined as "alarmins". These molecules signal tissue and cell damage, and they are also known as Damage

Associated Molecular Patterns (DAMPs) (Bianchi ME, 2007). Among these molecules, there is High-mobility group box 1 (HMGB1) protein, a ubiquitous nuclear protein acting as DAMP once released in the extracellular space, signaling cell damage and alerting the body to danger, thus initiating the immune response and finally promoting the regeneration process (Vénéreau E et al, 2012).

Inflammation can persist and become chronic, and this condition creates an environment conducive to cancer development. In fact, chronic inflammation has been linked to various steps involved in tumorigenesis, including cellular transformation, promotion, cell survival, proliferation, invasion, angiogenesis, and metastasis (Singh N et al, 2019). Chronic inflammation and the presence of an unfavorable inflammatory microenvironment can promote tumor development as observed in colon carcinoma (Terzić J et al, 2010), or even more clearly in malignant mesothelioma (MM), which comprises a large inflammatory component, in particular macrophages (Lievense LA et al, 2013). MM cells express high levels of HMGB1 and can secrete it. Moreover, MM patients show high level of HMGB1 in the serum, making this protein a possible biomarker for this tumor (Jube S et al, 2012).

1.4 Tumor microenvironment

The tumor microenvironment (TME) refers to the cellular environment in which tumor or cancer stem cells exist; these components evolve with cancer cells and provides support to malignant transformation.

The TME comprises blood vessels, extracellular matrix (ECM), signaling molecules, and cellular components (Arneth B et al, 2019) which include:

- endothelial cells acting in tumor development due to nutritional support, and cell protection from immune system (Hanahan D et al, 2011);
- immune cells (i.e., granulocytes, lymphocytes and macrophages) that are involved in various activities such as inflammatory reaction orchestrated by the tumor to promote survival (Mantovani A et al, 2008);
- fibroblasts that allow cancer cells to migrate from the primary tumor location into the bloodstream for systemic metastasis (LeBleu VS, 2015).

Due to its role in tumorigenesis, the TME has become an area of interest to control tumor cells and try to develop drugs and intervention to treat cancer (Guillerey C et al, 2016). Within this complex ecosystem, tumors can be classified according to the degree and quality of immune cell infiltration, with implications for prognosis and response to therapy. "Hot" tumors are typically characterized by abundant CD8+ T-cell infiltration, type I interferon signaling, expression of immune-activating

chemokines and active antigen-presentation machinery; all these features generally associate with better responses to immune checkpoint inhibitors (ICIs) (Gajewski TF et al, 2017; Chen DS & Mellman I, 2017). By contrast, "cold" tumors encompass very few cytotoxic T cells and several immunosuppressive cell populations (e.g. regulatory T cells, myeloid-derived suppressor cells, tumor-associated macrophages) and a dense, remodeling stroma that hinders antitumor immunity and limits responsiveness to ICIs (Liu YT & Sun ZJ, 2021; Khosravi GR et al, 2024; Vyhnánková S et al, 2025). Identifying strategies to convert a non–inflamed microenvironment into an inflamed one has therefore become a central goal in the development of new immunotherapies (Wu B et al, 2024).

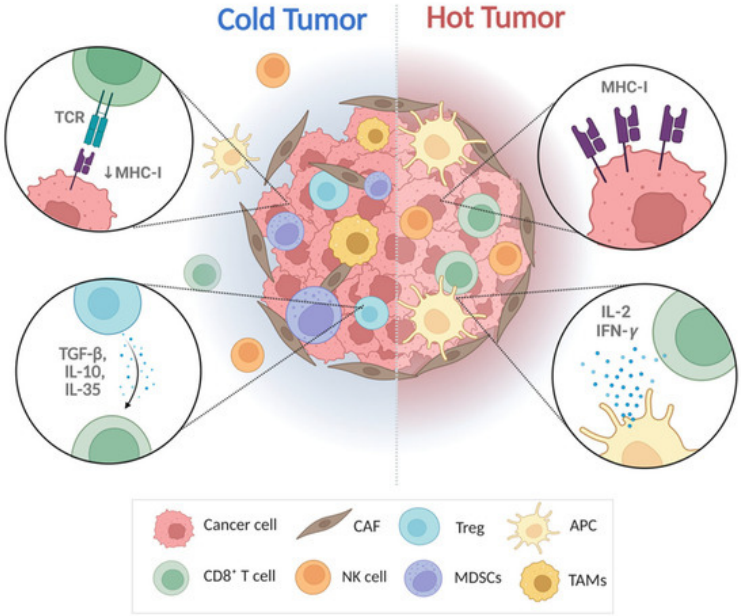

Figure 2. **Differences between "hot" and "cold" TME** from Yoon J et al 2025

Malignant mesothelioma (MM) represents a paradigmatic example in which a chronic inflammatory trigger does not translate into effective antitumor immunity. Asbestos exposure leads to persistent tissue damage and release of damage-associated molecular patterns (DAMPs) such as HMGB1 from mesothelial cells, driving a long-standing inflammatory response that ultimately supports malignant transformation and tumor progression (Suarez JS et al 2023; Cersosimo F et al, 2021; Hiltbrunner S et al, 2021). In this context, the TME is mainly immunosuppressive, enriched of regulatory T cells and myeloid populations –among which immunosuppressive macrophages– that correlate with poor outcome and limited efficacy of ICIs (Chu GJ et al, 2019; Désage AL et al, 2021).

Infiltrating and tissue resident macrophages are one of the most abundant non-malignant cell populations in the TME, playing a central role in tumor immunity (Zhou, D et al, 2021).

1.4.1 Macrophages

During embryogenesis, macrophages (MΦs) are derived from progenitors that start to develop from the primitive ectoderm of the yolk sac, followed by hematopoiesis in fetal liver, giving rise to circulating monocytes. In coincidence with the postnatal formation of bones, fetal liver hematopoiesis is replaced by bone marrow hematopoiesis, which is the source of circulating monocytes, from which derived most resident MΦs in tissues (Wynn TA et al, 2021).

In the context of cancer, MΦs are important innate immune cells that can engulf tumor cells and present tumor antigens for adaptive antitumor immunity and for this reason there is a growing interest in targeting phagocytosis for cancer immunotherapy (Zhou D et al, 2021). Thanks to their plasticity, they can polarize in a broad range of phenotypes depending on the local stimuli (Sica A et al, 2012). Activated macrophages are often classified into M1 (classical-activated MΦs) and M2 (alternative-activated MΦs) phenotypes (Biswas SK et al, 2010). In general, M1-like MΦs foster inflammation responses against invading pathogens and tumor cells, whereas M2-like MΦs tend to exert an immune suppressive phenotype, favoring tissue repair and tumor progression (Lievense LA et al, 2013). In this context, M1 secrete pro-inflammatory cytokines such as IL-12, TNFα, CXCL12 and INF-γ, while M2 release anti-inflammatory signals such as IL-10, IL-13 and IL-4 (Lin Y et al, 2019).

Most TAMs show an M2 phenotype, creating an immunosuppressive environment thus promoting tumor initiation and progression (Mantovani A et al, 2017).

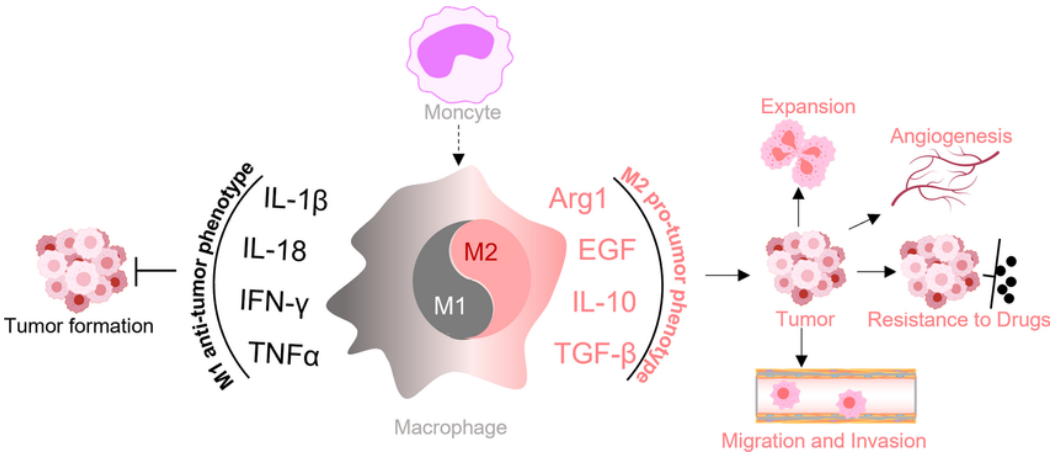

Figure 3. **Macrophage phenotypes in cancer** from Li M et al, 2023.

M1 and M2 represent the opposite ends of a continuum of intermediate phenotypes produced by different stimuli. The M1 pro-inflammatory profile is beneficial for pathogens/tumor elimination but is detrimental for the wound healing process. On the other hand, M2 anti-inflammatory profile improves chronic inflammatory diseases and regeneration (Funes SC et al, 2018).

Among specialized macrophage subsets, CD169+ MΦs have gained considerable attention for their unique role in antitumor immune surveillance. Found mainly in the subcapsular sinus of lymph nodes and in the marginal zone of the spleen, CD169+ (Siglec-1) MΦs specialize in capturing antigens, apoptotic bodies, and tumor-derived vesicles entering lymphatic circulation (Liu Y et al, 2021). Through the retention and transfer of these materials to dendritic cells, CD169+ MΦs form a crucial interface between innate recognition and the initiation of adaptive immune responses, supporting efficient CD8+ T-cell priming (Bernhard CA et al, 2015). Notably, a higher number of CD169+ MΦs within tumor-draining lymph nodes correlate with improved prognosis in several cancers (Asano K et al, 2011; Saito Y et al, 2015). Within the TME, CD169 expression marks MΦs with enhanced phagocytic and antigen-presenting capacities, counterbalancing the predominantly immunosuppressive M2-like TAM compartment. Type I interferons have been shown to induce CD169 expression, further promoting an immunostimulatory phenotype supporting robust antitumor surveillance (Kim, HJ et al 2022). Overall, CD169+ MΦs represent a key immunological niche that links innate capture of tumor-derived material with adaptive immunity.

1.4.2 T cells

Lymphocytes represent another essential immune component within the TME, with CD4+ and CD8+ T cells exerting distinct and complementary functions in antitumor immunity. CD8+ cytotoxic T lymphocytes (CTLs) are the principal effectors of tumor cell killing through the release of cytolytic molecules such as Granzyme B (GrzB) and perforin, as well as the secretion of pro-inflammatory cytokines like IFN-γ, which is cytotoxic and enhances antigen presentation (Zhang N & Bevan MJ, 2011). Their activation status is frequently assessed through expression of markers such as CD44, which is expressed in antigen-experienced or memory phenotypes and correlates with enhanced migratory and effector capabilities (Klement JD et al, 2018). However, within the chronically inflamed and immunosuppressive TME, persistent antigen exposure can drive CTLs toward functional exhaustion, thus impaired cytotoxic activity and upregulation of inhibitory receptors such as PD-1 (Wherry EJ & Kurachi

M, 2015). CD4+ T cells also play a pivotal role by providing essential help to CD8+ T cells, supporting dendritic cell priming, and shaping the cytokine milieu through Th1 polarization and IFN-γ production —features generally associated with improved antitumor responses (Zander R et al, 2019). Nevertheless, CD4+ T-cell subsets can also contribute to immune suppression, particularly in the case of regulatory T cells (Tregs), which dampen effector responses and facilitate tumor immune evasion (Tanaka A & Sakaguchi S, 2017). Altogether, the balance between activated, cytotoxic CD8+ T cells and supportive CD4+ helper T cells versus exhausted or suppressive lymphocyte populations critically influences whether the TME supports tumor eradication or tumor progression, making these subsets key targets for immunotherapeutic strategies.

1.5 High-mobility group box 1 (HMGB1)

HMGB1 is a highly conserved nuclear protein present in all cell types (Yang H et al, 2005). Together with HMGB2 and HMGB3, it is a member of the High Mobility Group Box (HMGB) family of chromosomal proteins with nuclear functions (Müller S et al, 2001). Despite its nuclear localization, HMGB1 has also been detected in the cytoplasm of cells undergoing necrosis (passive release) and in some types of immune cells, such as macrophages, that can also secrete it without dying (active release) (Bianchi ME et al, 2017). When outside the cell, HMGB1 triggers inflammation (Fiuza C et al, 2003) by binding to the Receptor for Advance Glycosylation End products (RAGE) (Hori O et al, 1995), to Toll-Like Receptors 2 and 4 (TLR2 and TLR4) (Park JS et al, 2004) and C-X-C chemokine Receptor type 4 (CXCR4) (Schiraldi M et al, 2012). Extracellular HMGB1 induces the secretion of TNF-α by MΦs and the activation of NF-kB, a key regulator of oncogenesis (Yang H et al, 2010), thus leading to cell proliferation and cell death inhibition.

1.5.1 HMGB1 structure and functions

Proteins belonging to the HMGB family share a highly conserved structure (>80% of amino acid identity): they are composed of two DNA-binding domains, BoxA and BoxB, and a highly negative C-terminal domain, the acidic tail (Yang H et al, 2013).

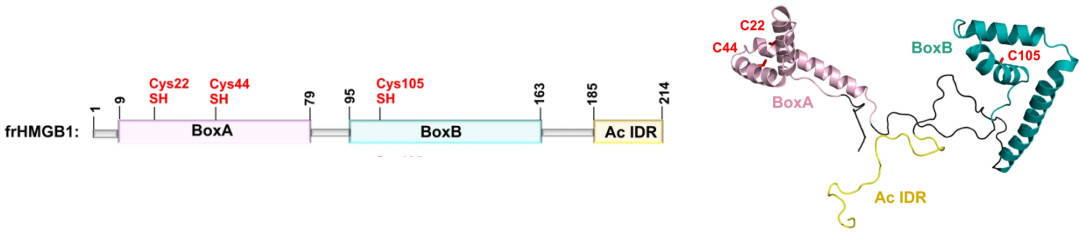

Figure 4. Structure of HMGB1 protein (adapted from Mantonico MV et al, 2024). HMGB1 protein has 215 amino acid residues divided in three domains: A-box, B-box and an acidic C-terminal tail. Three cysteines at positions 22, 44, and 105 are redox-sensitive and they regulate HMGB1 function in response to oxidative stress.

The canonical localization of HMGB1 is in the nucleus, due to the presence of two nuclear localization sequences (NLS) in the box domains. However, in case of damage or if the cell undergoes necrosis, HMGB1 can be released passively into the extracellular space. Moreover, HMGB1 is mobilized towards the cytoplasm when the NLS sequences are hyperacetylated. Thus, HMGB1 accumulates in the secretory lysosomes in the cytoplasm, allowing its active release into the extracellular environment (Lu B et al, 2014).

When HMGB1 is in the nucleus, it binds the minor groove of double-strand DNA causing a local distortion of the helix (Müller S et al, 2001). Therefore, this protein allows the interactions between DNA binding proteins and their cognate sequence, protein-protein interactions, recognition of DNA damage due to mismatch repair and, finally, it is also involved in the formation of nucleoprotein complexes (Agresti A et al, 2003; Yuan F et al, 2004). Thus, nuclear HMGB1 is engaged in many different activities, ranging from DNA stability and repair to transcription and recombination (He, SJ et al, 2017).

In the extracellular context HMGB1 plays a complex role: an infection or tissue damage can cause the release of the protein that acts as a DAMP, working either as a chemoattractant for leukocytes or as a proinflammatory mediator. Extracellular HMGB1 can stimulate the release of many different chemokines, such as TNF-α, IL-10, and IL-6, from both resident immune cells and recruited leukocytes. The redox state of its three cysteines C22, C44, and C105 influences the function of the protein. In particular, the disulfide form of HMGB1 mediates inflammatory activity, whereas the fully reduced form exerts chemoattractant activity (Venereau E et al, 2012).

When HMGB1 is secreted into the extracellular space, it can induce distinct cell activation/differentiation pathways through autocrine, paracrine and endocrine

mechanisms (Rapoport BL et al, 2020). Binding to the Receptor for Advanced Glycation End products (RAGE), HMGB1 axis contributes to numerous disorders from sepsis to cancer, as well as diabetes and neurological disorders (Kang R et al, 2010). Indeed, the inhibition of HMGB1-RAGE axis appears as a promising approach to interfere with the inflammatory activity of HMGB1.

Toll Like Receptors (TLR) are a family of pattern-recognition receptors which have a role in the host immune responses to infection. TLR2, TLR4, and TLR9 have been identified as receptors for HMGB1: in particular, HMGB1-TLR2 interactions were found to activate NK cells (Qiu Y et al, 2014) and cancer stem cells (CSCs) by promoting NF-kB, STAT3 and Smad3 signaling (Conti L et al, 2013): HMGB1-TLR4 signaling is implicated in models of various disorders such as liver and lung damage (Wang Y et al, 2013; Yang H et al, 2013); HMGB1-TLR9 interaction happens via the formation of complexes with other TLR9 ligands, such as short CpG oligodeoxynucleotides (ODNs) or nucleosomes (Ivanov S et al, 2007; Urbonaviciute V et al, 2008).

Notably, fully reduced HMGB1 (fr-HMGB1) forms a complex with CXCL12, which binds to the C-X-C chemokines receptor type 4 (CXCR4) (Schiraldi M et al, 2012).

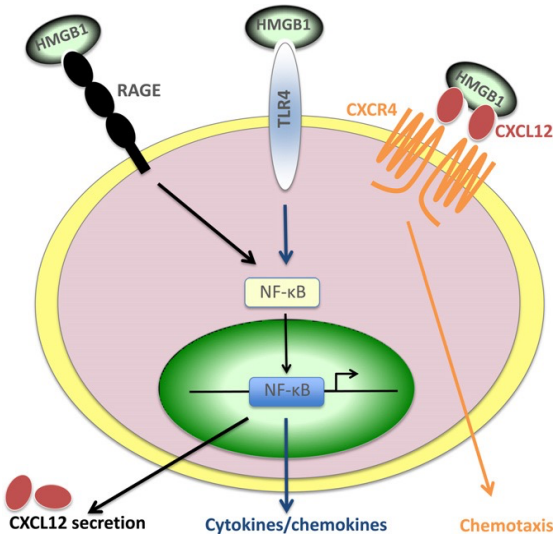

Figure 5. HMGB1 activities upon binding with its receptors (from Venereau E et al, 2013). HMGB1 binds CXCL12 and the heterocomplex activates CXCR4 to induce cell migration. HMGB1 alone binds to RAGE or TLR4, both ligations lead to NF-κB activation and the transcription of cytokines/chemokines genes.

1.5.2 HMGB1 in cancer

In the context of cancer, HMGB1 has been found highly expressed in various solid tumors, such as colon, lung, breast, ovarian, prostate cancers and mesothelioma (Kang R et al, 2013). HMGB1 has a paradoxical behavior: on one hand it supports

cell survival and tumor growth and progression, on the other hand it acts as a tumor suppressor by inducing cell death and regulating autophagy.

Once released by infiltrating leukocytes or by cancer cells themselves, HMGB1 sustains a protumor inflammatory microenvironment, and activates proinflammatory signaling pathways such as the NF-kB (Yang H et al, 2010) and inflammasome pathways, which in turn promote the release of proinflammatory cytokines and accelerate the inflammatory response by creating a positive loop via RAGE and TLR4-mediated signaling (Gebhardt C et al, 2008; Jube S et al, 2012).

Moreover, HMGB1 is involved in tumor energy metabolism: it was found to increase ATP production and cell proliferation in pancreatic tumor cells (Kang R et al, 2014). HMGB1 can also inhibit antitumor immunity by inducing apoptosis in macrophage-derived dendritic cells (Kusume A et al, 2009) or by enhancing tumor associated regulatory T cells to produce IL-10 and suppress CD8+ T cell-dependent response (Liu Z et al, 2011).

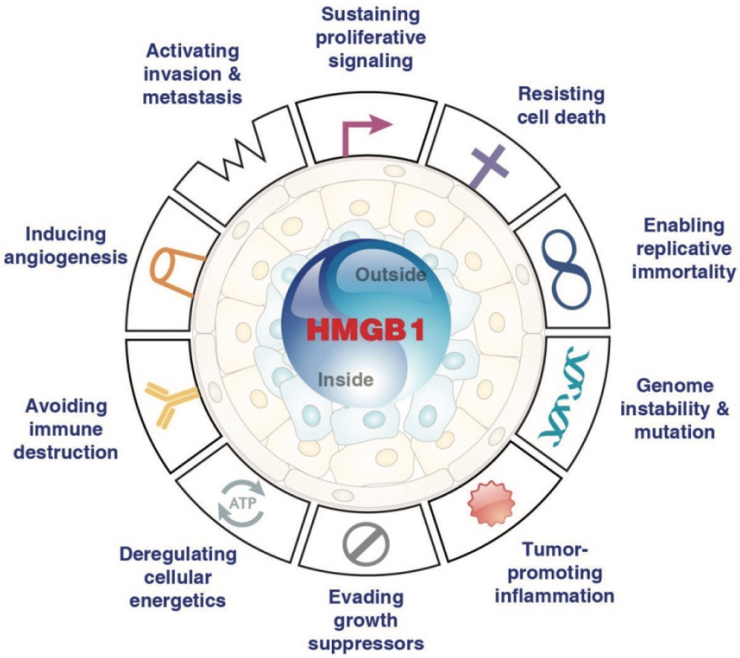

Figure 6. Schematic representation of the role of HMGB1 in cancer (from Guo ZS et al, 2013). HMGB1 is associated with the hallmarks of cancer.

Conversely, intracellular HMGB1 functions as a tumor suppressor by directly binding to Rb through the LXCXE motif, resulting in G1 phase arrest, apoptosis induction and tumorigenesis suppression in breast cancer (Jiao Y et al, 2007). HMGB1 plays an important role in maintaining genome stability (Giavara S et al, 2005):

telomeres are essential for chromosomal stability to protect them from recombination and degradation, and the loss of HMGB1 results in telomere shortening, thus favoring genome instability and tumorigenesis (Polanská E et al, 2012). Moreover, HMGB1 is a critical regulator of autophagy, which is a negative regulator of inflammasome activation by promoting its degradation or decreased ROS production (Tang D et al, 2010); loss of HMGB1 leads to autophagy deficiency that may cause genome instability and inflammation, thus favoring tumorigenesis (Kang R et al, 2013).

HMGB1 is also critical in immunogenic cell death (ICD) of tumor cells. ICD is a process of immunogenic apoptosis, induced by certain chemotherapeutic agents (e.g. mitoxantrone, oxaliplatin) and radiotherapy. ICD is characterized by the release or the surface exposure of damage associated molecular patterns (DAMPs), which help maturation, antigen uptake and presentation of dendritic cells (DC) and serve as powerful immunological adjuvants for the cytotoxic T lymphocytes (CTL) response (Barjij I & Meliani M, 2025). In this context, HMGB1 is released from dying cells and interacts with TLR4, stimulating ICD-associated anticancer immune response upon chemotherapy (Apetoh L et al, 2007).

1.6 CXCL12 and CXCR4

C-X-C Motif Chemokine Ligand 12 (CXCL12), also known as stromal cell-derived factor 1 (SDF-1), is an important chemokine playing a central role in different physiological and pathological processes, such as embryogenesis, hematopoiesis, angiogenesis and inflammation, because it activates and/or induces migration of hematopoietic progenitor and stem cells, endothelial cells and most leukocytes (Janssens R et al, 2018). A single gene located on chromosome 10q11 (Shirozu M et al, 1995), *CXCL12*, encodes for six protein isoforms in human, and three in mouse, all deriving from alternative splicing of the fourth and final exon (Bianchi ME & Mezzapelle R, 2020). The activity of CXCL12 is tightly regulated at many levels: transcription, differential mRNA splicing, posttranslational modifications and protein availability and cooperativity (Janssens R et al, 2018).

CXCL12 is the canonical ligand of C-X-C chemokine receptor type 4 (CXCR4); it can bind to CXCR4 in a monomeric or dimeric form, or in complex with HMGB1 (Bianchi ME & Mezzapelle R, 2020). CXCR4 is a G-protein-coupled receptor made up by an extracellular N-terminal domain, 7 transmembrane helices, 3 extra-cellular loops, 3 intra-cellular loops and an intracellular C-terminal domain (Wu B et al, 2010). The binding of CXCL12 to CXCR4 can drive both cell migration and proliferation by exploiting the same transduction pathways (PI3K-Akt and MEK1/2-Erk1/2).

Of note, the heterocomplex HMGB1•CXCL12 exerts a chemoattractant activity and promotes the recruitment of inflammatory cells via CXCR4 in a more efficient way compared to CXCL12 alone. Importantly, only fr-HMGB1 can form a complex with CXCL12 (Schiraldi M et al, 2012; Fassi EMA et al, 2019; Pirani E et al, 2024).

1.6.1 CXCR4 axis in tumor growth

CXCR4 is the most widely expressed among chemokines receptors, and it is involved in both physiological and pathological conditions. CXCR4 binds different ligands that trigger distinct signaling pathways, and is associated to G protein subunits that, through a conformational change, lead to Ca^{2+} mobilization culminating in activation of the PI3K/Akt and ERK1/2 pathways. Moreover, phosphorylation of CXCR4 intracellular domain of CXCR4 by GRKs can activate the JAK/STAT pathway by recruiting β-arrestins, inducing receptor internalization and desensitization (Bianchi ME & Mezzapelle R, 2020). CXCR4 orchestrates many functions, e.g. cell proliferation, survival, chemotaxis and migration, and also gene transcription.

High expression of CXCR4 is observed in many solid tumors, including melanomas and kidney, lung, brain, prostate, breast, pancreas and ovarian cancers (Zlotnik A, 2006). In the context of cancer, chemokines can coordinate immune cell trafficking and shape the TME immune profile (Bule P et al, 2021). CXCR4 and CXCL12 play an important role in driving leukocytes inside the tumor mass and they intervene in most aspect of tumor cell biology (Morein D et al, 2020). Their expression is controlled and modulated by specific miRNAs and partially depends on the hypoxic tumor microenvironment, in a HIF-1α-dependent manner (Zhu C et al, 2017). The binding of CXCL12 to CXCR4 leads to enhanced tumor cell proliferation, either via MAPK or PI3K/Akt pathways (Thomas RM et al, 2008; Barbero S et al, 2003) both in vitro and in vivo models. CXCR4 is also involved in metastasis formation, and in many types of tumors upregulation of CXCR4 and of its ligand CXCL12 are predictive of short disease-free survival (Guo F et al, 2016).

1.6.2 CXCR4-CD47 in cancer immunotherapy

We recently found that CXCR4 physically interacts with CD47, a transmembrane protein ubiquitously expressed on the membrane of all cells acting as "don't-eat-me" signal, thus inhibiting phagocytosis by binding to its receptor Signal Regulatory Protein α (SIRPα) on MΦs (Barclay AN & Van den Berg TK, 2014). Since the lack of CD47 on the cell surface leads to a quick clearance by MΦs, tumor cells increase the expression of CD47 to avoid phagocytosis; abundant expression of CD47 is associated with poor survival of patients (Liu X et al, 2015).

CD47 blockade by masking antibodies to prevent its interaction with SIRPα has remarkable therapeutic efficacy in various preclinical models of bladder, colon and breast cancer, glioblastoma, lymphoma, and acute lymphocytic leukemia (Jaiswal S et al, 2009; Willingham SB et al, 2012; Liu X et al, 2015). We showed that BoxA, a truncated form of HMGB1 with anti-inflammatory properties (Gong W et al, 2010), mediates the internalization of CD47 and induces macrophage phagocytosis. This allows processing of tumor antigens by innate cells and tumor-specific T-cell priming. We named this mechanism of immunosurveillance "Immunogenic Surrender" (Mezzapelle R et al, 2021).

ImmunoGenic Surrender (IGS) differs from Immunogenic cell death (ICD), which is induced by certain chemotherapeutics or radiotherapy. ICD is characterized by immunogenic apoptosis of tumor cells which follows endoplasmic reticulum (ER) stress and release of DAMPs. IGS does not promote apoptosis, which is functionally replaced by tumor cells phagocytosis via CD47 depletion from the cell surface. CXCL12 –the natural ligand of CXCR4– could also potentially induce IGS; in fact, *in vitro* experiments showed that CD47 expression is reduced on MM cells surface upon CXCL12 administration. On the plasma membrane, the physical interaction between CD47 and CXCR4 decreased following CXCL12 treatment in non-permeabilized cells and increased in permeabilized cells, suggesting the internalization of CD47. Accordingly, CXCL12 increased MM cells phagocytosis by MΦs.

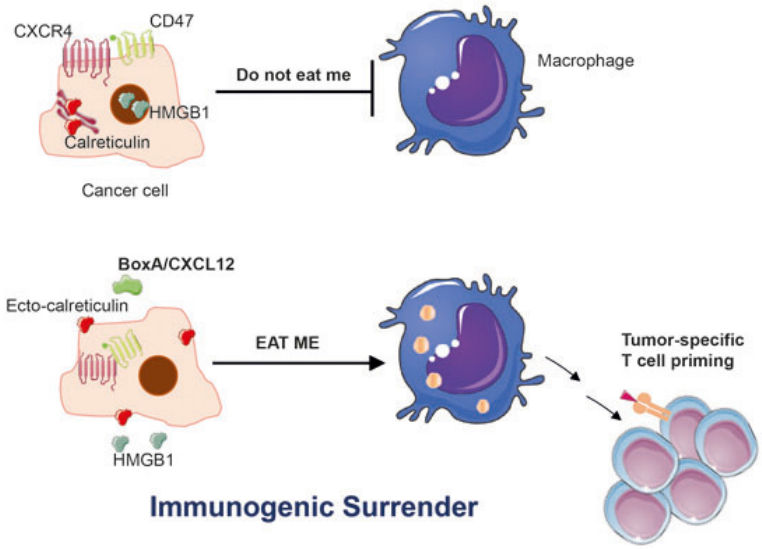

Figure 7 Schematic representation of ImmunoGenic Surrender mechanism (from Mezzapelle R et al, 2021). In the upper cartoon, tumor cell exposes CXCR4 and CD47 on its surface, the latter acting as "don't-eat me" signal; in the lower part, CD47 is internalized and thus tumor cell can be phagocyted by macrophages which can stimulates a T cell response against tumor antigens.

We were thus interested in knowing whether CXCL12 could exert an immunostimulatory activity in vivo and provide protection to mice with mesothelioma.

2. Aim of the work

Malignant mesothelioma (MM) is a very aggressive tumor which arises after a long period of asbestos-induced chronic inflammation, a process in which HMGB1 plays a pivotal role by activating inflammatory pathways through its receptors -among which CXCR4- to support the onset and progression of the disease. The chemokine CXCL12 binds to CXCR4 either alone or as heterocomplex with HMGB1, mediating chemoattraction and immune cell recruitment. In cancer, CXCL12-CXCR4 axis is typically associated with tumor progression and metastasis.

Recent findings from our group unraveled a CXCR4-dependent mechanism of immune surveillance, named ImmunoGenic Surrender (IGS), whereby engagement of CXCR4 by specific ligands, including CXCL12, drives the co-internalization of CXCR4 with CD47 ("don't-eat-me" signal), thus enabling the phagocytosis of some tumor cells by macrophages (MΦs). However, the overall impact of CXCL12 on the tumor microenvironment (TME) remains unclear.

The aim of my thesis was therefore to dissect the role of CXCL12 in MM progression and antitumor immunity, and to determine whether CXCL12 administration could be exploited as a potential therapeutic strategy. To this end, I used a syngeneic mouse model that recapitulates human MM, complemented by *in vitro* assays, and a simpler 3D co-culture system composed by MΦs and MM cells. I did try to: a) assess the effect of CXCL12 treatment *in vivo*, with particular focus on tumor growth, survival, and evidence of immune-mediated tumor control; b) investigate the transcriptional reprogramming elicited by CXCL12 in both MΦs and MM cells using single-cell transcriptomics in a 3D co-culture system; c) characterize the impact of CXCL12 on the immune composition of the TME, focusing on MΦs polarization and T-cell infiltration and activation.

3. Results

3.1 CXCL12 does not affect mesothelioma cell proliferation

It is reported that the chemokine CXCL12 can promote tumor cell proliferation and invasiveness by binding to CXCR4 (Bianchi ME & Mezzapelle R, 2020; Shi Y et al, 2020; Mezzapelle R et al, 2022). However, we have also shown that CXCL12 promotes the internalization of surface CD47 (Mezzapelle R et al, 2021), thus enhancing tumor cell phagocytosis by macrophages when in co-culture with malignant mesothelioma (MM) cells.

We then wondered whether CXCL12 could promote MM cell proliferation, and we tested this hypothesis on the mouse MM cell lines we had available in the lab, representing all mesothelioma histotypes (sarcomatoid, biphasic and epitheliod). I plated 3.5×10^4 cells, either AB1 [sarcomatoid], AB12 [biphasic], AB22 [epithelioid] or AE17 [epithelioid], per well in four 12-well plates. Sixteen hours after seeding I treated cells with increasing concentrations of CXCL12 (0, 1, 10, 100 nM) and I recorded cell confluence every 2 hours using an Incucyte S3. The graph in Figure 8 shows that even the highest dose of CXCL12 (100 nM) does not promote tumor cell growth compared to the untreated condition.

This result shows that CXCL12 does not boost MM cell proliferation, thus encouraging us to test its possible immunomodulatory role *in vivo*.

Figure 8

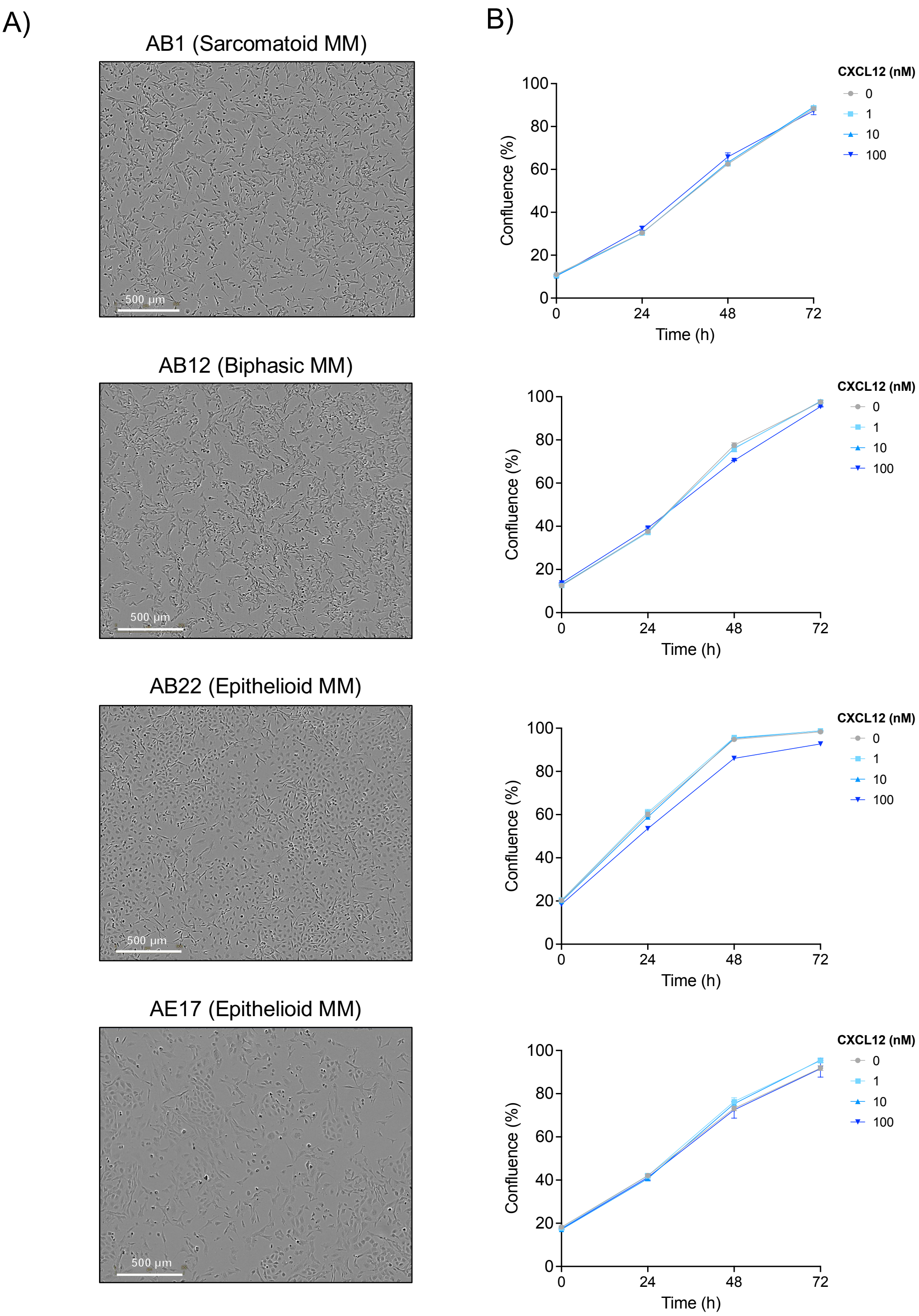

A)
AB1 (Sarcomatoid MM)
500 µm
AB12 (Biphasic MM)
500 µm
AB22 (Epithelioid MM)
500 µm
AE17 (Epithelioid MM)
500 µm
B)
Confluence (%)
Time (h)
0
24
48
72
0
20
40
60
80
100
CXCL12 (nM)
0
1
10
100

>>>

<<<

Figure 8. CXCL12 does not affect MM cell proliferation

A) Representative images of murine MM cell lines in culture. B) $3{,}5\times10^4$ MM cells were seeded in 12-well plates and treated after 16h with increasing concentrations (0-1-10-100 nM) of CXCL12. Cell confluence was recorded every 2 hours by IncuCyte C3, 4x objective. Four different timepoints are displayed in the graphs: 0, 24, 48, 72 hours post treatment administration. Statistical test: Two-way ANOVA, ns. The experiment shown is representative of three performed, in biological triplicate.

3.2 CXCL12 treatment delays tumor growth and extends survival in a syngeneic mouse model of mesothelioma

Since CXCL12 can induce CXCR4 co-internalization with CD47 (don't-eat-me signal) thus promoting tumor cells phagocytosis by macrophages (Mezzapelle R et al, 2021), we asked if *in vivo* it would promote tumor regression by triggering ImmunoGenic Surrender. So, we tested the effect of systemically injected CXCL12 in mice bearing MM. As a preliminary dose-response experiment, thirty-five BALB/c male mice, 8 weeks old, were randomly divided into 5 treatment groups and treated 3 times a week for 10 times:

- 7 control mice receiving 100 µL of PBS, 10 times;
- 7 mice receiving 3 µg CXCL12 per mouse, 10 times;
- 7 mice receiving 10 µg CXCL12 per mouse, 10 times;
- 7 mice receiving 30 µg CXCL12 per mouse, 10 times;
- 7 mice receiving 100 µg CXCL12 per mouse, 10 times.

At day 0 all mice were intraperitoneally (i.p.) injected with 7×10^4 AB1-B/c-Luc cells (herein referred to as MM cells) and engraftment was monitored by BLI. Starting from day 2 after MM cells injection, 100 µL/mouse of PBS (grey bars) for control group and various doses of CXCL12 (violet bars) for treated groups were administered i.p. (Figure 9A). Tumor growth was followed by BLI once a week (yellow arrow).

The BLI curves of control mice (grey lines) showed a rapid MM growth, and all mice were sacrificed by day 28 after tumor injection, while the CXCL12-treated mice (colored lines) developed MM more slowly. The administration of CXCL12 kept tumor growth under control in about half of the mice (in particular at the dose of 10 and 100 µg); however, as soon as we stopped the treatment the tumor re-started its growth (Figure 9B). Survival curves in Figure 9C show that CXCL12 confers a statistically significant survival advantage with respect to the control group, except for the 30 µg dose (3 µg P=0.0266; 10 µg P=0.0161; 30 µg P=0.1573; 100 µg P=0.0235).

Given the beneficial effect observed in the preliminary study, we selected 10 µg and 100 µg as the most effective doses in delaying MM progression, and we increased the number of mice per group:

- 30 control mice receiving 100 µL of PBS, 10 times;
- 12 mice receiving 10 µg CXCL12 per mouse, 10 times;
- 31 mice receiving 100 µg CXCL12 per mouse, 10 times.

We followed the same experimental scheme previously described, and we obtained comparable results. The BLI curves resemble the trend in the preliminary study, i.e. control mice (grey lines) displayed a rapid tumor growth and were sacrificed within day 28 post tumor injection, except for one mouse that rejected MM cells spontaneously, while in the CXCL12-treated groups (light blue and blue lines) we observed a slower MM growth for almost half of the mice (Figure 9D). Survival curves (Figure 9E) confirm that CXCL12 can extend the survival of MM bearing mice compared to the control group receiving PBS.

Figure 9

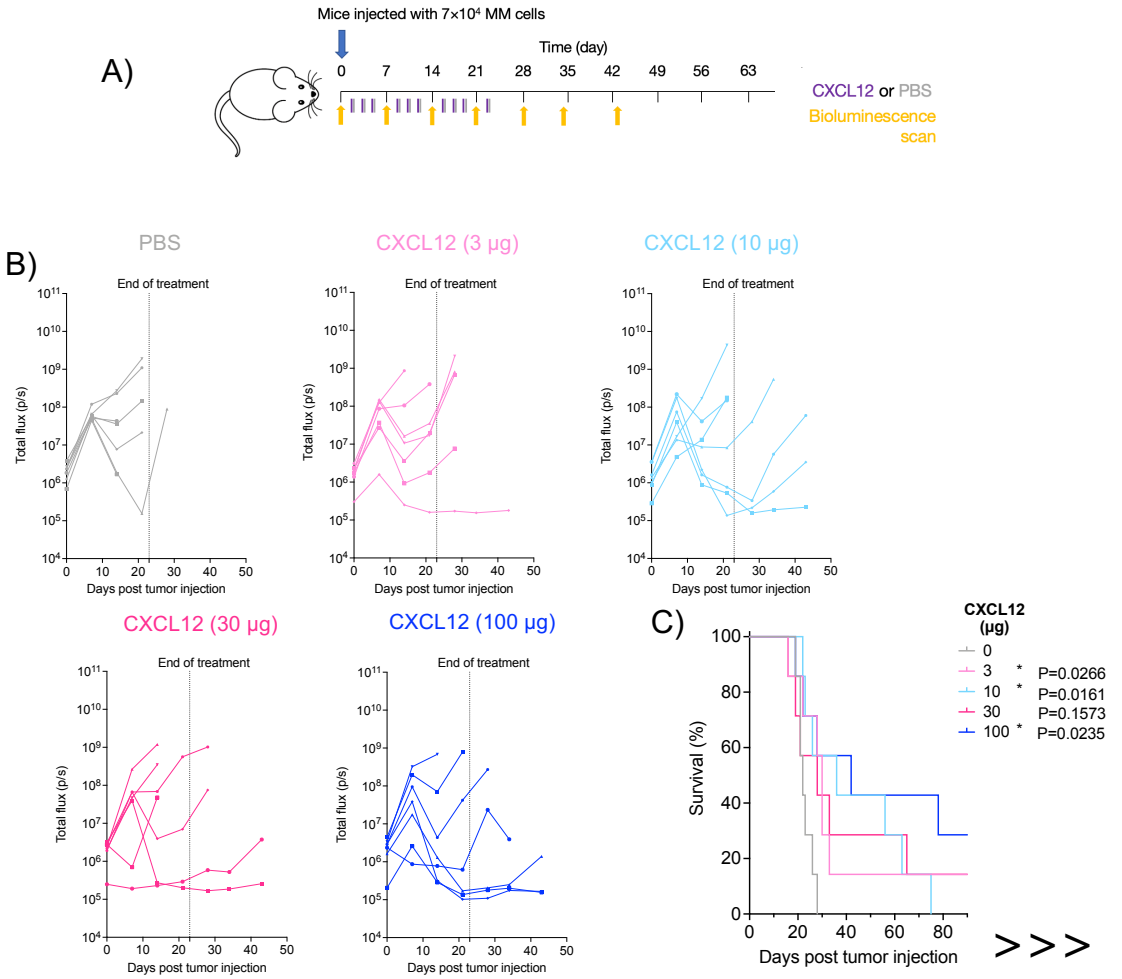

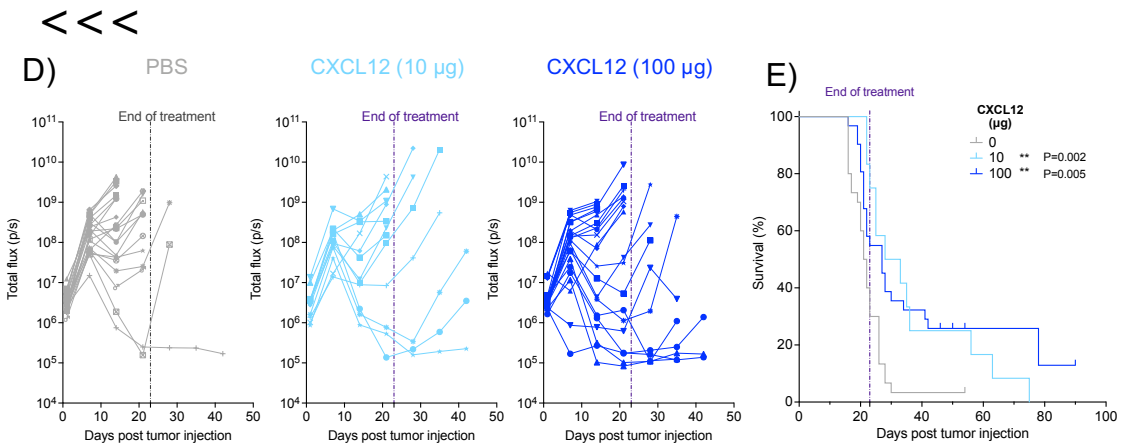

Figure 9. CXCL12 extends the survival of MM bearing mice

A) Scheme of the experiment. BALB/c mice were inoculated i.p. with 7 × 10^4 MM cells and treated with either CXCL12 (violet bars) or PBS (grey bars) three times a week, 10 times in total. Yellow arrows represent BLI imaging. B) Thirty-five mice were inoculated with MM cells and treated with increasing doses with CXCL12. C) Kaplan–Meier survival curves. Statistics: log-rank Gehan–Breslow–Wilcoxon test, p value vs PBS displayed. D) Fifty-four mice were inoculated with MM cells and treated or not with CXCL12. Tumor growth was detected via BLI. Lines that do not reach day 42 correspond to mice that were sacrificed for ethical reasons. E) Kaplan–Meier survival curves. Statistics: log-rank Gehan–Breslow–Wilcoxon test, P = 0.001.

3.3 CXCL12 does not affect the number of macrophages infiltrating the tumor nor their polarization status

Macrophages (MΦs) are myeloid cells which account for a substantial portion of immune infiltrate in biopsies from mesothelioma patients, and the largest fraction is represented by CD206+ M2-like tumor-associated macrophages (TAMs) (Laberiano-Fernandez C et al, 2023).

To test if CXCL12 administration was affecting directly TAMs, we used the syngeneic MM mouse model described in the previous section. At the day of sacrifice, tumor masses were excised from mice (n=3/group) and subsequently processed to formalin-fixed paraffin embedded (FFPE) 4 µm tissue sections. F4/80, CD86 and CD206 immunohistochemical (IHC) stainings were carried out. As shown in Figure 10A, the number of F4/80+ cells (macrophages) was not affected by CXCL12 treatment. Also, the count of CD86+ (representative for M1-like phenotype) and CD206+ (M2-like phenotype) cells was not altered by the treatment. Overall, despite the huge standard deviation present in the PBS-treated group, the ratio M1/M2 macrophages was comparable between the two experimental groups.

I.p. injection of MM cells in BALB/c wild-type immunocompetent mice recapitulates the human tumor (Mezzapelle et al, 2016) but causes a progressive and relatively

fast disease progression in mice receiving PBS; this does not allow us to monitor the control group longer than two weeks. For this reason, to follow the mice for up to three weeks we were forced to revise our model and to change the site of injection, moving from i.p to subcutaneous (s.c.) injection of MM cells. At day 0 all the mice were injected s.c. with 5×10^5 MM cells per flank, leading to an initial tumor burden of 10^6 MM cells/mouse. Starting from day 2 after MM cell injection, either PBS (grey bars) for the control group or 100 μg CXCL12 (violet bars) for the treated group was administered i.p. 3 times a week (Figure 10B). To monitor the effect of CXCL12 treatment on TAMs phenotype over time, mice were sacrificed at preset timepoints: day 7, 14 and 21. Each group of mice (n=7-8/group) was euthanized, necroscopy was performed and tumor masses were collected, enzymatically digested and stained for flow cytometry. The gating strategy was designed to identify MΦs in the tumor mass as single live cells simultaneously positive for CD45, CD11b and F4/80 (Figure 10C). I did not observe any perturbation of the polarization state of TAMs over time, indeed the M1/M2 ratio remained comparable between the two groups. However, there was an increase in the percentage of MΦs infiltrating the tumor in CXCL12-treated mice compared to the untreated ones at day 21.

To evaluate if CXCL12 was directly mobilizing monocytes from the bone marrow niches, we administered CXCL12 and we analyzed the number of circulating monocytes over time: two hours after injecting the chemokine, the number of circulating monocytes in the blood of mice receiving CXCL12 was almost double compared to the PBS-treated mice (Figure 10E).

Figure 10

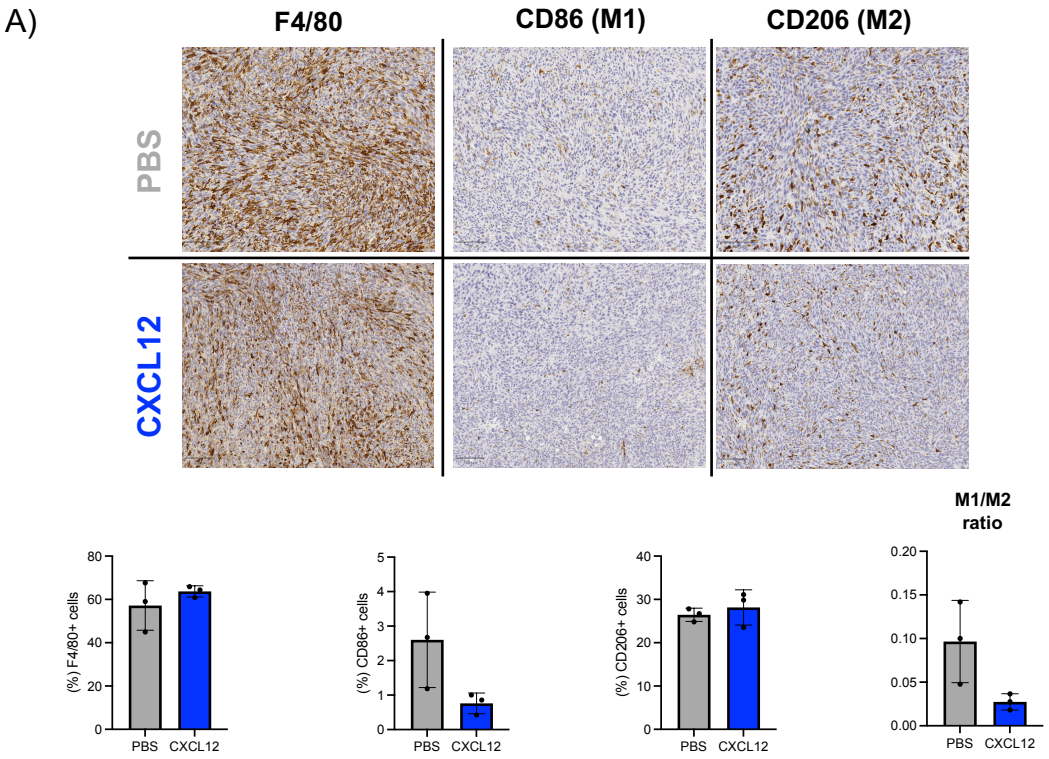
A)
F4/80
CD86 (M1)
CD206 (M2)
PBS
CXCL12
M1/M2 ratio
(%) F4/80+ cells
(%) CD86+ cells
(%) CD206+ cells
PBS
CXCL12
B)
Mice injected s.c. with 10⁶ MM cells
0
7
14
21
Time (day)
CXCL12 or PBS
Euthanasia
C)
FSC-A
SSC-A
FSC-H
singlets
Zombie Aqua
CD45 -Pacific Blue-A
F4/80 - APC-Cy7-A
CD11b - PE-Cy7-A
CD86 - FITC-A
CD206 -Alexa Fluor 647-A
Modal

>>>

<<<

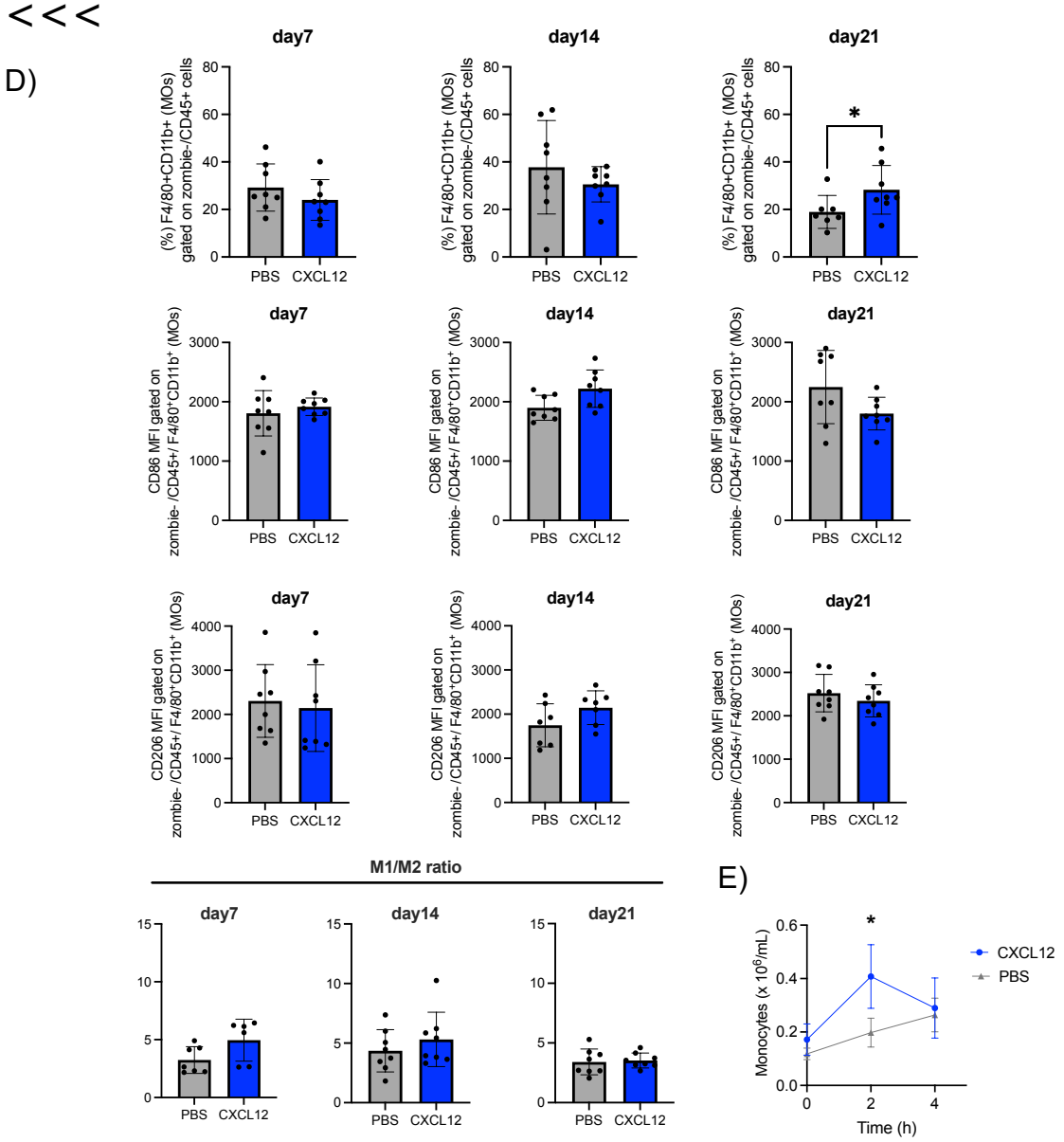

Figure 10. CXCL12 does not affect macrophages infiltration nor polarization but increases the number of circulating monocytes

A) Representative immunohistochemical staining for F4/80, CD86 and CD206 in tumor masses of control (PBS) and CXCL12-treated mice. Scale bar 100 μm. Quantification of F4/80, CD86 and CD206 positive cells via QuPath. B) Scheme of the experiment. C) Representative flow cytometry gating strategy of data present in panel D. D) Analysis of gated tumor infiltrating macrophages by flow cytometry. At day 7, 14 and 21 post engraftment of MM cells, tumor masses were excised from BALB/c mice (n=7-8 mice/group), digested and stained for CD45, CD11b, F4/80, CD86, CD206. Statistics: Mann-Whitney test for MOs (%) and M1/M2 ratio, $P < 0.05$; unpaired t test for CD86 and CD206 MFI, $P < 0.05$. The experiment shown is representative of three performed. E) Kinetics of circulating monocyte numbers in response to a single i.p. injection of 100 μg of CXCL12 (n=5 mice/group per time point; PBS injected in the control group). Statistics: Two-way ANOVA, (*) P=0.02.

3.4 Single cell RNA sequencing characterization of IGS triggers treatment in a 3D co-culture system of MM cells and MΦs

To investigate the effect of IGS triggers, i.e. BoxA and CXCL12, specifically on MΦs and MM cells, I exploited an *in vitro* approach of 3D co-culture system recently set up in the lab. Briefly, it is composed by MM spheroids (herein referred to as mesospheres, since they are MESOthelioma SPHERoids) and primary mouse bone marrow-derived macrophages (BMDMs). Mesospheres are generated from AB1 stably expressing GFP (AB1-GFP) to be tracked and easily distinguishable from MΦs (Figure 11A). I generated mesospheres using ultra-low attachment plates, then after 24 hours -needed for mesosphere formation- I seeded 1 mesosphere/well into a 24-well ultra-low adhesion plate +/- 3×10^4 MΦs/well. For seven consecutive days, I measured the cross-sectional area of mesospheres in the presence or absence of MΦs in three different conditions: untreated, treated with 800 nM BoxA or 100 nM CXCL12. The increase in area of mesospheres alone was comparable among treatments over time, but when MΦs were present in the co-culture, BoxA reduced mesospheres' growth significantly at day 7 of co-culture (Figure 11B).

To elucidate how IGS triggers influence the co-culture system over time, we performed single-cell transcriptomic analysis (Figure 11C). The dataset contains vital and high-quality cells which we identified as tumor cells by the expression of GFP, and MΦs (~5% of total cells) identified by the expression of specific lineage markers such as F4/80 and CD11b (referred to as *Adgre1* and *Itgam,* respectively). Cells in all experimental conditions, regardless of time and treatment, cluster similarly, meaning that neither BoxA nor CXCL12 undergo gross transcriptional alterations in the co-culture system (Figure 11D). We then proceeded with a separate analysis for each population, MM cells and MΦs.

Figure 11

A)

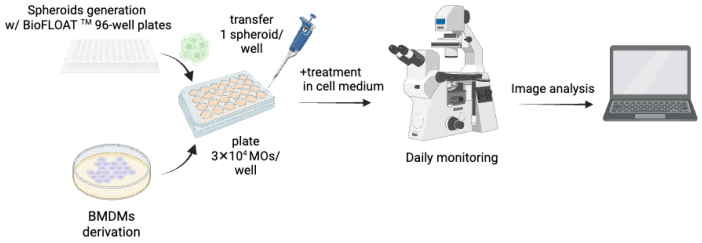

B)

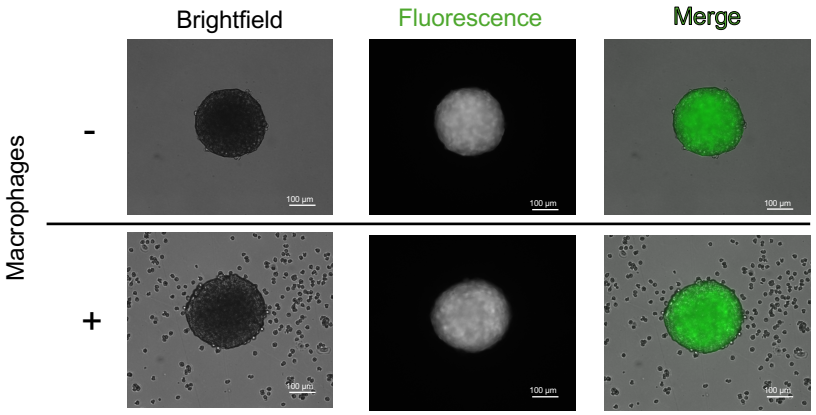

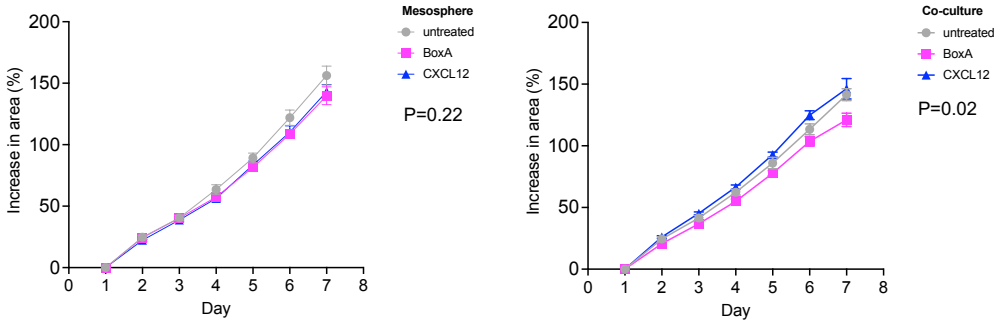

C)

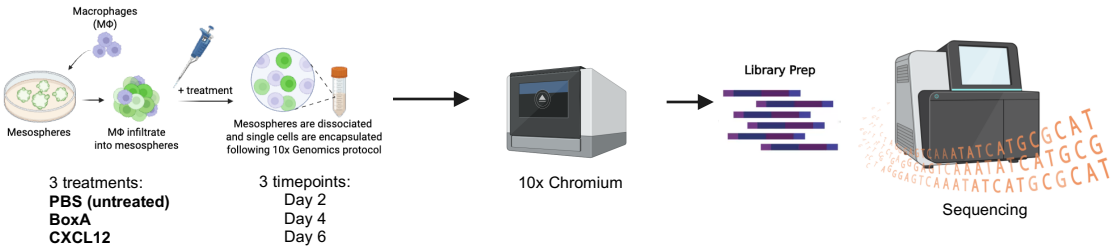

3 treatments:
PBS (untreated)
BoxA
CXCL12

3 timepoints:
Day 2
Day 4
Day 6

>>>

<<<

D)

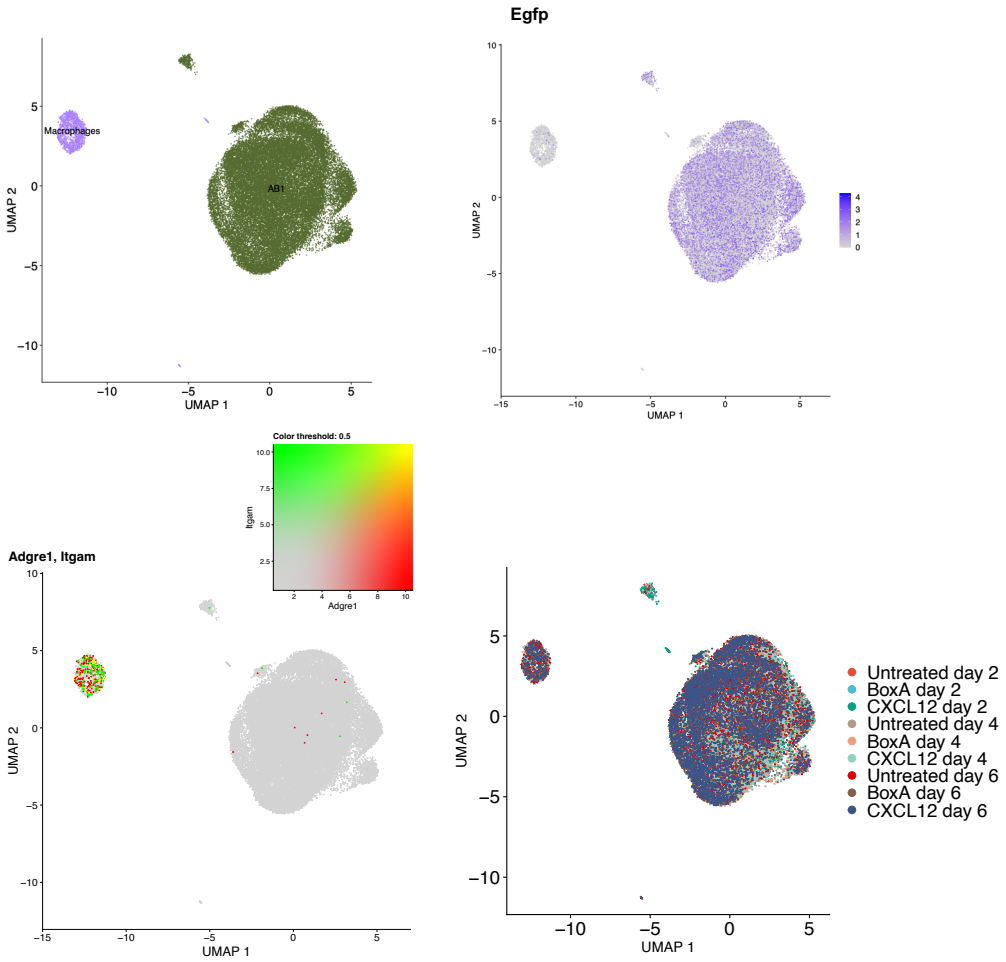

Figure 11. CXCL12 does not affect the growth of mesospheres nor clustering in a 3D co-culture system

A) Scheme of the experiment and representative brightfield and fluorescent images of AB1-GFP spheroids (mesospheres) alone or in co-culture with macrophages. Scale bar = 100 µm. B) Growth curves relative to day 1 of mesosperes alone (left) or in co-culture with macrophages (right) either untreated, BoxA or CXCL12-treated. Images were acquired by Axio microscope and mesosphere area was quantified via ImageJ. Statistics: n=8 spheroids/group, two-way ANOVA. The experiment is representative of three performed. C) Scheme of the scRNAseq experiment. D) UMAP visualization of AB1-GFP and macrophages cell identity and clustering at day 2, day 4 and day 6 of co-culture. Colored UMAP based on *Egfp*, *Adgre* and *Itgam* expression.

3.4.1 MΦs downregulate cellular responses at day 6 of co-culture

To elucidate the direct effect of IGS triggers directly on MΦs, we adopted two parallel and complementary approaches: a Gene Ontology (GO) and a Gene Set Enrichment Analysis (GSEA). Indeed, using a ranked list of all genes based on the

average log2 fold-change and p-value between treated and control conditions, GSEA reveals if the coordinated differential expression and significance of all genes determines the enrichment of specific biological pathways, while GO defines which biological pathways are overrepresented according to only upregulated (average log2fold-change > 1, p-value < 0.01) or downregulated genes (average log2fold-change < -1, p-value < 0.01).

Overall, the two approaches gave concordant and comparable outcomes, but only results of day 6 were statistically significant, whereas day 2 and 4 (not shown) did not return significant terms. As shown in Figure 12A,B on day 6 after CXCL12 administration, MΦs displayed a general negative regulation of cell growth and developmental processes, coupled with a downregulation of specific cellular processes, i.e. engulfment/phagocytosis, chemotaxis and leucocyte-mediated immunity or activation. Similarly, BoxA produced a downregulation of immune system processes such as T cell activation, coupled with reduced chemotaxis and cytokine production from MΦs (Figure 12C,D).

Taken together, these results show a general downregulation of cellular responses of MΦs upon either BoxA or CXCL12 treatment, and this could be due to receptor desensitization and long-term downregulation, which are common features for GPCRs as CXCR4.

Figure 12

A)

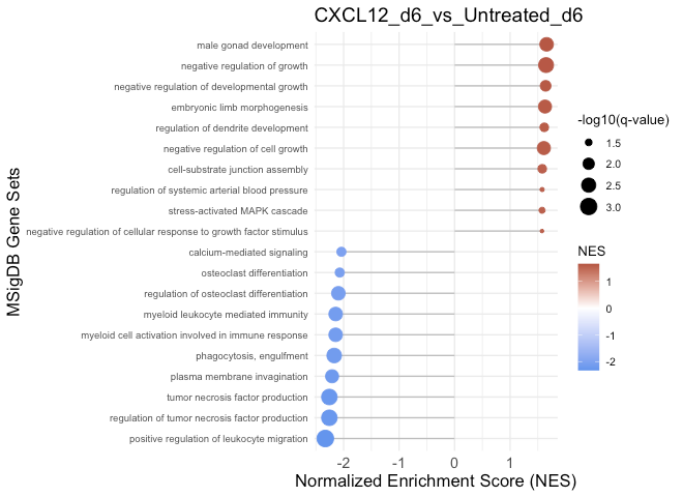

>>>

<<<

B)

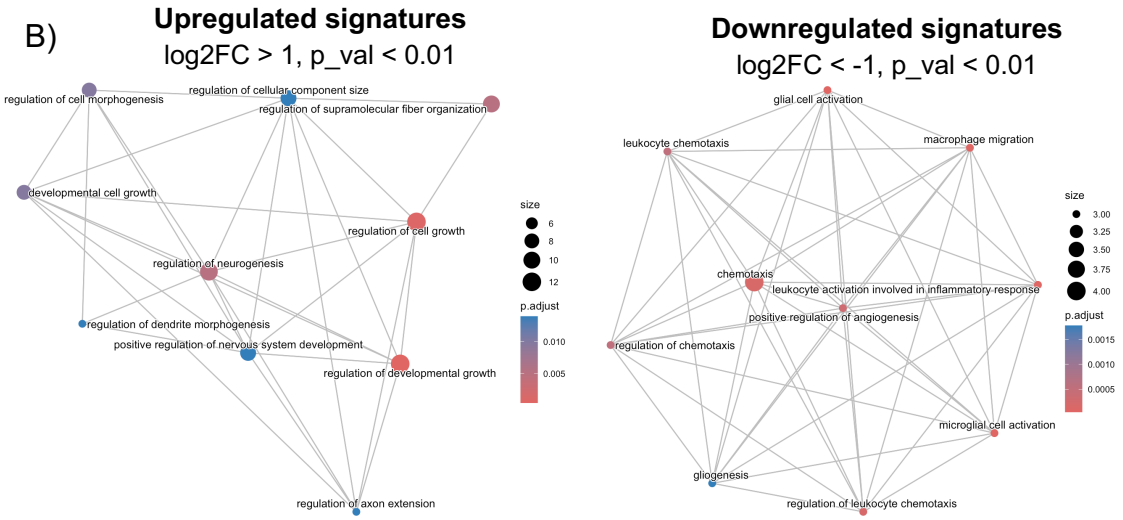
Upregulated signatures
log2FC > 1, p_val < 0.01
regulation of cell morphogenesis
regulation of cellular component size
regulation of supramolecular fiber organization
developmental cell growth
regulation of cell growth
regulation of neurogenesis
regulation of dendrite morphogenesis
positive regulation of nervous system development
regulation of developmental growth
regulation of axon extension
size
6
8
10
12
p.adjust
0.010
0.005
Downregulated signatures
log2FC < -1, p_val < 0.01
glial cell activation
leukocyte chemotaxis
macrophage migration
chemotaxis
leukocyte activation involved in inflammatory response
positive regulation of angiogenesis
regulation of chemotaxis
microglial cell activation
gliogenesis
regulation of leukocyte chemotaxis
size
3.00
3.25
3.50
3.75
4.00
p.adjust
0.0015
0.0010
0.0005

C)


BoxA_d6_vs_Untreated_d6
RNA localization
RNA processing
defense response
positive regulation of immune system process
positive regulation of T cell activation
negative regulation of T cell activation
immune response
regulation of cell activation
cell adhesion
cell chemotaxis
chemotaxis
regulation of cell adhesion
MSigDB Gene Sets
-2
-1
0
1
2
Normalized Enrichment Score (NES)
-log10(q-value)
2
3
4
5
NES
1
0
-1

D)

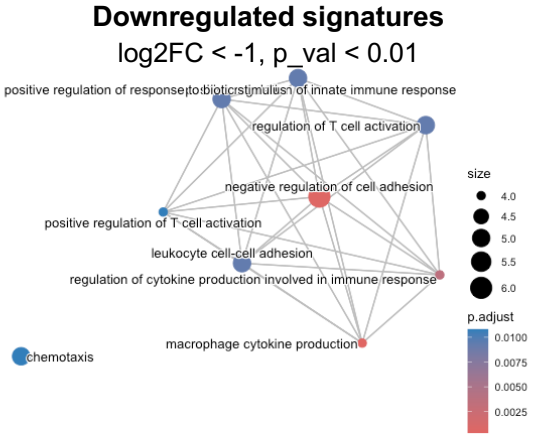
Downregulated signatures
log2FC < -1, p_val < 0.01
positive regulation of response to biotic stimulus
regulation of innate immune response
regulation of T cell activation
negative regulation of cell adhesion
positive regulation of T cell activation
leukocyte cell-cell adhesion
regulation of cytokine production involved in immune response
macrophage cytokine production
chemotaxis
phagocytosis
size
4.0
4.5
5.0
5.5
6.0
p.adjust
0.0100
0.0075
0.0050
0.0025

>>>

<<<

Figure 12. Macrophages display a general downregulation of cellular processes in response to treatments at day 6 of co-culture

A) Dot plot showing the significantly top 10 positively enriched (Normalized Enrichment Score (NES) > 0, q-value < 0.05) and top 10 negatively enriched (Normalized Enrichment Score (NES) < 0, q-value < 0.05) Gene Ontology terms from GSEA analysis for CXCL12 treatment vs untreated condition in macrophage cluster. Dot color gradient indicates positive (red) and negative (blue) NES, as reported in legend ("NES"). Dot size represents the significance as -log10(q-value), as reported in legend (-log10(q-value"). B) Enrichment network plots of overrepresented Gene Ontology biological pathways based on upregulated (left), and downregulated (right) genes for CXCL12 treatment vs untreated condition in macrophage cluster. Dot color gradient indicates the adjusted p-values of significance, as reported in legend ("p.adjust"). Dot size indicates the number of genes that are annotated to the GO term, as reported in legend ("size"). C) Same in A) for BoxA treatment vs untreated condition in macrophage cluster. D) Same in B) for BoxA treatment vs untreated condition in macrophage cluster.

3.4.2 MM cells undergo cellular reprogramming at day 6 of co-culture

MM represented the largest fraction (~95%) of cells in the co-cultures. We identified seven clusters, but none of them corresponded to a specific treatment. Notably, cluster6 was detached from the other ones in the UMAP visualization, and it was mainly composed by cells from day 2 samples, irrespective from treatment (Figure 13A,B). We then used for MM cells the same approach of GSEA and GO -as previously described for MΦ analysis– to investigate the biological pathways affected by either BoxA or CXCL12. Once again, only day 6 gave significant results, whereas day 2 and 4 (not shown) did not point to significant terms.

Following CXCL12 administration, MM cells showed a downregulation of integrin-mediated cell adhesion, proliferation and angiogenesis-related pathways, in addition to connective tissue development, suggesting a general cellular reprogramming toward a less adherent and more plastic de-differentiated status, potentially favoring cell motility. Similarly, BoxA treatment corresponded to several downregulated terms, consistent with a reduction in the development of mesenchymal-derived cell processes (Figure 13C,D). Overall, even if CXCL12 produced a broader effect, both IGS triggers seem to promote a de-differentiation of MM cells, probably to acquire greater cell plasticity, coupled with cellular modifications toward a migratory phenotype due to CXCR4-ligand interaction.

However, this represents only a preliminary result, because we are still working on cluster analysis to assign a signature to each cluster and especially to characterize better cluster6.

Figure 13

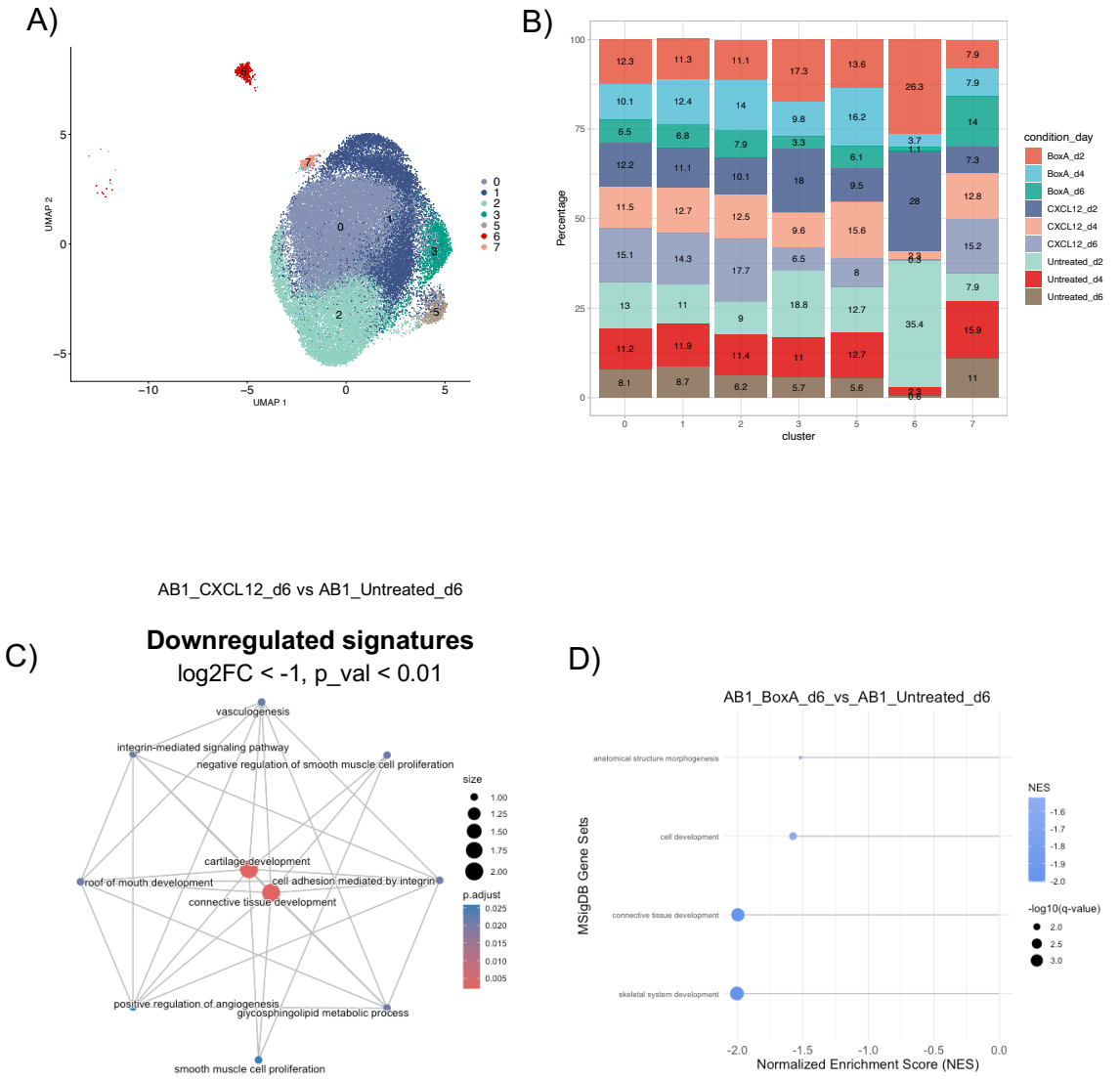

Figure 13. Mesospheres undergo cellular reprogramming at day6 following BoxA/CXCL12 administration

A) UMAP visualization of AB1-GFP clusters at day2, day4 and day6 of co-culture with macrophages (excluded from the graph). Clusters identification numbers are reported and associated at each color as in legend. B) Stacked bar plot representing the proportion ("Percentage", y-axis) of AB1-GFP cell identity per cluster ("cluster", x-axis). Percentage of cells are reported for each condition colored as in legend. C) Enrichment network plot of AB1 cluster at day6 of CXCL12 treatment vs untreated condition. D) Bar graph showing the gene set enrichment analysis (GSEA) of AB1 cluster at day6 of BoxA treatment vs untreated condition.

3.4.3 MΦs which had engulfed tumor cells clustered apart from the others

We performed a parallel analysis – considering only MΦs population and leaving out treatments – to assess if there were some phagocytic events in the 3D co-culture system. As shown in Figure 14A, a fraction of cells belonging cluster1 contained the *Efgp* transcript, belonging to MM cells; thus, these are MΦs which had engulfed tumor cells or fragments thereof. Other than *Efgp*, cluster1 showed typical tumor-associated RNAs such as epithelial structural genes (*Krt18*), growth factor and oncogenic signaling molecules (*Hbegf, Nrg1, Trib2*), extracellular matrix and adhesion components (*Col5a2, Col8a1, Sdc2, Tpm2, Cald1*), developmental regulators (*Bmp2, Inhba, Fstl1*), and cytoskeletal/motility genes (*Arhgap29, Gap43, Dpysl3, Tm4sf1*). Their presence in cluster1, despite being absent from the MΦ transcriptome, provides molecular evidence of completed phagocytosis and allow us to define a "predatory signature" hallmark. Notably, cluster1 is representative of day 2 of co-culture (Figure 14B,C), whereas late timepoints did not have a sizeable number of MΦs expressing *Egfp* or other tumor-associated markers.

Phagocytic MΦs (cluster1) showed a marked reduction in *Sirpa* expression and a concomitant decrease in *Cd47* levels compared to non-phagocytic MΦs (cluster0), consistently across all treatment conditions. In contrast, cluster0 displayed high expression of both transcripts (Figure 14D). These data indicate that MΦs which had phagocytosed tumor cells are characterized by attenuation of the CD47–SIRPα phagocytic axis, suggesting that MΦs which have phagocytosed are supposed to phagocytose a second time.

Differential gene expression analysis between the two clusters (cluster1 vs cluster0) revealed a clear transcriptional landscape associated with phagocytic activity (Figure 14E,F). The volcano plot -encompassing a total of 4,189 genes- shows numerous transcripts significantly differentially expressed ($|\log_2 FC| > 1$, adjusted $p < 0.05$): cluster1, identified as phagocytic, displayed upregulation of genes involved in tissue remodeling and cytoskeletal dynamics (*Aebp1, Cald1, Igfbp6, Fn1, Dkk2, Ghr, Baiap2l1)*; conversely, cluster0 was enriched in genes associated with immune and lysosomal functions (*Fth1, Ctss, Lyz2, Fcer1g, Tyrobp, H2-D1, Clec4d,* and *Ifitm3)*.

To further validate these findings, we performed Gene Ontology (GO) and a Gene Set Enrichment Analysis (GSEA) as described in the previous section. A comparison between cluster0 and cluster1 –non-phagocytic and phagocytic MΦs, respectively– showed for cluster0 an higher expression of antigen processing and presentation, leucocyte activation, cytokine production, together with a general activation of innate

immune response, reflecting a classical innate immune program, typical of active M1 MΦs. In contrast, gene sets enriched in cluster1 exhibited cell-adhesion and collagen biosynthesis-related processes, regulation of receptor internalization, together with connective tissue development, supramolecular fiber organization and TGF-β signaling pathways, mirroring a tissue remodeling phenotype (Figure 14G,H).

Collectively, these results indicate that the major transcriptional differences between the two clusters are driven by macrophage-intrinsic programs: cluster0 MΦs have not yet engaged in tumor cell engulfment and exhibited upregulation of classical innate immune and inflammatory genes (M1-like, classical inflammatory activation), whereas cluster1 MΦs, following phagocytosis, have been reprogrammed toward a remodeling-oriented and tissue repairing phenotype (M2-like, alternative activation).

Figure 14

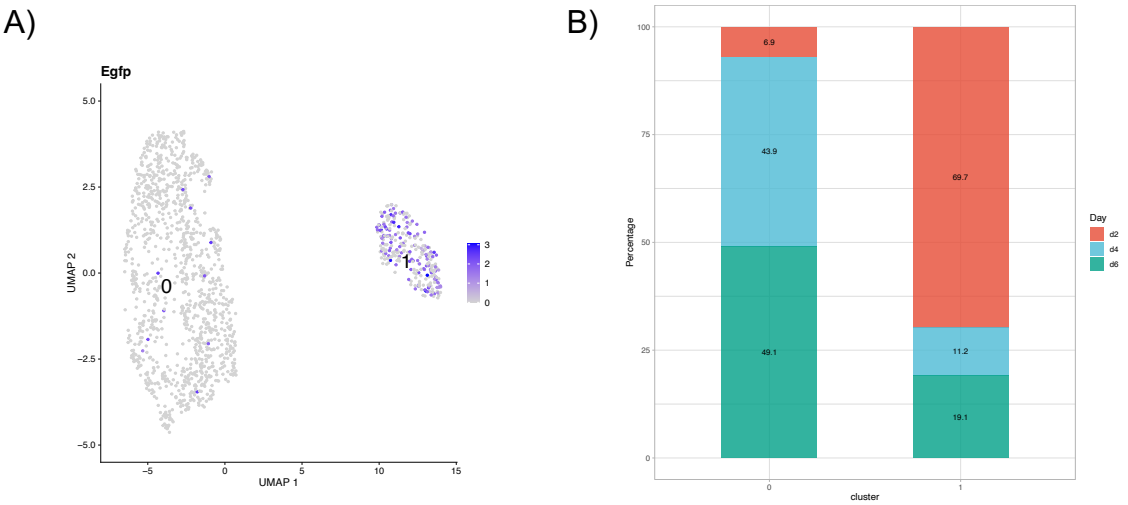

>>>

<<<

C)

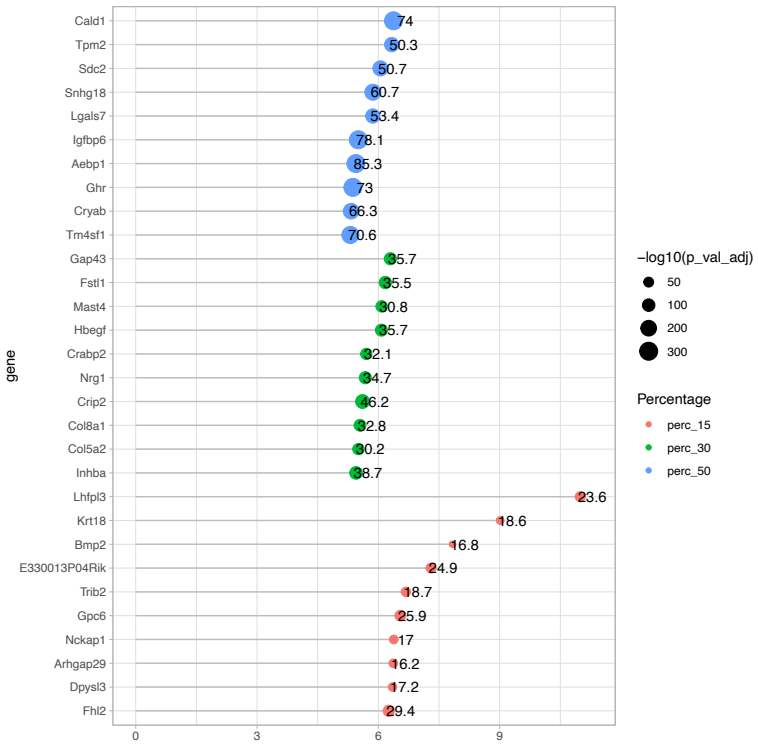
Cald1
Tpm2
Sdc2
Snhg18
Lgals7
Igfbp6
Aebp1
Ghr
Cryab
Tm4sf1
Gap43
Fstl1
Mast4
Hbegf
Crabp2
Nrg1
Crip2
Col8a1
Col5a2
Inhba
Lhfpl3
Krt18
Bmp2
E330013P04Rik
Trib2
Gpc6
Nckap1
Arhgap29
Dpysl3
Fhl2
74
50.3
50.7
60.7
53.4
78.1
85.3
73
66.3
70.6
35.7
35.5
30.8
35.7
32.1
34.7
46.2
32.8
30.2
38.7
23.6
18.6
16.8
24.9
18.7
25.9
17
16.2
17.2
29.4
gene
0
3
6
9
−log10(p_val_adj)
50
100
200
300
Percentage
perc_15
perc_30
perc_50

D)

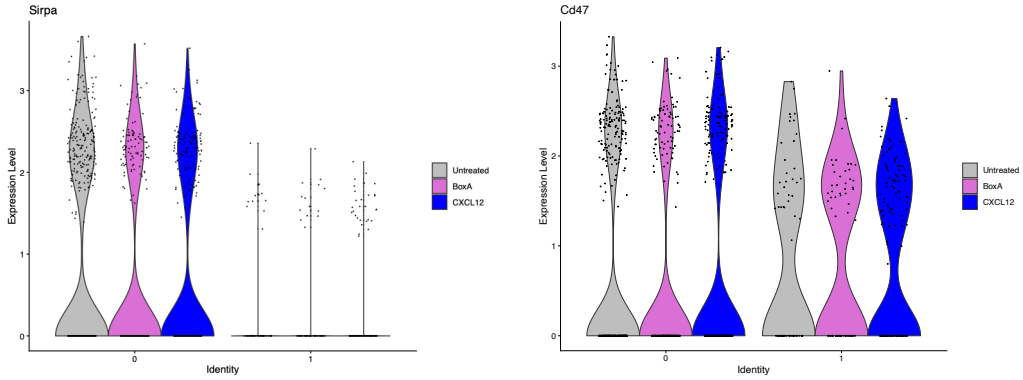
Sirpa
Cd47
Expression Level
Identity
Untreated
BoxA
CXCL12

>>>

<<<

E)

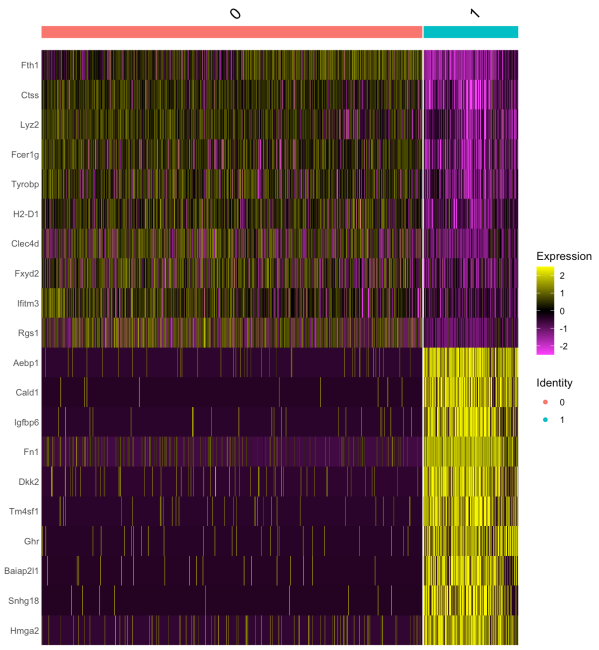
0
1
Fth1
Ctss
Lyz2
Fcer1g
Tyrobp
H2-D1
Clec4d
Fxyd2
Ifitm3
Rgs1
Aebp1
Cald1
Igfbp6
Fn1
Dkk2
Tm4sf1
Ghr
Baiap2l1
Snhg18
Hmga2
Expression
2
1
0
-1
-2
Identity
0
1

F)

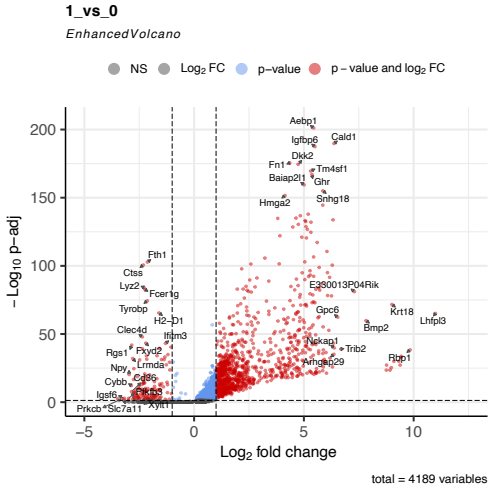
1_vs_0
EnhancedVolcano
NS
Log2 FC
p-value
p - value and log2 FC
−Log10 p−adj
Log2 fold change
total = 4189 variables
Aebp1
Igfbp6
Cald1
Dkk2
Fn1
Tm4sf1
Baiap2l1
Ghr
Hmga2
Snhg18
Fth1
Ctss
Lyz2
Fcer1g
E330013P04Rik
Tyrobp
Gpc6
Krt18
Lhfpl3
H2-D1
Clec4d
Ifitm3
Bmp2
Nckap1
Trib2
Rgs1
Fxyd2
Rbp1
Npy
Lrmda
Cybb
Cd86
Igsf6
Prkcb
Slc7a11

G)


0_vs_1
antigen processing and presentation of exogenous antigen
regulation of leukocyte degranulation
regulation of myeloid leukocyte mediated immunity
granulocyte activation
microglial cell activation
leukocyte degranulation
regulation of superoxide metabolic process
glial cell activation
negative regulation of exocytosis
regulation of leukocyte mediated cytotoxicity
response to estradiol
collagen biosynthetic process
positive regulation of substrate adhesion−dependent cell spreading
positive regulation of focal adhesion assembly
positive regulation of reproductive process
positive regulation of cell−substrate junction organization
regulation of receptor internalization
stress−activated protein kinase signaling cascade
postsynaptic neurotransmitter receptor internalization
postsynaptic endocytosis
MSigDB Gene Sets
Normalized Enrichment Score (NES)
−log10(q−value)
1.5
2.0
2.5
3.0
3.5
4.0
NES
2
1
0
−1

>>>

<<<

H)

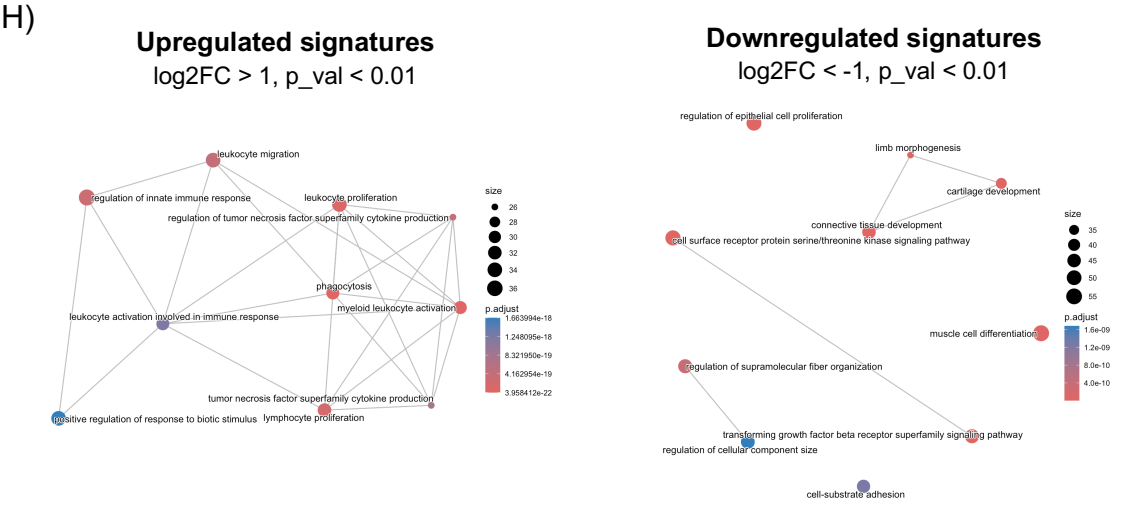

Figure 14. Day2 of co-culture displays the larger number of phagocytosis events

A) Colored UMAP visualization based on Egfp expression in macrophages co-cultured with mesospheres (excluded from the graph) at day2, day4 and day6. B) Stacked bar plot representing the proportion "Percentage", y-axis) of MΦs cell identity per cluster ("cluster", x-axis). Percentage of cells are reported for each condition colored as in legend. C) Lollipop plot of top10 marker genes (y-axis) identified by intersecting positively enriched genes in MM cells vs MΦs and positively enriched genes in MΦs cluster1 (*Egfp*+) vs cluster0 (*Egfp*-), grouped by range of proportions of MM cells expressing each marker ([15-30)%, [30-50]%, [50-100]% dot colors, as in legend). Marker genes are ordered from the highest to the lowest avg_log2fc; labels report the percentage of MM cells expressing each marker, dot sizes the -log10(p-value adjusted). D) Violin plots reporting *Sirpa* (left) and *Cd47* (right) expression levels (y-axis) in MΦs cluster0 and cluster1 grouped by condition (Untreated, BoxA and CXCL12) regardless of the day of treatment. E) Heat map of z-score of expression for the top 10 most significant marker genes for each of the 2 clusters. Each row represents a gene, and each column represents a single cell. Cell colors indicate z-score of expression as indicated in legend. F) Volcano plot of the differentially expression genes (DEGs) between cluster1 and cluster0. Dashed horizontal lines set a q-value < 0.05 threshold, while vertical dashed lines set an |average log2 fold-change| > 1. Red dots indicate DEGs with q-value < 0.05 and |average log2 fold-change| > 1. Blue dots DEGs with q-value < 0.05. Grey dots not significant genes. G) Bar graph showing the enriched gene sets for cluster0. H) Enrichment network plot of upregulated (left) and downregulated (right) signatures in cluster0 vs cluster1 of macrophages.

3.5 CXCL12 promotes CD169 expression on macrophages and favors T cell infiltration and activation in the tumor

Macrophages are professional antigen-presenting cells (APCs) which bridge the innate and adaptive immune system after phagocytosis (Barker RN et al, 2002). Siglec1 receptor (CD169)-positive MΦs have enhanced ability to phagocytose and crosstalk with CD8+ T cells (Grabowska J et al, 2019). CD169+ MΦs within tumors

contribute to tumor-infiltrating lymphocytes (TILs) activation and tumor elimination (Chavez M et al, 2018).

To test if IGS triggers were enhancing the ability of MΦs to present tumor antigen to lymphocytes, I obtained BMDMs and treated them overnight with either 800 nM BoxA or 100 nM CXCL12, then I looked at CD169 surface expression by flow cytometry (Figure 15A). Since CXCL12-treated MΦs displayed higher levels of CD169, I tested the if this upregulation was retained also by MΦs infiltrating the mesospheres upon CXCL12 administration (Figure 15B); the latter result displayed a general increase of surface CD169 over time regardless of the treatment. This could be due to the direct impact on MΦs of MM cells, which represents the largest part in the co-culture. To further validate this hypothesis, I tested the upregulation of CD169+ MΦs in MM tumors *in vivo*, using the experimental model already described in the previous section and depicted as scheme in Figure 15C. MΦs –identified as live single cells simultaneously positive for CD45, CD11b and F4/80– showed higher levels of CD169 expression in the CXCL12-treated group at day 14 post MM cells injection, whilst there was no variation in the earliest (day 7) and the latest (day 21) timepoints.

The previous results encouraged us to investigate if also the T cell compartment was affected directly by the CXCL12 treatment, since it is reported that, upon activation, CXCR4 and the TCR/CD3 complex interact and signal through each other, resulting in T cell proliferation and chemotaxis (Patrussi L et al, 2007; Wu CY et al, 2017; Mezzapelle R et al, 2022). TILs were characterized over time by flow cytometry analysis, and they were identified as live single cells simultaneously positive for CD45 and CD3, and positive or negative for CD8, as shown in Figure 15D. The first two timepoints (day 7 and 14, not shown) did not show any difference among treatments in the T cell count. At day 21, in tumor masses excised from mice receiving CXCL12, there was an increase in the percentage of TILs, which was significant for CD4+ T cells, whilst it was only moderately augmented for CD8+ T cells (Figure 15E). Simultaneously, I analyzed the expression of activation and effector markers such as interferon gamma (IFNγ), granzyme B (GrzB), CD44, and the exhaustion marker Programmed Death 1 (PD-1). As shown in Figure 15F, CXCL12 treatment increased the production of IFNγ by CD8+ T cells starting from day 7, and this trend was partially kept till day 21, when also GrzB levels were higher in the treated group compared to the untreated group (receiving PBS). In contrast, we did not observe any variation in CD44 nor PD-1 expression in TILs over time or among treatments. Taken together, these results support the notion that CXCL12 modulates the tumor microenvironment (TME), favoring an immune active context via modulating both

innate (i.e. increasing CD169+ MΦs) and adaptive (i.e. increasing the number and the activation of TILs) immune cells, with a beneficial effect for MM-bearing mice.

Figure 15

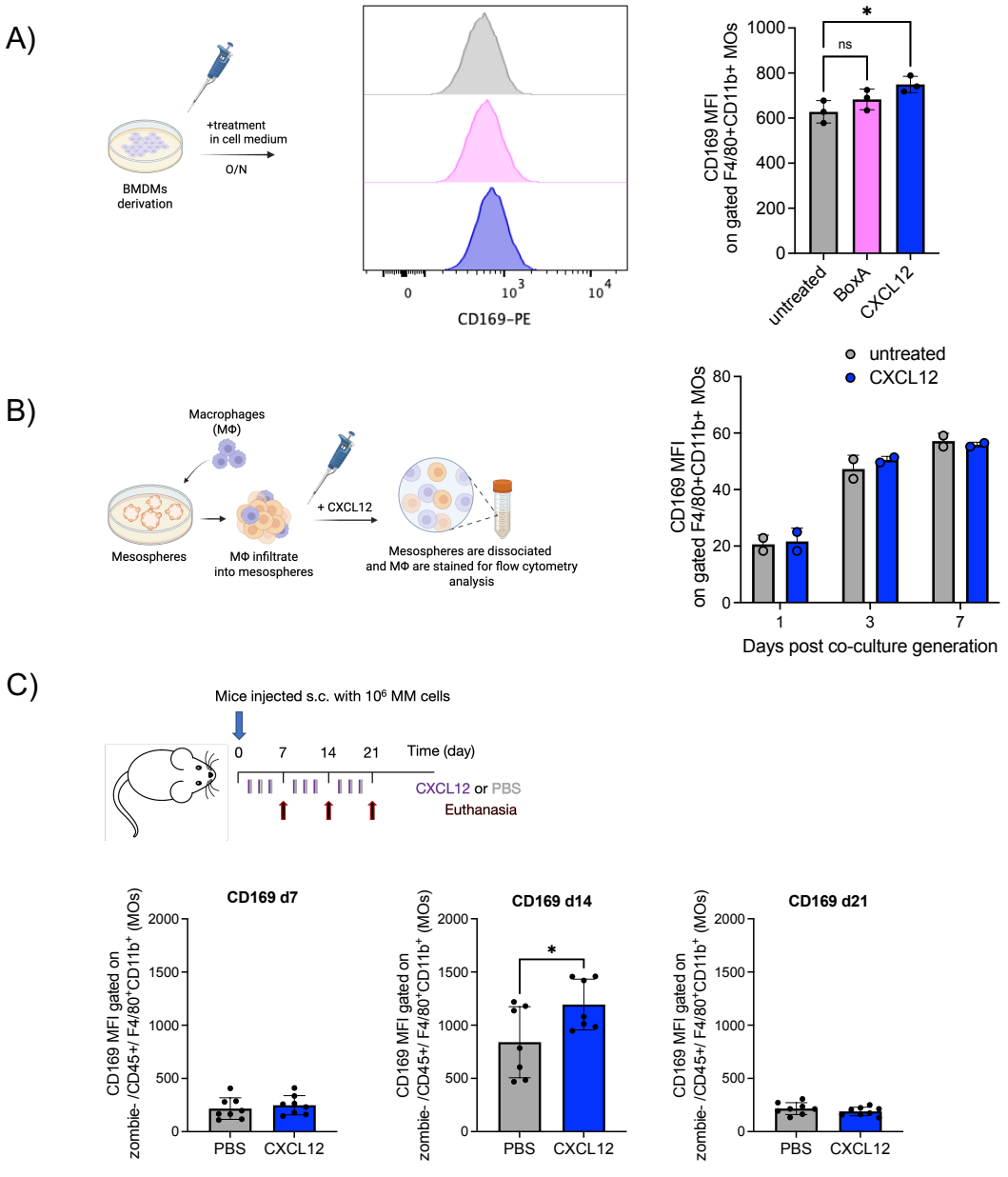

>>>

D)

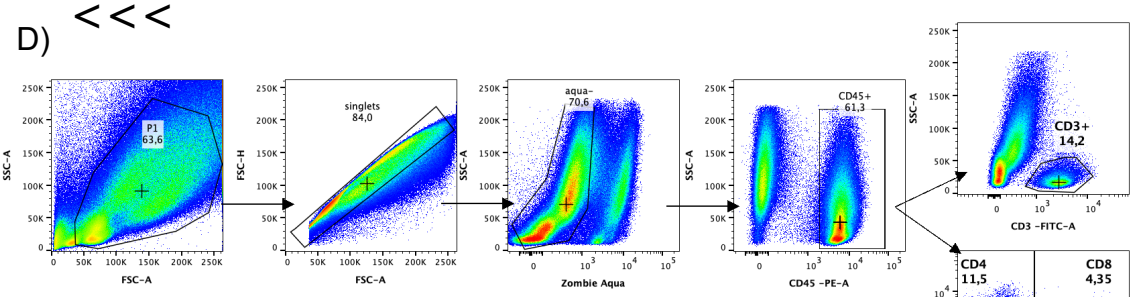
P1
63,6
FSC-A
SSC-A
singlets
84,0
FSC-H
aqua-
70,6
Zombie Aqua
CD45+
61,3
CD45 -PE-A
CD3+
14,2
CD3 -FITC-A
CD4
11,5
CD8
4,35
Q4
83,8
Q3
0,34
CD8 - PerCP-Cy5.5-A

E)

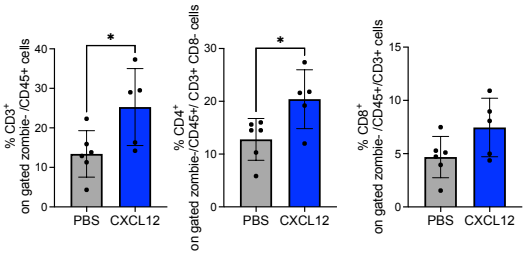
% CD3+ on gated zombie-/CD45+ cells
% CD4+ on gated zombie-/CD45+/ CD3+ CD8- cells
% CD8+ on gated zombie-/CD45+/CD3+ cells
PBS
CXCL12

F)

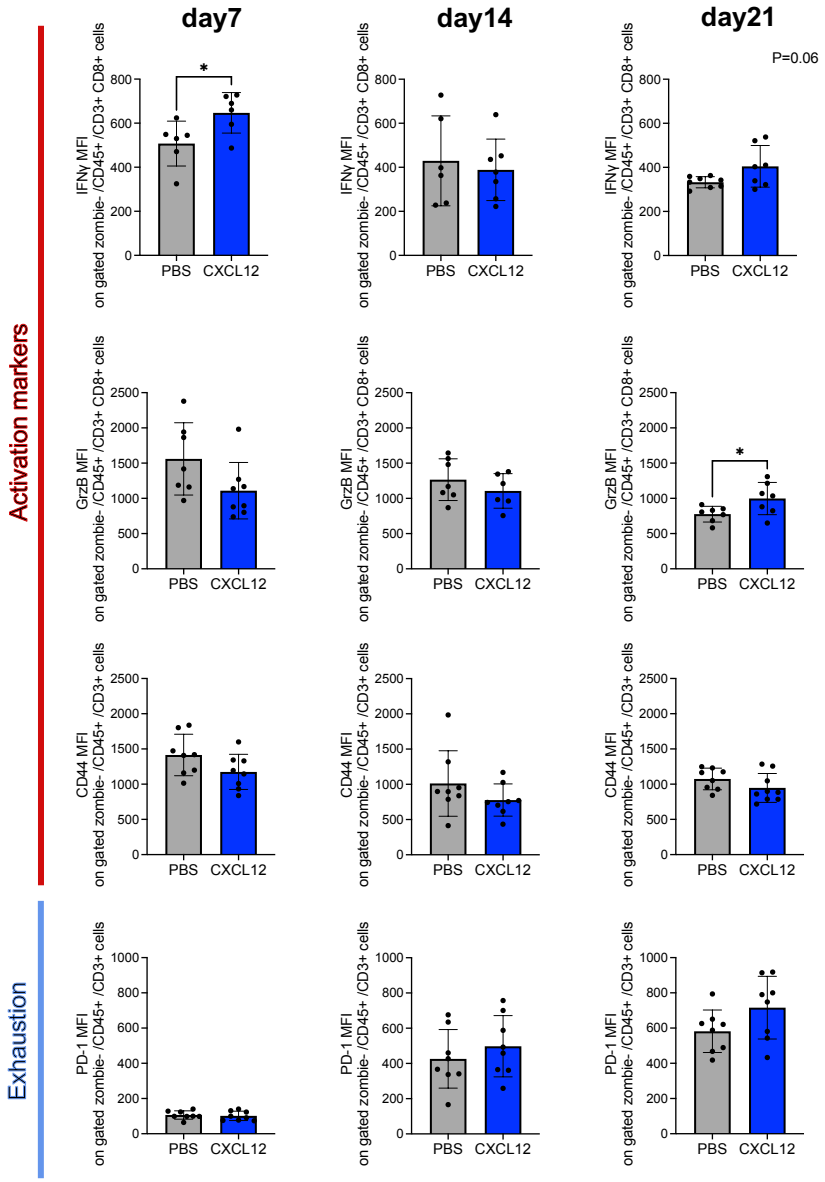
day7
day14
day21
P=0.06
Activation markers
Exhaustion
IFNγ MFI on gated zombie-/CD45+ /CD3+ CD8+ cells
GrzB MFI on gated zombie-/CD45+ /CD3+ CD8+ cells
CD44 MFI on gated zombie-/CD45+ /CD3+ cells
PD-1 MFI on gated zombie-/CD45+ /CD3+ cells
PBS
CXCL12

<<<

Figure 15. CXCL12 favors CD169 expression on macrophages and promotes T cell infiltration and activation in the tumor

A) Scheme of the experiment and surface expression of CD169 on bone marrow-derived macrophages (BMDMs) either untreated (grey) or treated with 800 nM BoxA (pink) or 100 nM CXCL12 (blue). Statistics: One-way ANOVA plus Dunnett's post-test, * P < 0.05. The experiment is representative of three performed in biological triplicate. B) Scheme of the experiment and surface expression of CD169 on macrophages (MΦ) infiltrating the mesospheres either untreated (grey) or treated 100 nM CXCL12 (blue), at day 1, day 3 and day 7 post-co-culture generation. Statistics: unpaired t test, ns. C) Analysis of gated tumor infiltrating macrophages by flow cytometry. At day 7, 14 and 21 post engraftment of MM cells, tumor masses were excised from BALB/c mice (n=7-8 mice/group), digested and stained for CD45, CD11b, F4/80, CD169. Statistics: unpaired t test, *P < 0.05. D) Representative flow cytometry gating strategy for tumor infiltrating lymphocytes (TILs). E) Analysis of gated TILs at day 21 post engraftment of MM cells; tumor masses were excised from BALB/c mice (n=5-6 mice/group), digested and stained for CD45, CD3, CD8. Statistics: Mann-Whitney test, *P < 0.05. F) Analysis for activation (IFNγ, GrzB on CD8+; CD44 on CD3+) and exhaustion (PD-1 on CD3+) on TILs at day7, day14 and day21 post engraftment of MM cells. Statistics: unpaired t test, *P < 0.05.

3.6 CXCL12 requires both CD4+ and CD8+ T cell populations to exert its effect on mesothelioma bearing mice

Given that, upon CXCL12 treatment, we observed a larger number of CD4+ T cells and a major activation of CD8+ T cells in tumor masses, we wanted to discriminate which of the two populations was responsible for extending the survival of MM-bearing mice. To answer this question, we selectively depleted either CD8+ or CD4+ T cells *in vivo* via i.p. injection of 100 µg depleting antibody (5 doses) starting three days prior to MM cells injection. Fifty-seven BALB/c male mice, 8 weeks old, were divided into 7 experimental groups and treated 3 times a week for 10 times:

- 11 control mice (receiving 100 µL of PBS, 10 times);
- 9 CXCL12-treated mice (receiving 100 µg CXCL12 per mouse, 10 times);
- 8 CXCL12-treated mice (receiving 100 µg CXCL12 per mouse, 10 times); depleted for CD4+ T cells;
- 8 CXCL12-treated mice (receiving 100 µg CXCL12 per mouse, 10 times); depleted for CD8+ T cells;
- 8 PBS-treated mice (receiving 100 µL of PBS per mouse, 10 times); depleted for CD4+ T cells;
- 8 PBS-treated mice (receiving 100 µL of PBS per mouse, 10 times); depleted for CD8+ T cells;
- 5 PBS-treated mice (receiving 100 µL of PBS per mouse, 10 times); injected with IgG control for the depletion antibodies.

At day 0 all mice were i.p. injected with with 7×10^4 MM cells and engraftment was assessed by BLI. Starting from day 2 after MM cells injection, 100 µL/mouse of PBS (grey bars) or CXCL12 (violet bars) were administered i.p. 3 times a week for 10 times (Figure 16A). To assess that T depletion was effective, I performed flow cytometry analysis to look at CD4+ and CD8+ cells circulating in peripheral blood: depletion was complete for populations (Figure 16B). Tumor growth was supposed to be followed by BLI scan, but unfortunately the institutional instrument (IVIS SpectrumCT) went out of order the day after we performed the first scan, and it was not fixed in time to be used for the experiment.

Survival curves showed that CXCL12 confers a statistically significant survival advantage with respect to the control group (P=0.04), whereas both CD4 and CD8-depleted groups, irrespective from additional CXCL12 treatment, survived less or were sacrificed for severe illness with respect to the control group (Figure 16C,D,E). Furthermore, between the two depleted groups receiving CXCL12, there was a statistically significant difference in the survival curves, highlighting a more prominent role for CD8+ T cells compared to CD4+ in mediating an effective anti-tumor immune response.

Overall, even lacking tumor growth curves, this experiment was informative and showed that both CD4+ and CD8+ cells are required to extend the survival upon treatment with CXCL12.

Figure 16

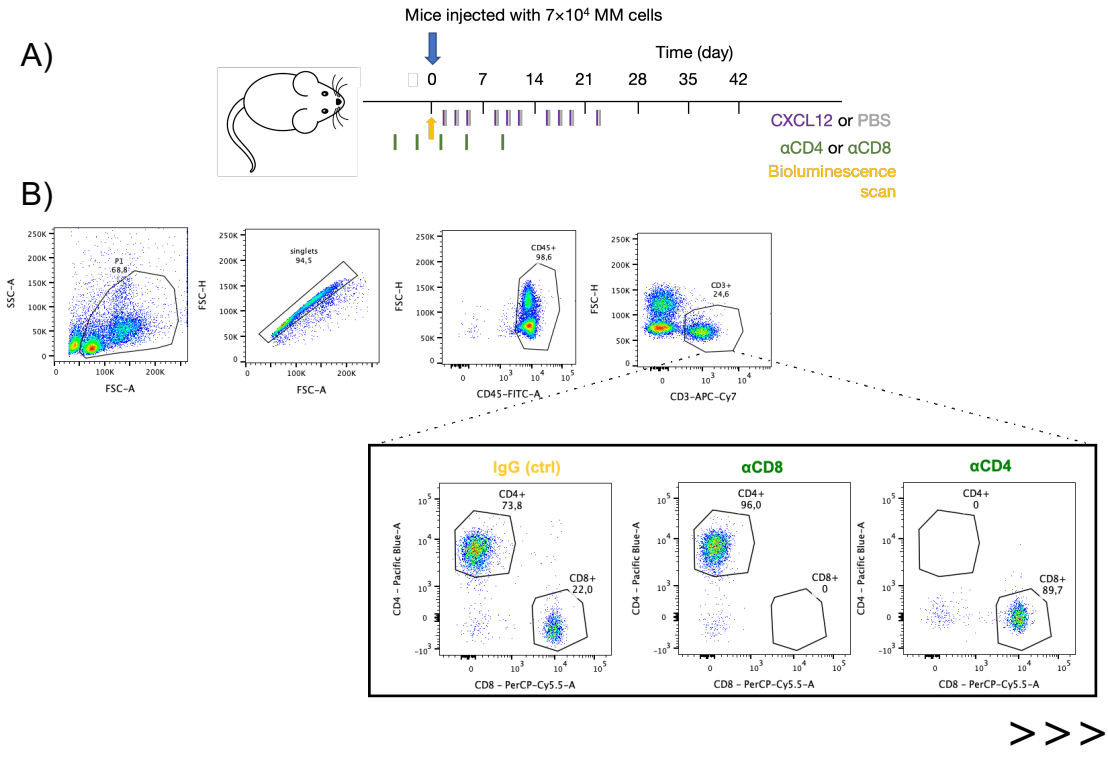

>>>

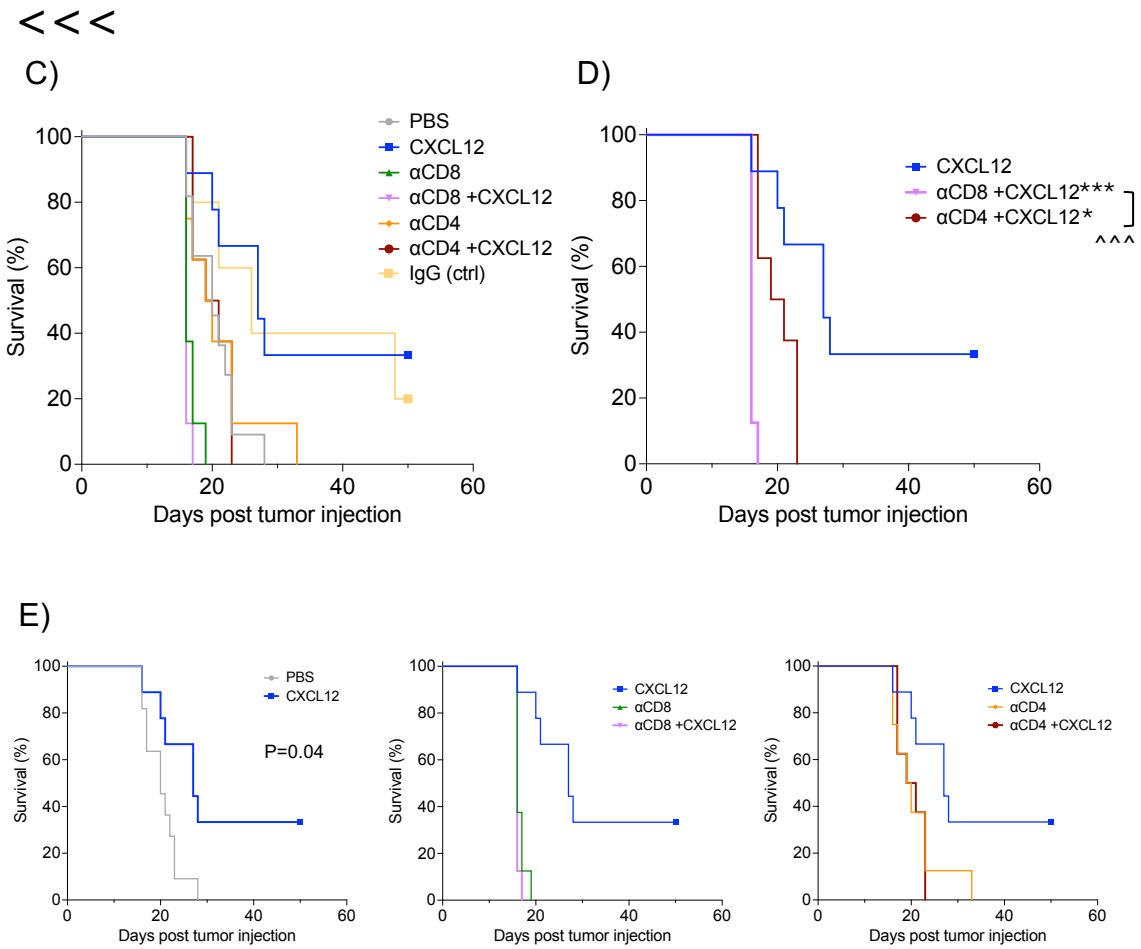

Figure 16. CXCL12 requires both CD4+ and CD8+ T cell populations to impact on survival of MM bearing mice

A) Scheme of the experiment. BALB/c mice were depleted either of CD8+ or CD4+ T cells, inoculated i.p. with MM cells and treated with PBS or 100 µg CXCL12 as previously described. B) Representative flow cytometry gating strategy to assess T cell depletion in peripheral blood. C, D, E) Kaplan–Meier survival curves. Statistics: log-rank Gehan–Breslow–Wilcoxon test, p value vs CXCL12 displayed (*) P<0.05, (***) P<0.001; p-value among depleted groups (^^^) P<0.001.

3.7 Some CXCL12-treated mice survived longer and rejected MM cells twice

We have shown in Figure 9 that CXCL12-treated mice survived longer compared to the untreated group, and a fraction of mice rejected the tumor at the end of treatment. To test if those mice were immunized against MM cells, at day 75 we re-challenged them with 7×10^4 MM cells and followed tumor growth via BLI (Figure 17A). For three mice out of four, the BLI signal goes back to basal level in two weeks, meaning they rejected MM for a second time (Figure 17B), thus suggesting they were immunized against tumor cells. We then wanted to repeat the rechallenge of MM cells

in a second cohort of surviving mice, but we were forced to change the route of injection of MM cells from i.p. to s.c. –to follow tumor growth– due to IVIS SpectrumCT unavailability. As shown in Figure 17C, all the naïve mice (n=4) –which were never injected with MM cells before– developed a tumor mass and were sacrificed within day25 post tumor injection. In the CXCL12-treated group we observed heterogeneity in tumor development: a mouse (#0) was found without any appreciable tumor, a second one (#1) had a very small tumor mass, and a third one (#2) had a visible tumor, comparable with tumor masses excised from the naïve group. At sacrifice, I tested the expression of MHC-I, as it is reported to be downregulated in several tumors to evade immune system recognition; in fact, MHC-I expression was low in naïve mice (#3, #4) and in even lower in mouse #2 which developed the biggest tumor mass among the CXCL12-treated mice. In contrast, the other mouse (#1) – which had received CXCL12 but developed a small tumor mass – displayed the highest expression of MHC-I (Figure 17D). Even if the number of mice was limited, this small experiment showed that CXCL12 promoted effective tumor immunization in a large fraction of mice and, in the case where it didn't, it was most likely due to a mechanism of tumor immune evasion rather than a lack of immunological memory.

Figure 17

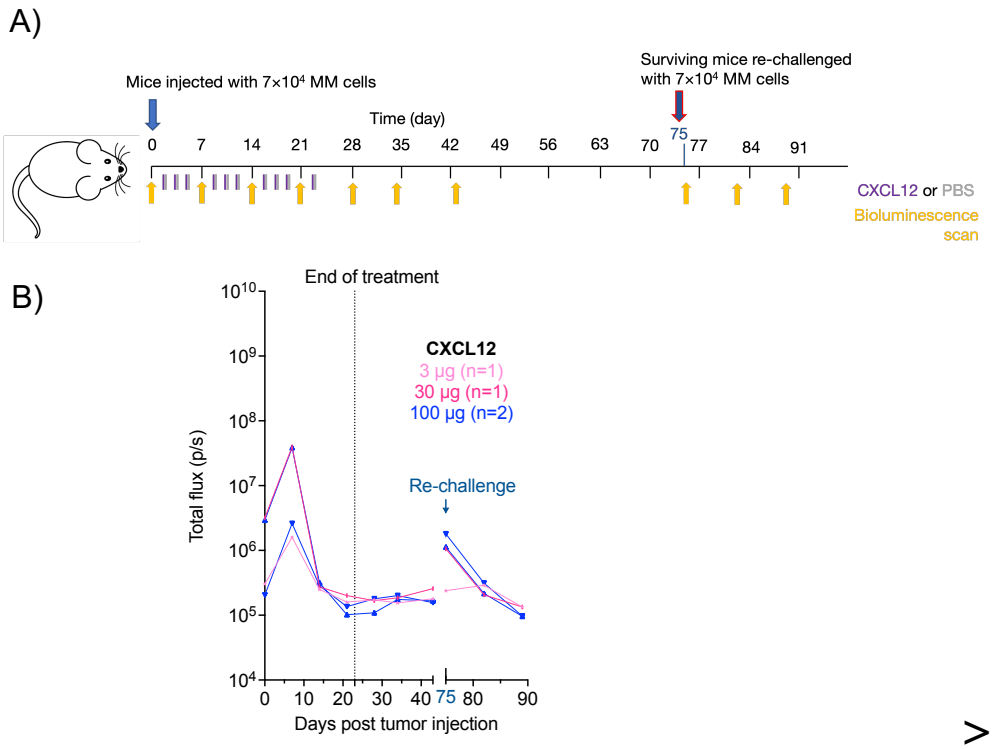

>>>

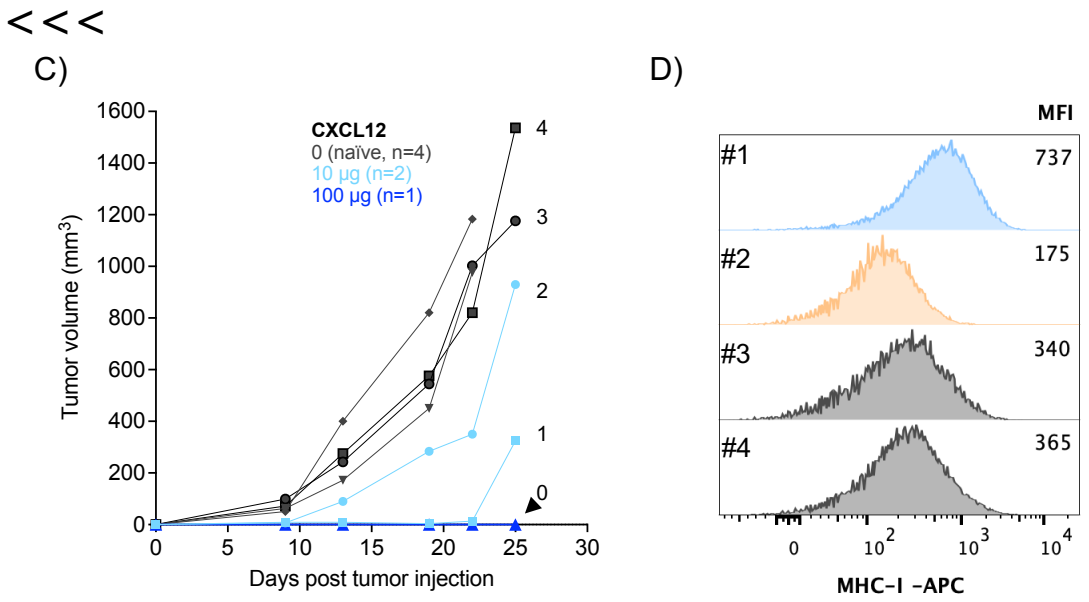

Figure 17. Some mice receiving CXCL12 rejected the MM cells twice

A) Scheme of the experiment. Surviving mice at the end of experiments -described in Fig.9- were inoculated i.p. with MM cells for a second time at day 75. B) Tumor growth was followed via BLI as previously. C) Tumor volume measured via caliper after s.c. re-challenge. Due to instrument unavailability, we had to change injection site to assess tumor engraftment. Naïve mice, i.e. never injected with MM cells before, were added as positive controls. D) At day 25 post rechallenge, surviving mice were euthanized, tumors were excised, digested and stained for CD45, MHC-I (flow cytometry analysis). MFI shown is gated on zombie-/CD45- cells.

3.8 CXCL12 modulates HMGB1 localization in the tumors favoring its nuclear localization

HMGB1 is a nuclear protein which can be found in the cytoplasm, from which it can be actively or passively released. It has been found highly expressed in various solid tumors, including mesothelioma (Kang R et al, 2013), where extracellular HMGB1 sustains chronic inflammation thus favoring MM progression (Bianchi ME et al, 2017).

Since HMGB1 can form a complex with CXCL12 (Schiraldi M et al, 2012), I tested if the administration of exogenous CXCL12 was modulating HMGB1 localization in the tumor masses of treated mice, as shown in Figure 10A. At the day of sacrifice, tumors were excised from mice (n=3/group) and subsequently processed to formalin-fixed paraffin embedded (FFPE) tissue sections. FFPE tissue sections were cut (4 µm) and HMGB1 staining was carried out. HMGB1 was mainly located in the cytoplasm in tumors coming from the untreated group, whereas the cytosolic fraction was restricted in tumors of mice receiving CXCL12 (Figure 18). This result may indicate MM cells limit the secretion of HMGB1 upon CXCL12 treatment, reducing overall a pro-tumoral signal in the tumor microenvironment.

Figure 18

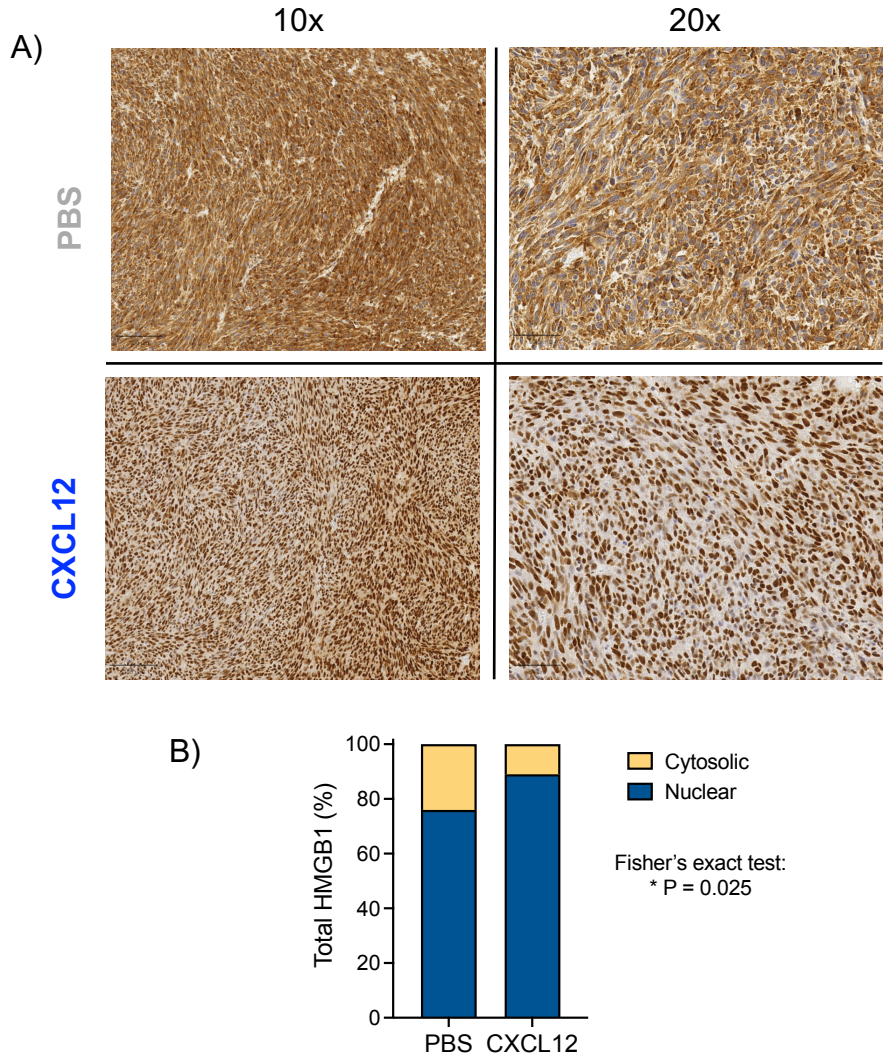

Figure 18. CXCL12 modulates HMGB1 localization in tumors

A) Representative immunohistochemical staining for HMGB1 in tumor masses of control (PBS) and CXCL12-treated mice. Scale bar 100 µm (10x magnification, left), 50 µm (20x magnification, right). B) Quantification of nuclear and cytosolic fractions in positive cells via QuPath, n=3 mice/group, 10 ROIs/sample. Statistics: Fisher's exact test, two-sided, * P=0.025.

3.9 CXCL12 does not promote MM proliferation nor modulate MΦs polarization in a human *in vitro* system

We finally wanted to confirm if the results shown in the previous sections, and obtained in a murine setting, were reproducible in a human system also. First, I tested CXCL12 effect on the proliferation of MSTO-211H and GO2 cell lines (both biphasic mesothelioma histotype): I plated 1.5×10^4 (MSTO) or 2.5×10^4 (GO2) cells

per well in a 24-well plate, and sixteen hours after seeding I treated or not cells with CXCL12 (100 nM) and I recorded cell confluence every 2 hours. As shown in Figure 19A, CXCL12 did not boost the proliferation neither of MSTO nor of GO2, even at the highest concentration (100 nM) previously used.

Since GO2 proliferate slowly and do not grow as a 3D structure over time, we proceeded only with MSTO cells for further experiments. I generated mesospheres starting from MSTO stably expressing GFP (MSTO-GFP) and I measured the area of mesospheres in the presence or absence of MΦs (obtained from healthy donor-derived CD14+ monocytes differentiation) and in two different conditions: untreated and treated with 100 nM CXCL12. The area of mesospheres increased over time, but when MΦs were present in the co-culture mesopheres grew more slowly (Figure 19B).

Then, we tested if CXCL12 could modulate MΦs polarization toward an M1 or M2-like phenotype. To overcome healthy donor-related variation, we obtained MΦs from the THP-1 (human monocytic) cell line via Phorbol 12-myristate 13-acetate (PMA, 150 nM) differentiation for 72 hours. Then, MΦs were exposed overnight to either PBS, 100 nM CXCL12, IFNγ plus LPS or IL-4 plus IL-13 (for M1 and M2-like phenotype, respectively). Total RNA was extracted from cells, 500 ng of RNA was reverse transcribed to cDNA that was later amplified by qRT-PCR for CD80 and CD206 transcripts – markers for M1 and M2-like macrophages, respectively. As shown in Figure 19C, CXCL12 did not polarize MΦs in any of the two directions, as the expression of both CD80 and CD206 was comparable to the unstimulated condition (M0).

Taken together, these results are in line with those obtained in the murine system.

Figure 19

A)

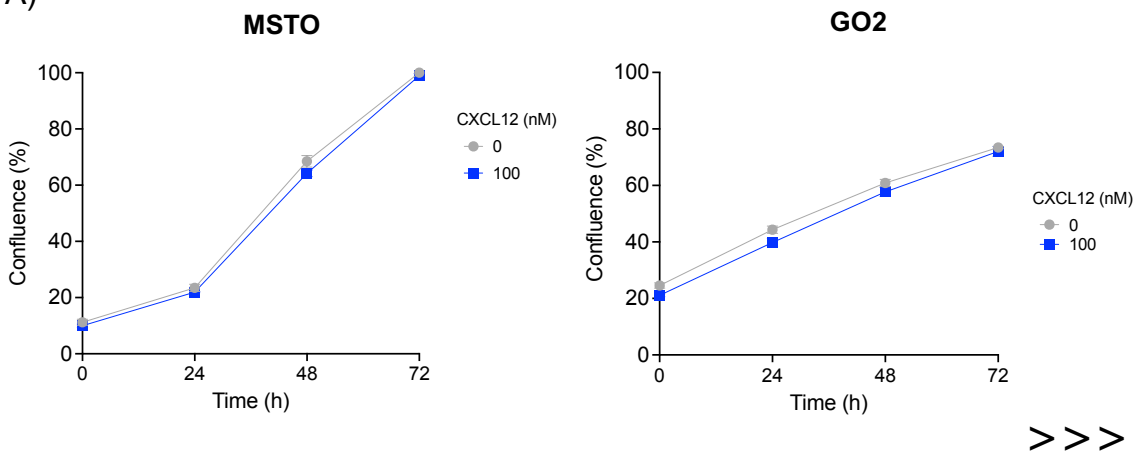

>>>

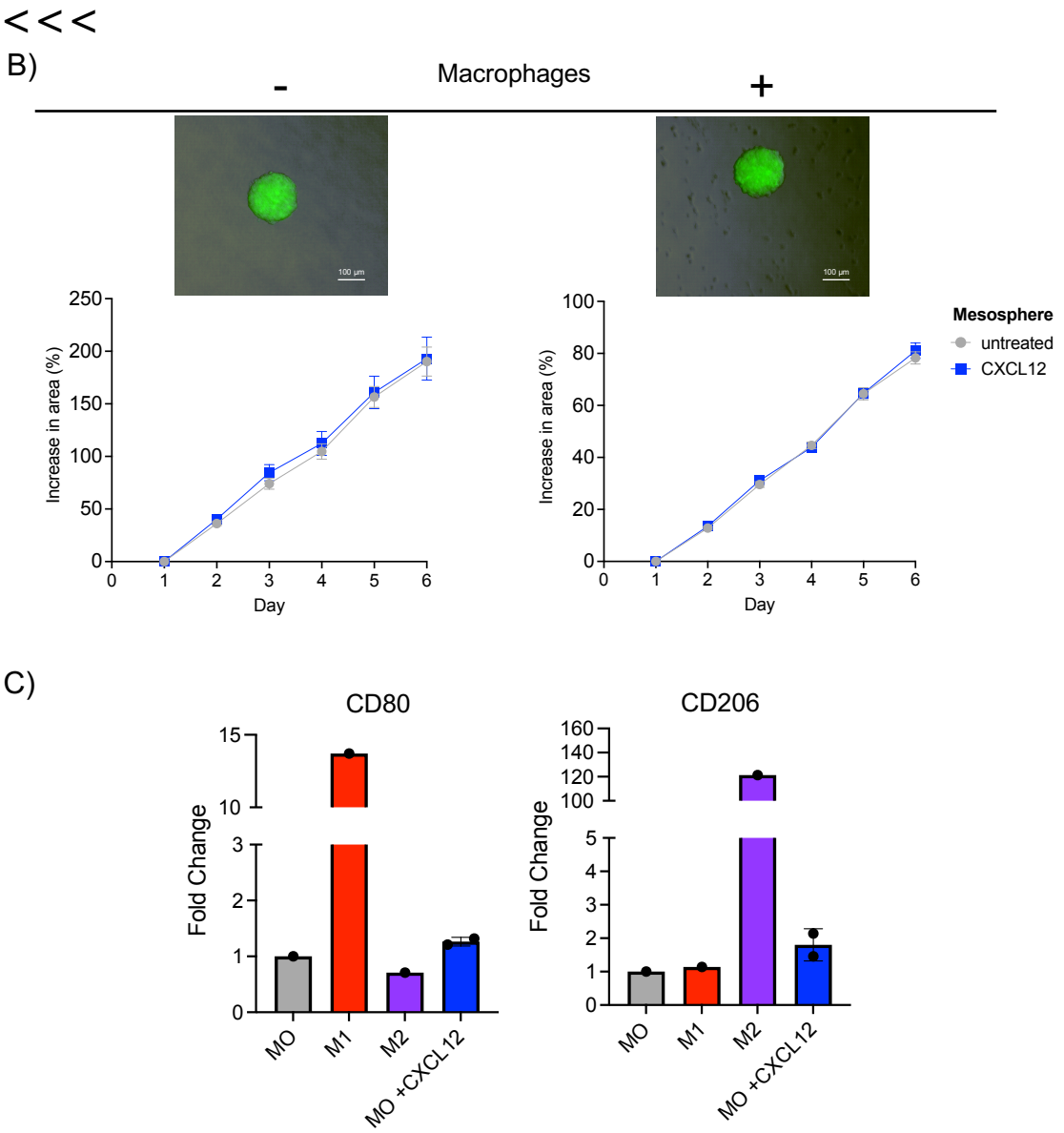

Figure 19. CXCL12 displays a similar behavior in a human system

A) MM cells (1,5×10⁴ cells/well for MSTO and 2,5×10⁴ cells/well for GO2) or were seeded in 24-well plates and treated after 16h with 100 nM CXCL12. Cell confluence was recorded every 2 hours by IncuCyte C3, 4x objective. Statistical test: Two-way ANOVA, ns. The experiment shown is representative of two performed, in biological triplicate. B) Representative images of MSTO spheroids (mesospheres) alone or in co-culture with macrophages, and growth curves relative to day 1 of mesosperes alone (left) or in co-culture with macrophages (right) either untreated or CXCL12-treated. Images were acquired by Axio microscope and mesosphere area was quantified via ImageJ. Statistics: n=10 spheroids/group, two-way ANOVA. The experiment is representative of two performed. C) Gene expression of CD80 (M1-like) and CD206 (M2-like) on macrophages derived from THP-1 cell line.

4. Discussion

Until now, the role of CXCL12-CXCR4 axis has been associated to tumor progression and metastatic formation in several solid tumors. However, we have previously demonstrated – in Mezzapelle R et al (2021) – that CXCL12 causes receptor co-internalization with CD47 (a don't-eat-me signal), thus unmasking tumor cells and enabling phagocytosis by macrophages (MΦs). Within this thesis, I investigated if and how the chemokine CXCL12 can activate an effective anti-tumor immune response.

First, I performed a proliferation assay by adding increasing doses of exogenous CXCL12 on MM cells, and I did not find enhancement in cell proliferation. Then, to test if it had immunomodulatory effect *in vivo*, we administered CXCL12 in a syngeneic model of mesothelioma (MM), and we found that CXCL12 treatment contributes to delay tumor growth in about half of mice (at the dose of 10 and 100 μg). In general, CXCL12 treated mice survived significantly longer compared to the untreated ones. Our results suggest that the chemokine CXCL12, so far known to promote tumor progression in other cancers (Guo Q et al, 2014; Anastasiadou DP et al, 2024) is instead beneficial *in vivo* in the context of MM, presumably by triggering ImmunoGenic Surrender (IGS). We hypothesize that a continuous administration of CXCL12 should be more beneficial to the MM bearing mice, since responding mice showed a low BLI signal so long as we administer CXCL12, but as soon as we stopped the treatment (day 23) tumor resumed its growth and the mice died or were sacrificed in the following weeks for severe illness. In five mice out of forty-eight the treatment with CXCL12 led to antitumor immunization: when re-challenged with the same tumor cells, they rejected the tumor within one week. Among the mice that received CXCL12 and were re-challenged, only one mouse developed a tumor mass comparable in size to the untreated group; in this mouse we observed the lowest MHC-I expression, suggesting a tumor immune-evasion mechanism (McGranahan N et al, 2017; Wu X et al, 2023; Lin P et al, 2025) frequently present in several tumor models, rather than a lack of immunological memory. Overall, this pattern of protection suggests that the administration of exogenous CXCL12 is engaging and reshaping the host immune system consistently with immunotherapy-mediated tumor control.

We then wanted to understand which immune population –focusing on macrophages and T cells– was modulated by CXCL12 treatment and eventually activated for mediating an effective anti-tumor response, and I will discuss the findings in the following sections.

4.1 A macrophage-T cell axis is activated following CXCL12 treatment

In many cancer models, CXCL12–CXCR4 signaling supports tumor progression by attracting immunosuppressive myeloid cells and facilitating tumor growth or metastasis (Zlotnik A et al, 2011; Teicher BA & Fricker SP, 2010). However, increasing evidence indicates that the functional outcome of CXCL12 signaling is highly context-dependent and can diverge substantially across tumor types, inflammatory states, and stromal compositions (Guyon A, 2014). In this study, exogenous CXCL12 administration did not alter the overall abundance of tumor-associated macrophages (TAMs) in the mesothelioma tumor microenvironment (TME); however, at day 21 there were more macrophages (MΦs) infiltrating the tumor in CXCL12-treated mice compared to the untreated ones, and this might be attributed to CXCL12 promoting the egress of CXCR4-positive myeloid cells from the bone marrow. We then conducted a preliminary experiment to test if systemic CXCL12 administration was affecting the number of circulating monocytes, and this was the case: two hours after injecting the chemokine, the number of circulating monocytes was almost doubled, supporting the notion that a CXCL12 gradient outside the bone marrow (BM) would cause the release of cells from the BM parenchymal niche. CXCL12 did not induce a classical polarization program, neither toward M1 (CD86+)- nor M2 (CD206+)-like states; this might mean that CXCL12 has no effect on polarization, or that the M1/M2 dichotomy fails to recapitulate the complexity of MΦs states in tumors (Xue J et al, 2014; Aras S & Zaidi MR, 2017).

4.1.1. CD169+ MΦs bridge over T cells

Overall, the data presented indicate that CXCL12 exerts a more qualitative effect on MΦs. In fact, *in vitro* experiments showed that BMDMs exposed to CXCL12 upregulate CD169 (Siglec-1) and MΦs infiltrating MM spheroids display an increase of surface CD169 levels over time –the latter irrespective from the treatment– supporting the appearance of a specialized population involved in antigen processing and lymphocyte crosstalk (Miyake Y et al, 2007; Grabowska J et al, 2018).

In vivo we observed an increased expression of this marker in MΦs infiltrating the tumor at day 14 post MM cells inoculation; this follows the increase observed in T cells at an earlier timepoint –day 7– of IFNγ, which is reported to induce CD169+ MΦs (Kim HJ et al, 2022). Moreover, the presence of CD169+ MΦs correlate with better clinical outcomes and enhanced anti-tumor immune responses (Saito Y et al, 2015; Edgar LJ et al, 2019).

The presence of CD169+ MΦs is strictly connected to enhanced T-cell mediated tumor control, in fact this MΦs population acts at the interface of innate and adaptive

immunity by cross-presenting antigens to dendritic cells, thus facilitating CD8+ T cell priming (Edgar LJ et al, 2019), and supporting local stromal re-organization into niches for activated T cells (Asano T et al, 2018). CD169+ MΦs are usually mainly located in the spleen and lymph nodes (Tacconi C et al, 2021), whereas our analysis was restricted to the tumor area; thus, many more CD169+ MΦs might be located in spleen and/or lymph nodes. In any case, our initial results are encouraging, and further investigation will determine the impact of this population in mediating the beneficial effect of CXCL12 on MM-bearing mice.

CXCL12 treatment also significantly reshaped the T-cell landscape *in vivo*. We observed increased infiltration of lymphocytes (CD3+ cells) within the tumor microenvironment –specifically CD4+ T cells and CD8+ T cells to a lower extent– alongside enhanced expression of functional activation markers, such as interferon gamma (IFNγ) and granzyme B (GrzB) in CD8+ T cells. All these features are typically associated with active cytotoxic immunity and better tumor control (Gajewski TF et al, 2013). The survival experiment supports the functional importance of T cells in mediating the therapeutic effect of CXCL12. The survival advantage induced by CXCL12 was fully abrogated upon depletion of either CD4+ or CD8+ T cells, highlighting the interdependent roles of helper and cytotoxic tumor-infiltrating lymphocytes (TILs) in mounting an effective anti-tumor response (Zander R et al, 2019). Moreover, among the T-cell depleted groups, CD8-depleted mice were the ones surviving less. This might be explained by the presence of some antitumor CD8+ T cell clones before the inoculation of tumor cells, which are maintained intact in the CD4-depleted group but not in the CD8-depleted group. The results obtained align with the work of Espinosa-Carrasco et al (2024), which demonstrates the importance of CD4+ T cells in instructing CD8+ T cells to their effector function, and the formation of immune triads made of three cell types: an antigen-presenting cell (APC), a CD4+ T cell and a CD8+ T cell. They found that the presence of triads correlates with better clinical outcome and response to immune checkpoint blockade (ICB) therapy. The data presented in my thesis do not retain spatial information to assess the formation of triads, but we plan to investigate further this path exploiting multiplex immunohistochemistry (mIHC) techniques on tumor masses collected from mice that received CXCL12 treatment, and compare them to PBS-treated ones.

Overall, these findings indicate that in our MM model, following CXCL12 administration, MΦs are reprogrammed not to kill tumor cells directly but rather to support and favor a more effective T-cell response.

4.2 HMGB1 is relocated by CXCL12

Mesothelioma is characterized by an immunosuppressive TME, thus displaying low response to immunotherapy (Cersosimo F et al, 2021). In this context, HMGB1 has been shown to be constitutively secreted by MM cells (Jube S et al, 2012) to support tumor progression. HMGB1 forms a complex with CXCL12, and the administration of exogenous CXCL12 favors the nuclear localization HMGB1 in the tumor masses. Cytoplasmic HMGB1 represents a proxy for the protein which will be released, thus exerting its pro-tumoral function; limiting the cytoplasmic fraction could decrease the availability of HMGB1 in the TME and thereby attenuate its pro-tumoral effects. This mechanism may ultimately contribute to improved outcomes in MM-bearing mice.

These observations, although promising, are based on preliminary results obtained retrospectively using standard IHC. Therefore, a crucial next step will be to validate and mechanistically refine this hypothesis. Specifically, we plan to characterize the redox-dependent isoforms of HMGB1 —determined by the oxidation state of cysteines C23, C45, and C106— which dictate whether the protein exerts pro-inflammatory activity (disulfide HMGB1) or chemoattractant properties (fully reduced HMGB1) (Schiraldi M et al, 2012). Defining which isoforms predominate under different experimental conditions will help clarify how CXCL12 modulates HMGB1 function *in vivo*. In parallel, we will quantify circulating HMGB1 levels, which are known to be elevated in the serum of mesothelioma patients (Napolitano A et al, 2016). Integrating tissue-level isoform analysis with systemic HMGB1 measurements will provide a more comprehensive picture of HMGB1 biology in MM and may support the development of HMGB1-targeted therapeutic strategies.

4.3 The transcriptomic landscape in mesosphere: the effect of IGS triggers on macrophages and MM cells, and a glance at phagocytosis

MΦs phenotypic plasticity is strongly shaped by local signals in the TME and understanding how MΦs and tumor cell states vary over time is crucial for defining therapeutic vulnerabilities in mesothelioma. A previous work from our lab showed that MΦs and MM cells mutually influence each other in a 3D co-culture system: MΦs infiltrating into mesospheres adopted an M2-like phenotype that supported spheroid growth over time, whereas M1-like MΦs limited spheroid expansion thus exerting an anti-tumoral effect (Andrea Lamarca, unpublished). Therefore, we adopted this simple 3D co-culture system made up by two cell types –MΦs and MM cells– to dissect the direct impact of CXCL12 and BoxA on these cell populations.

The treatment with CXCL12 induced a transcriptional profile consistent with MΦs dedifferentiation, reduced adhesion, and increased migratory potential, thus aligning with the acquisition of matrix-interacting and wound-remodeling functions reported in solid tumors (Wynn TA & Vannella KM, 2016). This is concordant with the well-established role of CXCL12-CXCR4 axis in activating chemotaxis, actin cytoskeleton remodeling and focal-adhesion turnover (Teicher BA & Fricker SP, 2010; Zlotnik A et al, 2011; Bianchi ME & Mezzapelle R, 2020). BoxA too produces a functional reprogramming characterized by downregulation of several pathways, particularly those associated with adhesion-related processes and chemotaxis. Taken together, these results highlight a general downregulation of MΦs cellular responses, aligning with long-term desensitization of GPCR signaling, which usually occurs following continuous and prolonged stimulation with agonists (Rajagopal S & Shenoy SK, 2018).

Upon CXCL12 and BoxA treatment, MM cells also undergo a transcriptional reprogramming that mirrors the MΦs response. CXCL12 appears to promote a more plastic, less adherent and dynamic phenotype, in line with CXCL12/CXCR4-driven tumor cell plasticity and motility reported for several cancers (Lazennec G & Richmond A, 2010). Similarly, BoxA produced a decrease in cellular processes, suggesting the disruption of HMGB1-dependent trophic and stress-adaptive programs (Bianchi ME et al, 2017).

Overall, my study reveals that MΦs and MM cells –in a simplified 3D co-culture system– undergo extensive and coordinated transcriptional reprogramming in response to IGS triggers, and combined targeting of both CXCR4 and HMGB1 could potentially reshape the TME.

Additionally, the temporal trajectory of MΦ–MM interactions revealed that phagocytic events peak early at day 2 of co-culture, and this aligns with previous observations that MΦs rapidly internalize apoptotic or stressed tumor cells shortly after contact (Voll RE et al, 1997; Elliott MR & Ravichandran KS, 2016).

Analysis of the SIRPα and CD47 expression revealed a clear association between MΦs phagocytic activity and inhibitory signaling status: MΦs that had not yet engaged in phagocytosis (cluster0) exhibited high expression of *Sirpa* together with elevated *Cd47*, in contrast, MΦs that had engulfed MM cells or tumor fragments (cluster1) showed a pronounced downregulation of both transcripts across all experimental conditions. This pattern is consistent with the established role of the CD47–SIRPα interaction as a dominant "don't-eat-me" signal that inhibits MΦs phagocytosis (Oldenborg PA et al, 2000). Importantly, the loss of *Sirpa* in phagocytic MΦs suggests that attenuation of inhibitory signaling represents a hallmark of the post-phagocytic

MΦs state, in line with previous studies showing that MΦs actively engaged in tumor clearance or remodeling display reduced sensitivity to CD47–SIRPα signaling and adopt alternative, M2-like phenotype (Gu S et al, 2018). Disengagement of the CD47–SIRPα axis accompanies and stabilizes the transition from an inflammatory, M1-like phenotype to a post-phagocytic, TAM-like state within the TME.

The phagocytic activity drives the divergence between two transcriptionally distinct macrophage populations:

- phagocytic MΦs –cluster1 in our scRNAseq experiment, which contain tumor-derived RNAs from engulfed cells (Qie J et al, 2022)– displayed a transcriptional reprogramming consistent with the transition toward a M2-like phenotype that is observed after phagocytosis of apoptotic cells (Martinez FO & Gordon S, 2014; Zilionis R et al, 2019) or exposure to tumor-derived signals (Mantovani A et al, 2002; Murray PJ & Wynn TA, 2011);
- non-phagocytic MΦs –cluster0, lacking tumor-derived RNAs– maintain a classical pro-inflammatory profile, consistent with M1-like phenotype responding to danger-associated signals in the tumor microenvironment, as extensively described in macrophage polarization studies (Gordon S & Martinez FO, 2010; Murray PJ et al, 2014).

This functional separation supports the concept of phagocytosis-induced reprogramming described in tumor-associated macrophages (TAMs) (Noy R & Pollard JW, 2014), and transcriptional rewiring from an inflammatory toward a tissue-repair phenotype. In fact, this result could also indicate that only M2-like MΦs perform phagocytosis in our system; to exclude this possibility, we plan to set up a phagocytosis assay using MΦs pre-polarized toward M1 or M2-like state. Moreover, in this study, we identified a robust and clear "predatory signature" that molecularly defines phagocytic MΦs, which are characterized by the combined presence of tumor-derived transcripts and a remodeling-oriented transcriptional shift. This provides a transcriptional fingerprint of MΦs which have engaged in tumor cell phagocytosis; this can represent a molecular tool to detect phagocytic MΦs directly within the native TME and could enable us to assess their prevalence and functional impact macrophage phagocytosis of tumor cells during MM progression.

These data have a limitation: from the scRNAseq data alone we cannot determine whether the macrophages phagocytose entire living tumor cells or cell fragments of apoptotic cells. Collectively, however, our data reveal a high-resolution view of how early physical interactions with tumor cells imprint long-lasting transcriptional states

on MΦs and provide data useful for targeting phagocytosis and modulating immunosuppression in mesothelioma.

4.3.1 Human mesospheres

To validate the translational relevance of our murine findings in an *in vitro* human setting, we established a 3D co-culture made up by human MΦs and MM cells grown as spheroids to test CXCL12 effect. Here, CXCL12 affected neither human MM cell proliferation nor mesosphere growth, and in parallel it failed to skew MΦs polarization toward either an M1- or M2-like phenotype, mirroring the absence of modulation of MΦs polarization observed in murine experiments *in vivo*. Notably, in the human system, the presence of MΦs -regardless of treatment- in the co-culture leads to reduced mesosphere growth, likely due to a more pronounced phagocytic activity compared to murine BMDMs (Suleimanov SK et al, 2024) and enhanced phagocytic capacity of THP-1-derived MΦs compared to primary cell-derived MΦs (Shiratori H et al, 2017).

Taken together, these findings support the evidence that CXCL12 is not tumor-promoting in the context of mesothelioma, and its effect could potentially be conserved across species.

4.4. Conclusion

Altogether, the results presented in this thesis refine our understanding of the CXCL12–CXCR4 axis in mesothelioma. CXCL12 in this context enhances anti-tumor immunity by promoting a macrophage phenotype conducive to T-cell recruitment and activation. Importantly, CXCL12 might have opposite effects at the same time: the pro-tumoral effects already known, plus an anti-tumoral effect that we found because we actually looked for it. Importantly, CD169+ macrophages might provide a mechanistic framework through which CXCL12 exerts its effects. This macrophage subset might serve as a potential therapeutic target for future immunomodulatory strategies in mesothelioma. Furthermore, the preliminary results collected in the human system -aligning with the those obtained in the murine one- point out the potential translational power of these findings.

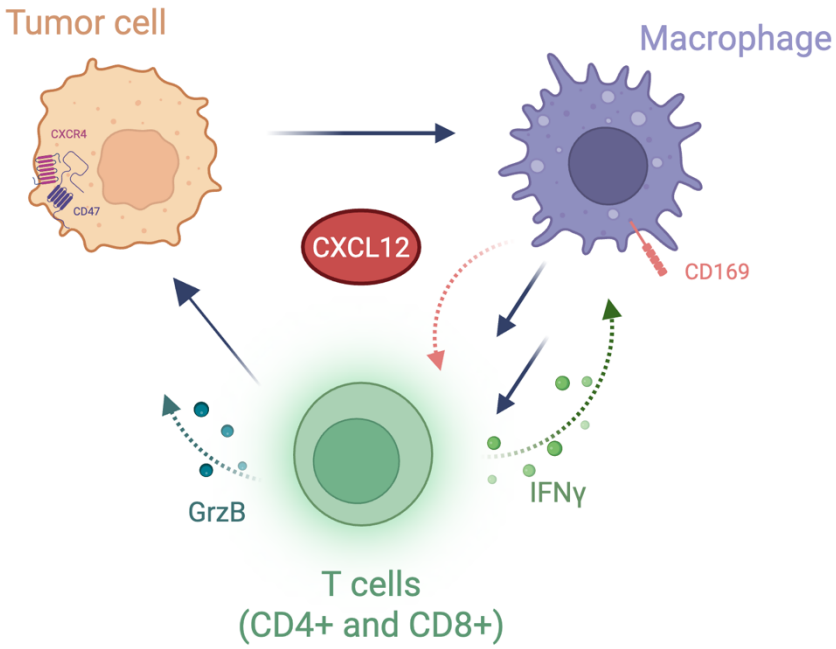

Figure 20. Schematic representation of the immune interactions elicited by CXCL12. CXCL12 engages CXCR4 on tumor cells, causing its co-internalization with the "don't-eat-me" signal CD47, while simultaneously promoting macrophage activation, marked by CD169 expression. Activated macrophages and CXCL12 enhance T-cell responses: CD4+ and CD8+ T cells increase effector functions, including Granzyme B (GrzB) and Interferon-γ (IFNγ). Together, these coordinated events support the initiation of antitumor immunity.

5. Materials and methods

5.1 Cell lines and drug compounds

AB1, AB12, AB22 and AE17 mouse mesothelioma cells (Cell Bank Australia) were cultured at 37°C under 5% CO2 in RPMI 1640 (Life Technologies) supplemented with 5 or 10% v/v fetal bovine serum (Life Technologies), respectively, 2 mM L-glutamine, 100 U/ml penicillin/streptomycin, and 10 mM HEPES. Luciferase-expressing AB1-B/c-LUC and AB1-GFP cells were previously described (Mezzapelle R et al, 2016; Mezzapelle R et al 2021). MSTO-211H (ATCC CRL-2081) human mesothelioma cells were cultured at 37°C under 5% CO2 in RPMI 1640 (Life Technologies) supplemented with 10% v/v fetal bovine serum (Life Technologies), 2 mM L-glutamine, 100 U/ml penicillin/ streptomycin. MSTO-GFP were obtained by transfecting MSTO cells with the PGK.GFP LV. GO2 cells were generated and kindly provided by Marion MacFarlane (MRC Toxicology Unit of University of Cambridge, Cambridge, UK).

All cell lines were passaged for no longer than 10 passages after thawing. Cell lines were routinely tested for mycoplasma contamination by PCR. BoxA and CXCL12 (LPS-free) were purchased from HMGBiotech (Milano, Italy).

5.2 Cell proliferation

$1{,}5\times10^4$ (either AB1 or AB12 or AB22 or AE17) or $1{,}5\times10^4$ MSTO or $2{,}5\times10^4$ GO2 cells were seeded in 24-well plates, grown overnight, and treated with CXCL12 (1, 10, 100 nM) for 72 h. Each condition was tested in triplicate. After treatment administration, cell confluence was recorded using IncuCyteS3. A scan was performed every 2 h. Cell confluence percentage was calculated by IncuCyte® Software (whole well analysis, segmentation adjustment: 0.2; filter: Area (μm^2) 400 as minimum value).

5.3 Mice

Animal experiments were approved by the Animal Care and Use Committee (IACUC #1322) of Ospedale San Raffaele in accordance with the Italian law. Eight-week-old male BALB/c mice were purchased from Charles River Laboratories (Calco, Italy). Animals were housed under specific pathogen-free conditions and allowed access to food and water ad libitum. Mice were inoculated intraperitoneally (i.p.) with 7×10^4 or subcutaneously (s.c.) with 5×10^5/flank MM cells. Cell engraftment was confirmed by bioluminescence imaging (BLI). Two days after inoculation, mice were

randomized into experimental groups and treatments started. CXCL12 (100 µg) was administered i.p. three times a week for 3 weeks (10 times in total). Control mice were injected i.p. with Phosphate Buffered Saline (PBS) solution. Tumor growth was assessed weekly by BLI. Mice were monitored daily and were sacrificed when severely distressed (BLI signal > 10^9 photons/s). In vivo BioLuminescence optical imaging (BLI) was performed using an IVIS SpectrumCT Preclinical In Vivo Imaging System (Perkin Elmer). The system is equipped with a low noise, back-thinned, back-illuminated CCD camera cooled at -90°C (quantum efficiency in the visible range above 85%). Before BLI, each mouse received an i.p. injection of 6 g luciferin/kg body weight. During image acquisition, the animals were kept at 37°C and under gaseous anesthesia (2–3% isoflurane and 1 lt/min O2). After luciferin injection, BLI was performed by acquiring an image every 2 min (exposure time = auto, binning = 8, f = 1 and a field of view equal to 23 cm (field D)) to detect the highest BLI signal. BLI image analysis was performed by measuring the total light flux (photons/s) in a uniform region of interest (ROI) placed over the animal abdomen. Images were acquired and analyzed using Living Image 4.4 (Perkin Elmer) and Aura In vivo Imaging software (Spectral Instruments Imaging).

5.4 Tumor re-challenge

BALB/c mice that rejected the first tumor challenge and naïve BALB/c mice were inoculated i.p. with 7×10^4 or s.c. with 10^6 MM cells. Tumor growth was followed by BLI or via caliper measurement (tumor volume calculated as follow: $V(mm^3) = 0.5 \times D \times d^2$). Mice were sacrificed when the bioluminescent signal remained at background levels for three consecutive scans.

5.5 Mouse samples

5.5.1 Tumors

Tumor masses were explanted from each sacrificed mouse, fixed in zinc formalin for 24 h, processed with Leica TP1020, embedded in paraffin, and slices were cut. Briefly, the sections (4 µm) were deparaffinized in xylene and rehydrated in graded alcohol. Immunohistochemical staining was performed using the following antibodies: anti-F4/80 (clone A3-1 Bio-Rad), anti-CD86 (clone E5W6H Cell Signaling), anti-CD206 (clone E6T5J Cell Signaling), and anti-HMGB1 (#18256 Abcam). Slides were counterstained with hematoxylin and mounted. If used for cytofluorimetry analysis, after excision, tumor masses were enzymatically digested

with digestion solution (collagenase A+B+D [15 µg/mL], Roche + DNase I [30 µg/mL] Thermo Fisher Scientific) for 1 hour, then mechanically dissociated and smashed through a 70 µm cell strainer. After filtration, cells were counted and stained for surface and intracellular markers.

5.5.2 Blood

Blood samples (~150 µL) were collected from mice via the retro-orbital sinus technique. A sterile heparinized glass capillary tube (Hirschmann Na-heparin, d=1,75 mm, 100mm/130 µL) was gently inserted into the medial canthus of the eye at a slight angle to access the retro-orbital sinus. Blood was collected by capillary action and immediately transferred into appropriate collection tubes (Microvette 200 EDTA K3E) for analysis at Idexx Procyte analyzer (Animal biochemistry facility, IRCCS San Raffaele Hospital).

5.6 Image acquisition and analysis

All images were scanned using the Aperio Scanscope C2 system (Leica Biosystems). After acquisition, staining quantification was carried out in QuPath and a script was created to segment nuclei and count the number of positively stained cells within the total sample. The script is as follows:

- CD86

```
setImageType('BRIGHTFIELD_H_DAB');

setColorDeconvolutionStains('{"Name" : "H-DAB", "Stain 1" : "Hematoxylin",
"Values 1" : "0.81041 0.56974 0.13652 ", "Stain 2" : "DAB", "Values 2" :
"0.26524 0.50132 0.8236 ", "Background" : " 254 190 154 "}');

// Only run detection in pre-selected annotations

selectAnnotations();

runPlugin('qupath.imagej.detect.cells.WatershedCellDetection',
'{"detectionImageBrightfield": "Optical density sum",
"requestedPixelSizeMicrons": 0.5,  "backgroundRadiusMicrons": 8,
"medianRadiusMicrons": 0.0, "sigmaMicrons": 1.5,  "minAreaMicrons": 10.0,
"maxAreaMicrons": 400,  "threshold": 0.1,  "maxBackground": 2.0,
"watershedPostProcess": true,  "excludeDAB": false,  "cellExpansionMicrons": 5.0,
"includeNuclei": true, "smoothBoundaries": true,  "makeMeasurements": true}');

setCellIntensityClassifications('Nucleus: DAB OD mean', 0.1);
```

- CD206 and F4/80

```
setImageType('BRIGHTFIELD_H_DAB');

setColorDeconvolutionStains('{"Name" : "H-DAB", "Stain 1" : "Hematoxylin",
"Values 1" : "0.81041 0.56974 0.13652 ", "Stain 2" : "DAB", "Values 2" :
"0.26524 0.50132 0.8236 ", "Background" : " 254 190 154 "}');
```

```
// Only run detection in pre-selected annotations

selectAnnotations();

runPlugin('qupath.imagej.detect.cells.WatershedCellDetection',
'{"detectionImageBrightfield": "Optical density sum",
"requestedPixelSizeMicrons": 0.5,  "backgroundRadiusMicrons": 8,
"medianRadiusMicrons": 0.0, "sigmaMicrons": 1.5,  "minAreaMicrons": 10.0,
"maxAreaMicrons": 400,  "threshold": 0.1,  "maxBackground": 2.0,
"watershedPostProcess": true,  "excludeDAB": false,  "cellExpansionMicrons": 5.0,
"includeNuclei": true, "smoothBoundaries": true,  "makeMeasurements": true}');

setCellIntensityClassifications('Nucleus: DAB OD mean', 0.1);
```

- HMGB1

```
// Set image type for H-DAB (Hematoxylin and DAB)
setImageType('BRIGHTFIELD_H_DAB')

// Create selection for all objects (optional)
createSelectAllObject(false)

// Set color deconvolution for Hematoxylin and DAB
setColorDeconvolutionStains('{"Name" : "H-DAB", "Stain 1" : "Hematoxylin",
"Values 1" : "0.81041 0.56974 0.13652 ", "Stain 2" : "DAB", "Values 2" :
"0.26524 0.50132 0.8236 ", "Background" : " 254 190 154 "}')

// Get the selected annotations
def selectedAnnotations = getSelectedObjects().findAll { it.isAnnotation() }

if (selectedAnnotations.isEmpty()) {println "No annotations selected. Please select
annotations to analyze." return}

selectedAnnotations.each { annotation -> println "Analyzing annotation:
${annotation.getName()}"

    // Select the annotation for analysis
    selectObjects([annotation])

    // Run the cell detection plugin with Watershed method
    runPlugin('qupath.imagej.detect.cells.WatershedCellDetection',
'{"detectionImageBrightfield": "Optical density sum",
"requestedPixelSizeMicrons": 0.5,  "backgroundRadiusMicrons": 8,
"medianRadiusMicrons": 0.0,  "sigmaMicrons": 1.5,  "minAreaMicrons": 10.0,
"maxAreaMicrons": 400,  "threshold": 0.1,  "maxBackground": 2.0,
"watershedPostProcess": true,  "excludeDAB": false,  "cellExpansionMicrons": 5.0,
"includeNuclei": true,  "smoothBoundaries": true,  "makeMeasurements": true}')

    // Set classification threshold for DAB intensity
    setCellIntensityClassifications('Cell: DAB OD mean', 0.1)
    // setCellIntensityClassifications('Cytoplasm: DAB OD mean', 0.1)

    // Initialize counters
    def dabPositiveNucleus = 0
    def dabPositiveCytoplasm = 0

    // Get the detected cells within the annotation
    def cells = getCellObjects().findAll {
annotation.getROI().contains(it.getROI().getCentroidX(),
it.getROI().getCentroidY()) }
```

```
    // Loop through each detected cell and analyze staining in both nucleus and
cytoplasm
    cells.each { cell ->
def dabNucleus = cell.getMeasurementList().getMeasurementValue('Nucleus: DAB
OD mean')
def dabCytoplasm =
cell.getMeasurementList().getMeasurementValue('Cytoplasm: DAB OD mean')
        if (dabNucleus != null && dabNucleus > 0.1) {dabPositiveNucleus++ }
        if (dabCytoplasm != null && dabCytoplasm > 0.1) {
dabPositiveCytoplasm++} }

    // Total DAB-positive cells
    def totalDabPositive = dabPositiveNucleus + dabPositiveCytoplasm

    // Fractions relative to all DAB+ cells
    def nucleusFraction = totalDabPositive > 0 ? dabPositiveNucleus /
totalDabPositive : 0
    def cytoplasmFraction = totalDabPositive > 0 ? dabPositiveCytoplasm /
totalDabPositive : 0

    // Output the results
    println "DAB-positive nuclei: ${dabPositiveNucleus}"
    println "DAB-positive cytoplasm: ${dabPositiveCytoplasm}"
    println "Total DAB-positive cells: ${totalDabPositive}"
    println "Fraction nuclear DAB+ (of all DAB+): ${nucleusFraction}"
    println "Fraction cytoplasmic DAB+ (of all DAB+): ${cytoplasmFraction}"

    // Add results to the annotation measurements
    annotation.getMeasurementList().putMeasurement("DAB Positive Nuclei",
dabPositiveNucleus)
    annotation.getMeasurementList().putMeasurement("DAB Positive Cytoplasm",
dabPositiveCytoplasm)
    annotation.getMeasurementList().putMeasurement("DAB Positive Cells (Total)",
totalDabPositive)
    annotation.getMeasurementList().putMeasurement("DAB Nucleus Fraction",
nucleusFraction)
    annotation.getMeasurementList().putMeasurement("DAB Cytoplasm Fraction",
cytoplasmFraction)
```

5.7 Cytofluorimetry staining

Cytofluorimetry staining on murine samples was performed on cells obtained from enzymatic and mechanic digestion of tumor tissue. Cells were stained first with Zombie Aqua fixable viability kit (1:500, #433102 BioLegend), then with Pacific Blue-conjugated anti-CD45 (1:500, clone 30-F11, BioLegend), APC-Cy7 conjugated anti-F4/80 (1:100, clone BM-8, BioLegend), PE-Cy7 conjugated anti-CD11b (1:100, clone M1/70, BD Biosciences), FITC conjugated anti-CD86 (1:100, clone GL-1, BioLegend), Alexa Fluor 647 conjugated anti-CD206 (1:100, clone C068C2, BioLegend), PE conjugated anti-CD169 (1:100, clone 3D6.112, BioLegend) antibodies to define macrophage phenotype. Cells were stained with PE conjugated or FITC conjugated anti-CD45 (1:500, clone 30-F11; BioLegend and BD Biosciences, respectively), FITC conjugated or APC-Cy7 conjugated anti-CD3 (1:400, clone 17A2, BioLegend), PerCP-

Cy5.5 conjugated anti-CD8 (1:200, clone 53-6.7, BioLegend), V450 conjugated anti-CD44 (1:200, clone IM7, BD Biosciences), PE conjugated or Alexa Fluor 647 conjugated anti-PD-1 (1:500, clone RMP1-30, BioLegend) antibodies to identify T cells. Cells from tumor masses were stained with APC-conjugated anti MHC-I (1:400, clone 28-14-8, eBioscience).

5.7.1 Intracellular staining

After surface marker staining, when necessary, cells were then fixed in 2% paraformaldehyde, permeabilized (0.5% saponin, 2% heat-inactivated FBS, 2% rat serum, 0.2% sodium azide), and further stained for intracellular IFNγ (APC conjugate, 1:200, Clone XMG1.2, BioLegend) and GrzB (PE-Cy7 conjugate, 5 µL/tube, clone QA16A02, BioLegend). Samples were acquired on a BD FACS Canto II, and data were analyzed using FlowJo v10.10 software.

5.7.2 Efficiency of T cell depletion

The efficiency of CD8 T-cell depletion in vivo was determined by flow cytometry in peripheral blood at day 2 after MM cell inoculation. Blood cells were stained first with Zombie Aqua fixable viability kit (1:500, #433102 BioLegend), then with APC-Cy7 conjugated anti-CD3 (1:400, clone 17A2, BioLegend), PerCP-Cy5.5 conjugated anti-CD8 (1:200, clone 53-6.7, BioLegend), Pacific Blue conjugated anti-CD4 (1:400, clone RM4-5, BioLegend) antibodies. Samples were analyzed on a BD FACS Canto II apparatus and data analyzed using FlowJo v10.10 software

5.8 Depletion of CD4 and CD8 T cells *in vivo*

A hundred µg of either anti-mouse CD8 monoclonal antibody (Clone 2.43, BioXcell) or anti-mouse CD4 monoclonal antibody (Clone GK1.5, BioXcell) or IgG control (IgG2b, clone LTF-2, BioXcell) were injected i.p. at day -3, -1, +1, +6, +10 relative to the inoculation of MM cells (day 0). CD4 and CD8 T-cell depletion in the peripheral blood was assessed by flow cytometry and confirmed to exceed 98%.

5.9 Generation of macrophages

Bone marrow cells were isolated from the femurs of 8-week-old male BALB/c mice. Macrophages were obtained by culturing bone marrow cells in complete DMEM containing 10% (v/v) FCS, 2 mM L-glutamine, 100 U/ml penicillin/streptomycin, 1x non-essential amino acids, 1x sodium pyruvate, 1% (v/v) β-mercaptoethanol supplemented with macrophage colony-stimulating factor (M-CSF, 20 ng/ml) for 6

days. At day 4, the medium was replaced with fresh M-CSF, and at day 6, adherent macrophages were harvested, counted and used for co-culture generation.

Human macrophages were obtained either by healthy donor-derived isolated CD14+ monocytes (differentiated with 20 ng/mL human M-CSF for 6 days) or by differentiation of THP-1 cell line (human monocytic leukemia, TIB-202 ATCC) with 150 nM Phorbol 12-myristate 13-acetate (PMA) for 72 hours.

5.10 RNA extraction and real-time PCR analysis

Total RNA was extracted from cells using NucleoSpin RNA (Macherey-Nagel) and treated with DNase I. The amount of total RNA was determined by UV spectrophotometry using a Nano-Drop Spectrophotometer (Thermo Fisher Scientific). Next, 500 ng of total RNA was reversed transcribed using the Superscript IV Reverse Transcriptase (Thermo Fisher Scientific) following the manufacturer's protocol. PCR analysis was carried out using SYBR Green Master Mix (Roche Diagnostics).

Receptor expression was evaluated using the following primers:

- CD80 Forward: 5' GAAGAGCTGGCACAAACTCG 3'
  Reverse: 5' CGCAGAGCCAGGATCACAAT 3'
- CD206 Forward: 5' AGCCAACACCAGCTCCTCAAGA 3'
  Reverse: 5' CAAAACGCTCGCGCATTGTCC A 3'
- β-actin (normalizer) Forward: 5' GCACCACACCTTCTACAATGA 3'
  Reverse: 5' GTCATCTTCTCGCGGTTGGC 3'

5.11 Generation of MM spheroids

AB1-GFP spheroids were generated by using BIOFLOAT™ 96-Well Plate, an ultra-low attachment plate, or by force floating technique. 1000 cells/well were seeded in a total volume of 100 µL, cells started to aggregate and spheroids were fully formed in 24 hours. MSTO-GFP spheroids were generated using the same technology (cell density: 750 cells/well in a total volume of 100 µL).

Bulk spheroids generation was achieved by plating 10^6 AB1-GFP cells in 5 mL of DMEM complete medium in a 6 cm non-adherent bacterial cell culture dish for 3 days. The lack of adherence to the culture plate forced the cells to float and assemble into spheroids.

5.11.1 Spheroids co-culture

BMDMs were detached after differentiation using Versene solution (0.5 mM EDTA in PBS), counted, and resuspended in complete DMEM medium. A suspension of

3×10^4 BMDMs/500µL was aliquoted in each well of an ultra-low adhesion 24-well plate (Corning product #3473). One spheroid was then transferred to each well. Co-cultures were carried on for 7 days and 100 µL of fresh medium was added every other day to each well. Bulk co-cultures were performed by harvesting fully differentiated BMDMs and adding 2×10^6 BMDMs into the spheroid suspension generated from forced floating.

Spheroids were imaged daily by fluorescent microscopy at Zeiss Axio Observed inverted microscope. Green color thresholding was applied by ImageJ software to measure the area of AB1-GFP spheroids.

5.12 Preparation of single cell suspensions from spheroids co-culture

Bulk co-cultures (AB1-GFP spheroids plus BMDMs) were dissociated to single cells using TrypLE Express (Gibco). Cells were finally suspended in 100 µL of PBS containing 0.04% BSA in 1.5 mL tubes and processed immediately for scRNAseq analysis; final cell density was 1500 cells/µL for a total cell number of 15000 cells.

5.13 Chromium Next GEM Single Cell 3' v3.1: Cell Multiplexing

We followed these protocols: Cell Multiplexing Oligo Labeling for Single Cell RNA Sequencing Protocols with Feature Barcode technology (CG000391 | Rev B, 10x Genomics) and Chromium Next GEM Single Cell 3’ Reagent Kits v3.1 (Dual Index) with Feature Barcode technology for Cell Multiplexing User Guide (CG000388 | Rev C, 10x Genomics). Single-cell transcriptomic was conducted on the 10x platform in COSR Facility of San Raffaele Hospital. scRNA-seq libraries were pooled and sequenced on the NextSeq2000 instrument (Illumina). The sequencing setup included an 8-base index read, a 28-base Read 1 containing 10X cell-identifying barcodes (CBs) and unique molecular identifiers (UMIs), and a 100-base Read 2 containing the transcript sequence.

Raw sequencing data underwent processing using the cellranger pipeline (v6.3; https://www.10xgenomics.com/support/software/cell-ranger). This process generated digital gene expression matrices, which were then analyzed.

5.14 scRNAseq analysis

Analysis of single-cell RNAseq libraries was performed in RStudio using ‟Seurat‟ package. All the libraries were merged into one Seurat object and filtered for low-

quality cells (percentage of mitochondrial genes < 5%, number of features > 500, number of counts > 1000) and for multiplets using *scDblFinder* function. Libraries were then normalized, scaled and layers were integrated using *HarmonyIntegration* method. Cell clusters were defined after computation of nearest-neighbor graph and integrated UMAP were generated. To determine differentially expressed markers, we used *FindAllMarkers* function, setting a min.pct = 0.10 threshold. After annotation of clusters, cells belonging to the "Macrophage" cluster were selected, scaled, integrated and clustered to determine potential subgroups. UMAP and feature plots were generated using *DimPlot* and *FeaturePlot* functions from "Seurat" package.

GSEA was performed using the *gseGO* function from "clusterprofiler" package using a list of markers ranked by average $\log_2$ fold change * -$\log_{10}$(p-value) and the Gene Ontology "org.Mm.eg.db" database of biological processes. The Overrepresentation analysis (ORA) was performed using the enrichGO function from "clusterprofiler" package using a list of upregulated (average $\log_2$ fold change > 1) or downregulated (average $\log_2$ fold change < -1) markers and the Gene Ontology "org.Mm.eg.db" database of biological processes. Dot plots were generated using *ggplot* function from "ggplot2" package.

To determine the "predatory signature" set of genes, we firstly generated the list of DEG between "AB1" and "Macrophage" clusters and a list of DEG between "Cluster 1" and "Cluster 0" in "Macrophages" dataset. Then, we selected the shared markers and grouped them according to the proportion of cells expressing each marker in AB1 cluster.

5.15 Statistical analyses

I performed all experiments in duplicate, triplicate. For animal studies, the sample size estimate was indicated in the application to obtain an IACUC. There were no pre-established criteria for animal exclusion and, in general, we did not exclude animals, save the ones which did not display any tumor signal after MM cells engraftment. Statistical analyses were performed with GraphPad Prism software, version 10.6.0 (GraphPad software, Inc.).

References

Agresti A, Bianchi ME. (2003) HMGB proteins and gene expression. *Curr Opin Genet Dev*.13(2):170-178.

Anastasiadou DP, Quesnel A, Duran CL, Filippou PS, Karagiannis GS. (2024) An emerging paradigm of CXCL12 involvement in the metastatic cascade. *Cytokine Growth Factor Rev.* Feb;75:12-30

Apetoh L, Ghiringhelli F, Tesniere A, Obeid M, Ortiz C, Criollo A, Mignot G, Maiuri MC, Ullrich E, Saulnier P, Yang H, et al. (2007) Toll-like receptor 4-dependent contribution of the immune system to anticancer chemotherapy and radiotherapy. *Nat Med.* Sep;13(9):1050-9.

Aras S, Zaidi MR. (2017) TAMeless traitors: macrophages in cancer progression and metastasis. *Br J Cancer*. 117(11):1583-1591.

Arneth B. (2019) Tumor Microenvironment. Medicina (Kaunas). Dec 30;56(1):15.

Asano K, Nabeyama A, Miyake Y, Qiu CH, Kurita A, Tomura M, Kanagawa O, Fujii S, Tanaka M. (2011) CD169-positive macrophages dominate antitumor immunity by crosspresenting dead cell-associated antigens. *Immunity*. Jan 28;34(1):85-95.

Asano T, Ohnishi K, Shiota T, Motoshima T, Sugiyama Y, Yatsuda J, Kamba T, Ishizaka K, Komohara Y. (2018) CD169-positive sinus macrophages in the lymph nodes determine bladder cancer prognosis. *Cancer Sci.* May;109(5):1723-1730.

Baas P, Scherpereel A, Nowak AK, Fujimoto N, Peters S, Tsao AS, Mansfield AS, Popat S, Jahan T, Antonia S, Oulkhouir Y, Bautista Y, Cornelissen R, Greillier L, Grossi F, Kowalski D, Rodríguez-Cid J, Aanur P, Oukessou A, Baudelet C, Zalcman G. (2021) First-line nivolumab plus ipilimumab in unresectable malignant pleural mesothelioma (CheckMate 743): a multicentre, randomised, open-label, phase 3 trial. *Lancet*. Jan 30;397(10272):375-386.

Barbero S, Bonavia R, Bajetto A, Porcile C, Pirani P, Ravetti JL, Zona GL, Spaziante R, Florio T, Schettini G. (2003) Stromal cell-derived factor 1alpha stimulates human glioblastoma cell growth through the activation of both extracellular signal-regulated kinases 1/2 and Akt. *Cancer Res.* Apr 15;63(8):1969-74.

Barclay AN, Van den Berg TK. (2014) The interaction between signal regulatory protein alpha (SIRPα) and CD47: structure, function, and therapeutic target. *Annu Rev Immunol.* 32:25-50.

Barjij I, Meliani M. (2025) Immunogenic Cell Death as a Target for Combination Therapies in Solid Tumors: A Systematic Review Toward a New Paradigm in Immuno-Oncology. *Cureus*.17(6):e85776.

Barker RN, Erwig LP, Hill KS, Devine A, Pearce WP, Rees AJ. (2002) Antigen presentation by macrophages is enhanced by the uptake of necrotic, but not apoptotic, cells. *Clin Exp Immunol.* Feb;127(2):220-5.

Bernhard CA, Ried C, Kochanek S, Brocker T. (2015) CD169+ macrophages are sufficient for priming of CTLs with specificities left out by cross-priming dendritic cells. Proc Natl Acad Sci U S A. 112(17):5461-5466.

Bianchi C, Bianchi T, Tommasi M. (2007) Mesotelioma della pleura nella Provincia di Trieste [Mesothelioma of the pleura in the Province of Trieste]. *Med Lav*. Sep-Oct;98(5):374-80.

Bianchi ME & Mezzapelle R. (2020) "The Chemokine Receptor CXCR4 in Cell Proliferation and Tissue Regeneration." *Frontiers in immunology* vol. 11 2109.

Bianchi ME, Crippa MP, Manfredi AA, Mezzapelle R, Rovere Querini P, Venereau E. (2017) High-mobility group box 1 protein orchestrates responses to tissue damage via inflammation, innate and adaptive immunity, and tissue repair. *Immunol Rev.* Nov;280(1):74-82.

Bianchi ME. DAMPs, PAMPs and alarmins: all we need to know about danger. (2007) *J Leukoc Biol.* Jan;81(1):1-5

Binazzi A, Marinaccio A, Corfiati M, Bruno C, Fazzo L, Pasetto R, Pirastu R, Biggeri A, Catelan D, Comba P, Zona A. (2017) Mesothelioma incidence and asbestos exposure in Italian national priority contaminated sites. Scand J Work Environ Health. Nov 1;43(6):550-559.

Biswas SK, Mantovani A. (2010) Macrophage plasticity and interaction with lymphocyte subsets: cancer as a paradigm. *Nat Immunol.* 11(10):889-896.

Brcic L, Kern I. (2020) Clinical significance of histologic subtyping of malignant pleural mesothelioma. *Transl Lung Cancer Res*. Jun;9(3):924-933.

Bule P, Aguiar SI, Aires-Da-Silva F, Dias JNR. (2021) Chemokine-Directed Tumor Microenvironment Modulation in Cancer Immunotherapy. Int J Mol Sci. 22(18):9804.

Carbone M, Ly BH, Dodson RF, Pagano I, Morris PT, Dogan UA, Gazdar AF, Pass HI, Yang H. (2012) Malignant mesothelioma: facts, myths, and hypotheses. *J Cell Physiol*. Jan;227(1):44-58.

Cersosimo F, Barbarino M, Lonardi S, Vermi W, Giordano A, Bellan C, Giurisato E. (2021) Mesothelioma Malignancy and the Microenvironment: Molecular Mechanisms. *Cancers (Basel)*. Nov 12;13(22):5664.

Chavez M, Silvestrini MT, Ingham ES, Fite BZ, Mahakian LM, Tam SM, Ilovitsh A, Monjazeb AM, Murphy WJ, Hubbard NE, Davis RR, et al. (2018) Distinct immune signatures in directly treated and distant tumors result from TLR adjuvants and focal ablation. *Theranostics.* Jun 7;8(13):3611-3628.

Chen DS, Mellman I. (2017) Elements of cancer immunity and the cancer-immune set point. *Nature*. Jan 18;541(7637):321-330.

Chu GJ, van Zandwijk N, Rasko JEJ. (2019) The Immune Microenvironment in Mesothelioma: Mechanisms of Resistance to Immunotherapy. *Front Oncol.* Dec 6; 9:1366

Conti L, Lanzardo S, Arigoni M, Antonazzo R, Radaelli E, Cantarella D, Calogero RA, Cavallo F. (2013) The noninflammatory role of high mobility group box 1/Toll-like receptor 2 axis in the self-renewal of mammary cancer stem cells. *FASEB J*. Dec;27(12):4731-44.

Désage A-L, Karpathiou G, Peoc'h M, Froudarakis ME. (2021) The Immune Microenvironment of Malignant Pleural Mesothelioma: A Literature Review. *Cancers*; 13(13):3205.

Edgar LJ, Kawasaki N, Nycholat CM, Paulson JC. (2019) Targeted Delivery of Antigen to Activated $CD169^+$ Macrophages Induces Bias for Expansion of $CD8^+$ T Cells. *Cell Chem Biol*. 26(1):131-136.e4.

Elliott MR, Ravichandran KS. (2016) The Dynamics of Apoptotic Cell Clearance. *Dev Cell*. 38(2):147-160.

Espinosa-Carrasco G, Chiu E, Scrivo A, Zumbo P, Dave A, Betel D, Kang SW, Jang HJ, Hellmann MD, Burt BM, Lee HS, Schietinger A. (2024) Intratumoral immune triads are required for immunotherapy-mediated elimination of solid tumors. *Cancer Cell.* Jul 8;42(7):1202-1216.e8.

Fang YJ, Chuang HY, Pan CH, Chang YY, Cheng Y, Lee LJ, Wang JD. (2021) Increased Risk of Gastric Cancer in Asbestos-Exposed Workers: A Retrospective Cohort Study Based on Taiwan Cancer Registry 1980-2015. *Int J Environ Res Public Health*. Jul 15;18(14):7521.

Fassi EMA, Sgrignani J, D'Agostino G, Cecchinato V, Garofalo M, Grazioso G, Uguccioni M, Cavalli A. (2019) Oxidation State Dependent Conformational Changes of HMGB1 Regulate the Formation of the CXCL12/HMGB1 Heterocomplex. *Comput Struct Biotechnol J.* Jun 21;17:886-894.

Fiuza C, Bustin M, Talwar S, Tropea M, Gerstenberger E, Shelhamer JH, Suffredini AF. (2003) Inflammation-promoting activity of HMGB1 on human microvascular endothelial cells. *Blood*. Apr 1;101(7):2652-60.

Funes SC, Rios M, Escobar-Vera J, Kalergis AM. (2018) Implications of macrophage polarization in autoimmunity. *Immunology.* 154(2):186-195.

Gajewski TF, Corrales L, Williams J, Horton B, Sivan A, Spranger S. (2017) Cancer Immunotherapy Targets Based on Understanding the T Cell-Inflamed Versus Non-T Cell-Inflamed Tumor Microenvironment. *Adv Exp Med Biol*. 1036:19-31.

Gajewski TF, Schreiber H, Fu YX. (2013) Innate and adaptive immune cells in the tumor microenvironment. *Nat Immunol*. 14(10):1014-1022.

Gebhardt C, Riehl A, Durchdewald M, Németh J, Fürstenberger G, Müller-Decker K, Enk A, Arnold B, Bierhaus A, Nawroth PP, Hess J, Angel P. (2008) RAGE signaling sustains inflammation and promotes tumor development. *J Exp Med*. Feb 18;205(2):275-85.

Giavara S, Kosmidou E, Hande MP, Bianchi ME, Morgan A, d'Adda di Fagagna F, Jackson SP. (2005) Yeast Nhp6A/B and mammalian Hmgb1 facilitate the maintenance of genome stability. *Curr Biol.* Jan 11;15(1):68-72.

Gong W, Zheng Y, Chao F, Li Y, Xu Z, Huang G, Gao X, Li S, He F. (2010) The anti-inflammatory activity of HMGB1 A box is enhanced when fused with C-terminal acidic tail. *J Biomed Biotechnol*. 2010:915234

Gordon S, Martinez FO. (2010) Alternative activation of macrophages: mechanism and functions. *Immunity*. 32(5):593-604.

Grabowska J, Lopez-Venegas MA, Affandi AJ, den Haan JMM. (2018) $CD169^+$ Macrophages Capture and Dendritic Cells Instruct: The Interplay of the Gatekeeper and the General of the Immune System. *Front Immunol*. Oct 26;9:2472.

Gu S, Ni T, Wang J, Liu Y, Fan Q, Wang Y, Huang T, Chu Y, Sun X, Wang Y. (2018) CD47 Blockade Inhibits Tumor Progression through Promoting Phagocytosis of Tumor Cells by M2 Polarized Macrophages in Endometrial Cancer. *J Immunol Res.* Nov 7; 2018:6156757.

Guillerey C, Huntington ND, Smyth MJ. (2016) Targeting natural killer cells in cancer immunotherapy. *Nat Immunol.* Aug 19;17(9):1025-36.

Guo F, Wang Y, Liu J, Mok SC, Xue F, Zhang W. (2016) CXCL12/CXCR4: a symbiotic bridge linking cancer cells and their stromal neighbors in oncogenic communication networks. *Oncogene*. Feb 18;35(7):816-26.

Guo Q, Gao BL, Zhang XJ, Liu GC, Xu F, Fan QY, Zhang SJ, Yang B, Wu XH. (2014) CXCL12-CXCR4 Axis Promotes Proliferation, Migration, Invasion, and Metastasis of Ovarian Cancer. *Oncol Res.* 22(5-6):247-58.

Guo ZS, Liu Z, Bartlett DL, Tang D, Lotze MT. (2013) Life after death: targeting high mobility group box 1 in emergent cancer therapies. *Am J Cancer Res*. 3(1):1-20.

Guyon A. (2014) CXCL12 chemokine and its receptors as major players in the interactions between immune and nervous systems. *Front Cell Neurosci*. Mar 6;8:65.

Hanahan D, Weinberg RA. (2011) Hallmarks of cancer: the next generation. *Cell.* Mar 4;144(5):646-74.

He SJ, Cheng J, Feng X, Yu Y, Tian L, Huang Q. (2017) The dual role and therapeutic potential of high-mobility group box 1 in cancer. *Oncotarget*. 8(38):64534-64550.

Hiltbrunner S, Mannarino L, Kirschner MB, Opitz I, Rigutto A, Laure A, Lia M, Nozza P, Maconi A, Marchini S, D'Incalci M, Curioni-Fontecedro A, Grosso F. (2021) Tumor Immune Microenvironment and Genetic Alterations in Mesothelioma. *Front Oncol*. Jun 23;11:660039.

Hori O, Brett J, Slattery T, Cao R, Zhang J, Chen JX, Nagashima M, Lundh ER, Vijay S, Nitecki D, et al. (1995) The receptor for advanced glycation end products (RAGE) is a cellular binding site for amphoterin. Mediation of neurite outgrowth and co-expression of rage and amphoterin in the developing nervous system. *J Biol Chem*. Oct 27;270(43):25752-61.

https://www.cancer.org/cancer/cancer-causes/asbestos.html

https://www.cdc.gov/niosh/topics/asbestos/default.html

https://www.nhsinform.scot/illnesses-and-conditions/cancer/cancer-types-inadults/mesothelioma

Ivanov S, Dragoi AM, Wang X, Dallacosta C, Louten J, Musco G, Sitia G, Yap GS, Wan Y, Biron CA, Bianchi ME, Wang H, Chu WM. (2007) A novel role for HMGB1 in TLR9-mediated inflammatory responses to CpG-DNA. *Blood.* Sep 15;110(6):1970-81.

Jaiswal S, Jamieson CH, Pang WW, Park CY, Chao MP, Majeti R, Traver D, van Rooijen N, Weissman IL. (2009) CD47 is upregulated on circulating hematopoietic stem cells and leukemia cells to avoid phagocytosis. *Cell.* Jul 23;138(2):271-85.

Janssens R, Struyf S, Proost P. (2018) The unique structural and functional features of CXCL12. *Cell Mol Immunol*. 15(4):299-311.

Jiao Y, Wang HC, Fan SJ. Growth suppression and radiosensitivity increase by HMGB1 in breast cancer. (2007) *Acta Pharmacol Sin*. 28(12):1957-1967.

Jube S, Rivera ZS, Bianchi ME, Powers A, Wang E, Pagano I, Pass HI, Gaudino G, Carbone M, Yang H. (2012) Cancer cell secretion of the DAMP protein HMGB1 supports progression in malignant mesothelioma. *Cancer Res*. Jul 1;72(13):3290-301.

Kang R, Chen R, Zhang Q, Hou W, Wu S, Cao L, Huang J, Yu Y, Fan XG, Yan Z, Sun X, Wang H, Wang Q, Tsung A, Billiar TR, Zeh HJ 3rd, Lotze MT, Tang D. (2014) HMGB1 in health and disease. *Mol Aspects Med*. Dec;40:1-116.

Kang R, Livesey KM, Zeh HJ, Loze MT, Tang D. (2010) HMGB1: a novel Beclin 1-binding protein active in autophagy. *Autophagy*. 6(8):1209-1211.

Kang R, Zhang Q, Zeh HJ 3rd, Lotze MT, Tang D. (2013) HMGB1 in cancer: good, bad, or both? *Clin Cancer Res.* Aug 1;19(15):4046-57.

Khosravi GR, Mostafavi S, Bastan S, Ebrahimi N, Gharibvand RS, Eskandari N. (2024) Immunologic tumor microenvironment modulators for turning cold tumors hot. *Cancer Commun (Lond)*. May;44(5):521-553.

Kim HJ, Park JH, Kim HC, Kim CW, Kang I, Lee HK. (2022) Blood monocyte-derived CD169^{+} macrophages contribute to antitumor immunity against glioblastoma. *Nat Commun.* Oct 20;13(1):6211.

Kim HJ, Park JH, Kim HC, Kim CW, Kang I, Lee HK. (2022) Blood monocyte-derived CD169^{+} macrophages contribute to antitumor immunity against glioblastoma. *Nat Commun*. 13(1):6211.

Klement JD, Paschall AV, Redd PS, Ibrahim ML, Lu C, Yang D, Celis E, Abrams SI, Ozato K, Liu K. (2018) An osteopontin/CD44 immune checkpoint controls CD8+ T cell activation and tumor immune evasion. *J Clin Invest.* Dec 3;128(12):5549-5560

Kuroda A. (2021) Recent progress and perspectives on the mechanisms underlying Asbestos toxicity. *Genes Environ*. Oct 12;43(1):46

Kusume A, Sasahira T, Luo Y, Isobe M, Nakagawa N, Tatsumoto N, Fujii K, Ohmori H, Kuniyasu H. (2009) Suppression of dendritic cells by HMGB1 is associated with lymph node metastasis of human colon cancer. *Pathobiology.* 76(4):155-62.

Laberiano-Fernandez C, Baldavira CM, Machado-Rugolo J, Tamegnon A, Pandurengan RK, Ab'Saber AM, Balancin ML, Takagaki TY, Nagai MA, Capelozzi VL, Parra ER. (2023) The Immunological Landscape of M1 and M2 Macrophages and Their Spatial Distribution in Patients with Malignant Pleural Mesothelioma. *Cancers (Basel)*. Oct 24;15(21):5116.

Lazennec G, Richmond A. (2010) Chemokines and chemokine receptors: new insights into cancer-related inflammation. *Trends Mol Med*. 16(3):133-144.

LeBleu VS. (2015) Imaging the Tumor Microenvironment. *Cancer J.* May-Jun;21(3):174-8.

Li M, Yang Y, Xiong L, Jiang P, Wang J, Li C. (2023) Metabolism, metabolites, and macrophages in cancer. *J Hematol Oncol*. 16(1):80.

Lievense LA, Bezemer K, Aerts JG, Hegmans JP. (2013) Tumor-associated macrophages in thoracic malignancies. *Lung Cancer*. Jun;80(3):256-62.

Lin P, Lin Y, Chen X, Zhao X, Cui L. (2025) Decoding MHC loss: Molecular mechanisms and implications for immune resistance in cancer. *Clin Transl Med*. Jul;15(7):e70403.

Lin Y, Xu J, Lan H. (2019) Tumor-associated macrophages in tumor metastasis: biological roles and clinical therapeutic applications. *J Hematol Oncol*. 12(1):76.

Liu X, Pu Y, Cron K, Deng L, Kline J, Frazier WA, Xu H, Peng H, Fu YX, Xu MM. (2015) CD47 blockade triggers T cell-mediated destruction of immunogenic tumors. *Nat Med.* Oct;21(10):1209-15.

Liu Y, Xia Y, Qiu CH. (2021) Functions of CD169 positive macrophages in human diseases (Review). *Biomed Rep*. 14(2):26.

Liu YT, Sun ZJ. (2021) Turning cold tumors into hot tumors by improving T-cell infiltration. *Theranostics.* Mar 11;11(11):5365-5386.

Liu Z, Falo LD Jr, You Z. (2011) Knockdown of HMGB1 in tumor cells attenuates their ability to induce regulatory T cells and uncovers naturally acquired CD8 T cell-dependent antitumor immunity. *J Immunol.* Jul 1;187(1):118-25.

Lu B, Wang C, Wang M, Li W, Chen F, Tracey KJ, Wang H. (2014) Molecular mechanism and therapeutic modulation of high mobility group box 1 release and action: an updated review. *Expert Rev Clin Immunol*. Jun;10(6):713-27.

Magnani C, Ferrante D, Barone-Adesi F, Bertolotti M, Todesco A, Mirabelli D, Terracini B. (2008) Cancer risk after cessation of asbestos exposure: a cohort study of Italian asbestos cement workers. *Occup Environ Med*. Mar;65(3):164-70.

Magnani C, Terracini B, Ivaldi C, Botta M, Mancini A, Andrion A. (1995) Pleural malignant mesothelioma and non-occupational exposure to asbestos in Casale Monferrato, Italy. *Occup Environ Med*. Jun;52(6):362-7.

Mantonico MV, De Leo F, Quilici G, Colley LS, De Marchis F, Crippa M, Mezzapelle R, Schulte T, Zucchelli C, Pastorello C, Carmeno C, Caprioglio F, Ricagno S, Giachin G, Ghitti M, Bianchi ME, Musco G. (2024) The acidic intrinsically disordered region of the inflammatory mediator HMGB1 mediates fuzzy interactions with CXCL12. *Nat Commun.* Feb 8;15(1):1201.

Mantovani A, Allavena P, Sica A, Balkwill F. (2008) Cancer-related inflammation. *Nature*. Jul 24;454(7203):436-44.

Mantovani A, Marchesi F, Malesci A, Laghi L, Allavena P. (2017) Tumour-associated macrophages as treatment targets in oncology. *Nat Rev Clin Oncol*. 14(7):399-416.

Mantovani A, Sozzani S, Locati M, Allavena P, Sica A. (2002) Macrophage polarization: tumor-associated macrophages as a paradigm for polarized M2 mononuclear phagocytes. *Trends Immunol.* Nov;23(11):549-55.

Martinez FO, Gordon S. (2014) The M1 and M2 paradigm of macrophage activation: time for reassessment. *F1000Prime Rep*. 2014;6:13.

McGranahan N, Rosenthal R, Hiley CT, Rowan AJ, Watkins TBK, Wilson GA, Birkbak NJ, Veeriah S, Van Loo P, Herrero J, Swanton C; TRACERx Consortium. Allele-Specific HLA Loss and Immune Escape in Lung Cancer Evolution. Cell. 2017 Nov 30;171(6):1259-1271.e11.

Mezzapelle R, Leo M, Caprioglio F, Colley LS, Lamarca A, Sabatino L, Colantuoni V, Crippa MP, Bianchi ME. (2022) CXCR4/CXCL12 Activities in the Tumor Microenvironment and Implications for Tumor Immunotherapy. Cancers (Basel). May 6;14(9):2314.

Mezzapelle R, De Marchis F, Passera C, Leo M, Brambilla F, Colombo F, Casalgrandi M, Preti A, Zambrano S, Castellani P, Ertassi R, Silingardi M, Caprioglio F, et al. (2021) CXCR4 engagement triggers CD47 internalization and antitumor immunization in a mouse model of mesothelioma. *EMBO Mol Med*. Jun 7;13(6):e12344.

Miyake Y, Asano K, Kaise H, Uemura M, Nakayama M, Tanaka M. (2007) Critical role of macrophages in the marginal zone in the suppression of immune responses to apoptotic cell-associated antigens. *J Clin Invest*. 117(8):2268-2278

Morein D, Erlichman N, Ben-Baruch A. (2020) Beyond Cell Motility: The Expanding Roles of Chemokines and Their Receptors in Malignancy. *Front Immunol*. 11:952.

Müller S, Scaffidi P, Degryse B, Bonaldi T, Ronfani L, Agresti A, Beltrame M, Bianchi ME. (2001) New EMBO members' review: the double life of HMGB1 chromatin protein: architectural factor and extracellular signal. *EMBO J*. Aug 15;20(16):4337-40.

Murray PJ, Allen JE, Biswas SK, Fisher EA, Gilroy DW, Goerdt S, Gordon S, Hamilton JA, Ivashkiv LB, Lawrence T, et al. (2014) Macrophage activation and polarization: nomenclature and experimental guidelines. *Immunity*. Jul 17;41(1):14-20.

Murray PJ, Wynn TA. (2011) Protective and pathogenic functions of macrophage subsets. *Nat Rev Immunol*. 2011;11(11):723-737.

Napolitano A, Antoine DJ, Pellegrini L, Baumann F, Pagano I, Pastorino S, Goparaju CM, Prokrym K, Canino C, Pass HI, Carbone M, Yang H. (2016) HMGB1 and Its Hyperacetylated Isoform are Sensitive and Specific Serum Biomarkers to Detect Asbestos Exposure and to Identify Mesothelioma Patients. *Clin Cancer Res.* Jun 15;22(12):3087-96

Noy R, Pollard JW. (2014) Tumor-associated macrophages: from mechanisms to therapy. *Immunity.* Jul 17;41(1):49-61.

Oldenborg PA, Zheleznyak A, Fang YF, Lagenaur CF, Gresham HD, Lindberg FP. (2000) Role of CD47 as a marker of self on red blood cells. *Science*. Jun 16;288(5473):2051-4

Park JS, Svetkauskaite D, He Q, Kim JY, Strassheim D, Ishizaka A, Abraham E. (2004) Involvement of toll-like receptors 2 and 4 in cellular activation by high mobility group box 1 protein. *J Biol Chem*. Feb 27;279(9):7370-7.

Patrussi L, Ulivieri C, Lucherini OM, Paccani SR, Gamberucci A, Lanfrancone L, Pelicci PG, Baldari CT. (2007) p52Shc is required for CXCR4-dependent signaling and chemotaxis in T cells. *Blood*. Sep 15;110(6):1730-8.

Pirani E, Paparoditis P, Pecoraro M, Danelon G, Thelen M, Cecchinato V, Uguccioni M. (2024) Tumor cells express and maintain HMGB1 in the reduced isoform to enhance CXCR4-mediated migration. *Front Immunol*. May 13;15:1358800.

Polanská E, Dobšáková Z, Dvořáčková M, Fajkus J, Štros M. (2012) HMGB1 gene knockout in mouse embryonic fibroblasts results in reduced telomerase activity and telomere dysfunction. *Chromosoma*. Aug;121(4):419-31.

Qie J, Liu Y, Wang Y, Zhang F, Qin Z, Tian S, Liu M, Li K, Shi W, Song L, et al. (2022) Integrated proteomic and transcriptomic landscape of macrophages in mouse tissues. Nat Commun. Nov 30;13(1):7389.

Qiu Y, Yang J, Wang W, Zhao W, Peng F, Xiang Y, Chen G, Chen T, Chai C, Zheng S, Watkins DJ, Feng J. (2014) HMGB1-promoted and TLR2/4-dependent NK cell maturation and activation take part in rotavirus-induced murine biliary atresia. *PLoS Pathog*. Mar 20;10(3):e1004011.

Rajagopal S, Shenoy SK. (2018) GPCR desensitization: Acute and prolonged phases. *Cell Signal*. 41:9-16.

Rapoport BL, Steel HC, Theron AJ, Heyman L, Smit T, Ramdas Y, Anderson R. (2020) High Mobility Group Box 1 in Human Cancer. *Cells*. Jul 10;9(7):1664.

Saito Y, Ohnishi K, Miyashita A, Nakahara S, Fujiwara Y, Horlad H, Motoshima T, Fukushima S, Jinnin M, Ihn H, Takeya M, Komohara Y. (2015) Prognostic Significance of CD169+ Lymph Node Sinus Macrophages in Patients with Malignant Melanoma. *Cancer Immunol Res.* Dec;3(12):1356-63.

Saito Y, Ohnishi K, Miyashita A, Nakahara S, Fujiwara Y, Horlad H, Motoshima T, Fukushima S, Jinnin M, Ihn H, Takeya M, Komohara Y. (2015) Prognostic Significance of CD169+ Lymph Node Sinus Macrophages in Patients with Malignant Melanoma. *Cancer Immunol Res.* Dec;3(12):1356-63

Schiraldi M, Raucci A, Muñoz LM, Livoti E, Celona B, Venereau E, Apuzzo T, De Marchis F, Pedotti M, Bachi A, Thelen M, Varani L, Mellado M, Proudfoot A, Bianchi ME, Uguccioni M. (2012) HMGB1 promotes recruitment of inflammatory cells to damaged tissues by forming a complex with CXCL12 and signaling via CXCR4. *J Exp Med.* Mar 12;209(3):551-63.

Sekido Y. (2013) Molecular pathogenesis of malignant mesothelioma. *Carcinogenesis*. Jul;34(7):1413-9.

Shi Y, Riese DJ 2nd, Shen J. (2020) The Role of the CXCL12/CXCR4/CXCR7 Chemokine Axis in Cancer. *Front Pharmacol*. 11:574667.

Shiratori H, Feinweber C, Luckhardt S, Linke B, Resch E, Geisslinger G, Weigert A, Parnham MJ. (2017) THP-1 and human peripheral blood mononuclear cell-derived macrophages differ in their capacity to polarize in vitro. *Mol Immunol*. Aug;88:58-68.

Shirozu M, Nakano T, Inazawa J, Tashiro K, Tada H, Shinohara T, Honjo T. (1995) Structure and chromosomal localization of the human stromal cell-derived factor 1 (SDF1) gene. *Genomics*. 28(3):495-500.

Sica A, Mantovani A. (2012) Macrophage plasticity and polarization: in vivo veritas. *J Clin Invest.* 122(3):787-795.

Singh N, Baby D, Rajguru JP, Patil PB, Thakkannavar SS, Pujari VB. (2019) Inflammation and cancer. *Ann Afr Med*. Jul-Sep;18(3):121-126.

Solbes E, Harper RW. (2018) Biological responses to asbestos inhalation and pathogenesis of asbestos-related benign and malignant disease. *J Investig Med*. Apr;66(4):721-727.

Suleimanov SK, Efremov YM, Klyucherev TO, Salimov EL, Ragimov AA, Timashev PS, Vlasova II. (2024) Radical-Generating Activity, Phagocytosis, and Mechanical Properties of Four Phenotypes of Human Macrophages. *Int J Mol Sci.* Feb 3;25(3):1860.

Suarez JS, Novelli F, Goto K, Ehara M, Steele M, Kim JH, Zolondick AA, Xue J, Xu R, Saito M, Pastorino S, Minaai M, Takanishi Y, Emi M, Pagano I, Wakeham A, Berger T, Pass HI, Gaudino G, Mak TW, Carbone M, Yang H (2023) HMGB1 released by mesothelial cells drives the development of asbestos-induced mesothelioma. Proc Natl Acad Sci U S A; 120(39):e2307999120.

Tacconi C, Commerford CD, Dieterich LC, Schwager S, He Y, Ikenberg K, Friebel E, Becher B, Tugues S, Detmar M. (2021) $CD169^+$ lymph node macrophages have protective functions in mouse breast cancer metastasis. *Cell Rep.* Apr 13;35(2):108993.

Tanaka A, Sakaguchi S. Regulatory T cells in cancer immunotherapy. *Cell Res*. 2017;27(1):109-118.

Tang D, Kang R, Livesey KM, Cheh CW, Farkas A, Loughran P, Hoppe G, Bianchi ME, Tracey KJ, Zeh HJ 3rd, Lotze MT. (2010) Endogenous HMGB1 regulates autophagy. *J Cell Biol.* Sep 6;190(5):881-92.

Teicher BA, Fricker SP. (2010) CXCL12 (SDF-1)/CXCR4 pathway in cancer. *Clin Cancer Res.* Jun 1;16(11):2927-31.

Terzić J, Grivennikov S, Karin E, Karin M. (2010) Inflammation and colon cancer. *Gastroenterology*. Jun;138(6):2101-2114.e5.

Thomas RM, Kim J, Revelo-Penafiel MP, Angel R, Dawson DW, Lowy AM. (2008) The chemokine receptor CXCR4 is expressed in pancreatic intraepithelial neoplasia. *Gut*. 57(11):1555-1560.

Toyokuni S. (2009) Mechanisms of asbestos-induced carcinogenesis. *Nagoya J Med Sci*. Feb;71(1-2):1-10.

Urbonaviciute V, Fürnrohr BG, Meister S, Munoz L, Heyder P, De Marchis F, Bianchi ME, Kirschning C, Wagner H, Manfredi AA, Kalden JR, Schett G, Rovere-Querini P, Herrmann M, Voll RE. (2008) Induction of inflammatory and immune responses by HMGB1-nucleosome complexes: implications for the pathogenesis of SLE. *J Exp Med.* Dec 22;205(13):3007-18.

Venereau E, Casalgrandi M, Schiraldi M, Antoine DJ, Cattaneo A, De Marchis F, Liu J, Antonelli A, Preti A, Raeli L, Shams SS, Yang H, Varani L, Andersson U, Tracey KJ, Bachi A, Uguccioni M, Bianchi ME. (2012) Mutually exclusive redox forms of HMGB1 promote cell recruitment or proinflammatory cytokine release. *J Exp Med*. Aug 27;209(9):1519-28.

Venereau E, Schiraldi M, Uguccioni M, Bianchi ME. (2013) HMGB1 and leukocyte migration during trauma and sterile inflammation. *Mol Immunol.* Aug;55(1):76-82.

Voll RE, Herrmann M, Roth EA, Stach C, Kalden JR, Girkontaite I. (1997) Immunosuppressive effects of apoptotic cells. *Nature*. 390(6658):350-351.

Vogelzang NJ, Rusthoven JJ, Symanowski J, Denham C, Kaukel E, Ruffie P, Gatzemeier U, Boyer M, Emri S, Manegold C, Niyikiza C, Paoletti P. (2003) Phase III study of pemetrexed in combination with cisplatin versus cisplatin alone in patients with malignant pleural mesothelioma. *J Clin Oncol*. Jul 15;21(14):2636-44.

Vyhnánková S, Lacina L, Chovanec M, Plzák J, Smetana K Jr., Netušil J, Kolář M, Šindelka R. (2025) Cold, Hot, and Lethal—The Tumour Microenvironment and the Immunology of Head and Neck Squamous Cell Carcinoma. *International Journal of Molecular Sciences*. 26(18):8844.

Wang Y, Ge P, Zhu Y. (2013) TLR2 and TLR4 in the brain injury caused by cerebral ischemia and reperfusion. *Mediators Inflamm*. 124614.

Wherry EJ, Kurachi M. (2015) Molecular and cellular insights into T cell exhaustion. *Nat Rev Immunol*. Aug;15(8):486-99.

Willingham SB, Volkmer JP, Gentles AJ, Sahoo D, Dalerba P, Mitra SS, Wang J, Contreras-Trujillo H, Martin R, Cohen JD, et al. (2012) The CD47-signal regulatory protein alpha (SIRPa) interaction is a therapeutic target for human solid tumors. *Proc Natl Acad Sci U S A*. Apr 24;109(17):6662-7.

Wu B, Chien EY, Mol CD, Fenalti G, Liu W, Katritch V, Abagyan R, Brooun A, Wells P, Bi FC, Hamel DJ, Kuhn P, Handel TM, Cherezov V, Stevens RC. (2010) Structures of the CXCR4 chemokine GPCR with small-molecule and cyclic peptide antagonists. *Science*. Nov 19;330(6007):1066-71.

Wu B, Zhang B, Li B, Wu H, Jiang M. (2024) Cold and hot tumors: from molecular mechanisms to targeted therapy. *Signal Transduct Target Ther*. 9(1):274.

Wu CY, Tsai YY, Chen SY, Lin YP, Shin JW, Wu CC, Yang BC. (2017) Interaction of Zap70 and CXCR4 receptor at lamellipodia that determines the directionality during Jurkat T cells chemotaxis. *Mol Immunol.* Oct; 90:245-254.

Wu X, Li T, Jiang R, Yang X, Guo H, Yang R. (2023) Targeting MHC-I molecules for cancer: function, mechanism, and therapeutic prospects. *Mol Cancer*. Dec 2;22(1):194.

Wynn TA, Chawla A, Pollard JW. (2013) Macrophage biology in development, homeostasis and disease. *Nature*. 496(7446):445-455.

Wynn TA, Vannella KM. (2016) Macrophages in Tissue Repair, Regeneration, and Fibrosis. *Immunity*. 44(3):450-462.

Xue J, Schmidt SV, Sander J, Draffehn A, Krebs W, Quester I, De Nardo D, Gohel TD, Emde M, Schmidleithner L, et al. (2014) Transcriptome-based network analysis reveals a spectrum model of human macrophage activation. *Immunity.* Feb 20;40(2):274-88.

Yang H, Antoine DJ, Andersson U, Tracey KJ. (2013) The many faces of HMGB1: molecular structure-functional activity in inflammation, apoptosis, and chemotaxis. *J Leukoc Biol.* Jun;93(6):865-73.

Yang H, Bocchetta M, Kroczynska B, Elmishad AG, Chen Y, Liu Z, Bubici C, Mossman BT, Pass HI, Testa JR, Franzoso G, Carbone M. (2006) TNF-alpha inhibits asbestos-induced cytotoxicity via a NF-kappaB-dependent pathway, a possible mechanism for asbestos-induced oncogenesis. *Proc Natl Acad Sci U S A*. Jul 5;103(27):10397-10402.

Yang H, Rivera Z, Jube S, Nasu M, Bertino P, Goparaju C, Franzoso G, Lotze MT, Krausz T, Pass HI, Bianchi ME, Carbone M. (2010) Programmed necrosis induced by asbestos in human mesothelial cells causes high-mobility group box 1 protein release and resultant inflammation. *Proc Natl Acad Sci U S A*. Jul 13;107(28)

Yang H, Wang H, Czura CJ, Tracey KJ. (2005) The cytokine activity of HMGB1. *J Leukoc Biol.* 78(1):1-8.

Yoon J, Moon H, Jeon Y, Choe S, Yoon H. (2025) Signature Gene Mutations in Colorectal Cancer: Potential Neoantigens for Cancer Vaccines. *Int J Mol Sci.* 26(10):4559

Yuan F, Gu L, Guo S, Wang C, Li GM. (2004) Evidence for involvement of HMGB1 protein in human DNA mismatch repair. *J Biol Chem*. 279(20):20935-20940.

Zander R, Schauder D, Xin G, Nguyen C, Wu X, Zajac A, Cui W. (2019) CD4+ T Cell Help Is Required for the Formation of a Cytolytic CD8+ T Cell Subset that Protects against Chronic Infection and Cancer. *Immunity*. Dec 17;51(6):1028-1042.e4.

Zhang N, Bevan MJ. (2011) CD8(+) T cells: foot soldiers of the immune system. *Immunity*. 35(2):161-168.

Zhou D, Luan J, Huang C, Li J. Tumor-Associated Macrophages in Hepatocellular Carcinoma: Friend or Foe?. *Gut Liver*. 2021;15(4):500-516.

Zhu C, Yao WL, Tan W, Zhang CH. (2017) SDF-1 and CXCR4 play an important role in adult SVZ lineage cell proliferation and differentiation. *Brain Res*. 1657:223-231.

Zilionis R, Engblom C, Pfirschke C, Savova V, Zemmour D, Saatcioglu HD, Krishnan I, Maroni G, Meyerovitz CV, Kerwin CM, et al. (2019) Single-Cell Transcriptomics of Human and Mouse Lung Cancers Reveals Conserved Myeloid Populations across Individuals and Species. *Immunity*. May 21;50(5):1317-1334.e10.

Zlotnik A, Burkhardt AM, Homey B. (2011) Homeostatic chemokine receptors and organ-specific metastasis. *Nat Rev Immunol.* Aug 25;11(9):597-606.

Zlotnik A. (2006) Chemokines and cancer. *Int J Cancer*. 119(9):2026-2029.

Milano, 30/11/2025